KfK 4004
Januar 1986

Experimental Modal Survey of a Vertical Cylindrical Shell Partly Filled with Water

F. Eberle, J. Kadlec, G. Hailfinger, R. Scharnowell
Institut für Reaktorentwicklung
Projekt Nukleare Sicherheit

Kernforschungszentrum Karlsruhe

KERNFORSCHUNGSZENTRUM KARLSRUHE
Institut für Reaktorentwicklung
Projekt Nukleare Sicherheit

KfK 4004

Experimental modal survey of a vertical cylindrical shell partly filled with water

by

F. Eberle, J. Kadlec, G. Hailfinger and R. Scharnowell

Kernforschungszentrum Karlsruhe GmbH, Karlsruhe

Als Manuskript vervielfältigt
Für diesen Bericht behalten wir uns alle Rechte vor

Kernforschungszentrum Karlsruhe GmbH
Postfach 3640, 7500 Karlsruhe 1

ISSN 0303-4003

Experimental modal survey of a vertical cylindrical shell partly filled with water

Summary

The report deals with an experimental modal survey of a vertical cylindrical shell, requested for experimental verification of the SING-S coupled fluid/structure-interaction computer program. The eigenfrequencies, the mode shapes and the critical damping ratios of the test cylinder used (ϕ 1000 x 3 x 1600 mm, empty or partly filled with water, water level 1350 mm) were extracted from the set of simultaneously measured relaxation response signals. The response was achieved via a snapback process, e.g. sudden release of the test cylinder shell previously loaded with a concentrated load by means of a simple mechanical device. The EVA computer program was used to extract the modal characteristics from the acceleration response signals. A total number of 93 eigenmodes were identified - 55 eigenmodes of the test cylinder partly filled with water and 38 eigenmodes of the empty test cylinder. The majority of these eigenmodes are the multiple modes (preferably doublets) of equal axial and circumferential orders but different eigenfrequencies, critical damping ratios and orientations in space. A secondary objective of the modal investigations performed was the experimental verification by means of a comparative modal survey of the extraction subroutines of the EVA computer program. Three alternative experimental procedures - the modified relaxation procedure with preselected excitation frequencies, the single point random excitation procedure, and the impact method - were successively applied to furnish the supplementary modal characteristics needed for the comparison. They yielded consistent results confirming the correctness of all four experimental and evaluation procedures used.

Experimentelle Modalanalyse einer vertikalen, zum Teil mit Wasser gefüllten Zylinderschale.

Zusammenfassung

Der Bericht befaßt sich mit experimentellen, für die Verifizierung des gekoppelten fluid-strukturdynamischen Rechenprogrammes SING-S benötigten, modalanalytischen Untersuchungen einer vertikalen Zylinderschale. Die Eigenfrequenzen, die Eigenschwingungsformen und die modalen Dämpfungsquotienten der untersuchten Schale (ø1000 x 3 x 1600 mm, leer oder z.T. gefüllt mit Wasser, Wasserspiegelhöhe 1350 mm) wurden aus einem Satz von simultan gemessenen, frei ausschwingenden Antwortsignalen extrahiert, die über eine sprunghafte Anregung der Schale induziert wurden (Snapback-Vorgang). Die Extraktion der modalen Kennwerte erfolgte mit dem Rechenprogramm EVA. Insgesamt wurden 93 Eigenmodes identifiziert und für die Verifizierungszwecke bereitgestellt. Davon entfallen 38 auf die leere und 55 auf die z.T. mit Wasser gefüllten Zylinderschale. Viele davon sind mehrfache Modes (hauptsächlich Dubletts) mit jeweils gleicher Axial- und Umfangsordnung und unterschiedlichen Eigenfrequenzen, modalen Dämpfungsquotienten und Orientierungen im Raum. Das Sekundärziel der Untersuchungen war die experimentelle Überprüfung der Extraktionsroutinen des Rechenprogrammes EVA. Sie basierte auf einem Vergleich der modalen Kennwerte, die wahlweise mit sprunghafter, harmonischer, randomer oder impulsartiger Schwingungsanregung erzielt wurden. Diese Untersuchungen lieferten konsistente Ergebnisse, wodurch die Korrektheit aller vier benutzten Verfahren bestätigt wurde.

Contents

1. Introduction

The experimental modal analysis is one of the few means available to verify the structure dynamic codes or the coupled fluid/structure interaction codes currently developed in the reactor safety domain. However, application of this analysis to the real systems in reactor engineering is subjected to several severe constraints, which must be taken into account by the choice of a suitable experimental procedure. The most important of these constraints are: a) hostile environmental conditions met when the analysed structures are located inside of the reactor confinement; b) presence of massive steel or concrete walls surrounding the structure; c) tight time schedule for performing the necessary measurements. The conditions a) and b) practically exclude the possible application of the multiple-point sine dwell method developed and widely used in aerospace research /1/. The possibilities of applying under such conditions the single-or multiple-point random excitation methods /2, 3/ as well as the impact methods /4/ are also restricted. To meet all requirements above the EVA computer code was developed and combined with the step relaxation method /5/. The resulting procedure was used to extract from the step relaxation signals the eigenfrequencies, the mode shapes, and the critical damping ratios of a specifically designed reactor core barrel mockup installed in the pressure vessel of the HDR-reactor and excited by a snapback device /6/. The corresponding modal investigations yielded a set of the modal characteristics of the core barrel with numerous multiple modes, preferably doublets. The appearance of the multiple modes is rarely reported in the literature; consequently this phenomenon must be studied in more detail. This demand could be fulfilled by combination of the study with an experimental modal survey of a vertical cylindrical shell as reported here. The principal goal of this survey was to furnish the set of eigenfrequencies and mode shapes required for experimental verification of the SING-S coupled fluid/structure-interaction code /7/. The second goal of this work was to provide the corresponding set of the critical damping ratios and to verify experimentally the extraction subroutines used by the EVA computer code. Four different experimental procedures were successively applied in this second verification task, yielding four sets of eigenfrequencies (up to 100 Hz), mode shapes and critical damping ratios of the test cylinder partly filled with water. These sets were compared with each other and with the corresponding theoretical set provided by the SING-S computer code.

The experimental setup and the four experimental identification procedures used are described in section 2. The experimental results obtained are presented and compared with the corresponding theoretical predictions in section 3. Section 4 contains the conclusions.

2. Experimental setup and mode identification procedures

The sectional view of the stainless-steel test cylinder used in our experiments and its principal dimensions are given in fig. 1. Four lead blocks weighting 47 kg each were attached on the upper flange to increase the inertial mass of the system. The test cylinder was empty or partly filled with water; the corresponding water level equals 1350 mm. Fig. 2 shows the general view of the testing bench, the experimental setup is given in fig. 3. The test cylinder was installed on a fastening plate approx. 3.3 tons in weight and instrumented with piezoresistive accelerometers type 2264-200 (Endevco) or GY-155-200 (Kulite), which were fed by 5 kHz carrier frequency amplifiers type VD6 (Elan) or KWS 3028A (Hottinger). The maximal number of the complete chains available for the acceleration measurements was restricted to 17. The following accelerometer positions were used (see fig. 4 and table I):

a) 17 equidistantly positions (1 through 17) on the generatrix of the cylindrical shell on the reference plane (denoted by the azimuthal angle $\psi = 0^{o}$);

b) 30 equidistant positions (18 through 48) on the circular circumference of the shell at the vertical coordinate z = 1000 mm;

c) 16 regularly distributed positions (49 through 64) on the upper flange and several complementary positions on the shell (65 through 81).

For the vibration excitation of the test cylinder and extraction from response signals of the modal parameters required four alternative procedures were used (see fig. 3).

2.1 Procedure I (snapback excitation and computer code EVA)

The characteristic features of this procedure are the transient, step relaxation response of the test cylinder and the evaluation of the corresponding response signals with the computer code EVA. The snapback device (Ⓘ in fig. 3) used to induce the step relaxation response is shown in fig. 5. The test cylinder was locally preloaded by means of a tensioned

steel wire before the experiment started. The transient response obtained after shearing the wire was simultaneously measured by all accelerometers installed (one of them is shown in the upper right corner of fig. 5). The corresponding response signals were simultaneously digitized (the compputer facility used is described in / 8 /) and stored on magnetic tape. The computer code EVA implemented on a type 3033 computer (IBM) and used to extract the eigenfrequencies, the mode shapes and the critical damping ratios of the test cylinder from the response signals recorded performs in two steps of evaluation:

a) In the first step the weighted spectral density function constructed from the whole assembly of the response signals recorded is used and the eigenfrequencies and the corresponding critical damping ratios are extracted.

b) In the second evaluation step the corresponding mode shapes are extracted from the Fourier transforms of individual response signals.

The mathematical background of the computer code EVA is given in detail in the report / 5 /.

Typical time history plots of the transient response signals and the moduli of the corresponding Fourier transforms illustrating the procedure are presented in fig. 6. The upper left diagram shows the time history of the accelertion signal a (t), measured on the generatrix on the vertical coordinate z = 800 mm; the corresponding snapback excitation was performed on the same generatrix at the position z = 1000 mm (the test cylinder was partly filled with water). The upper right diagram shows the modulus $|\hat{a}(f)| = |\mathcal{F}\{a(t)\}|$ of the corresponding Fourier transform. The energy rich peaks in the second diagram indicate the eigenfrequencies of the numerous shell modes of the test cylinder. The lower left diagram shows the time history of acceleration, excited on the upper flange and measured on the same generatrix on the vertical coordinate z = 800 mm. This particular experiment showed the excitation of the low-frequency beam modes of the test cylinder, indicated by three small peaks situated approximately at 20.4, 25.8 and 31 Hz in the diagram of $|a(f)|$ on the right. The disadvantage of the second excitation type was the low acceleration level obtained, yielding signals with poor signal/noise-ratios.

Procedure I turned out to be a very effective method of mode identification. It enabled to analyse a relatively broad frequency interval in one run (0-300 Hz in the case of a partly filled test cylinder and 0-355 Hz in the case of an empty cylinder), preserving a good frequency resolution of 0.157 Hz. Owing to the restricted number of the measuring chaines available, six different experiments were necessary to complete the mode identification in each frequency band of interest. Moreover, it proved to be useful to repeat each individual experiment twice in order to guarantee the storage of reliable data sets for the subsequent evaluation.

2.2 Procedure II (harmonic excitation and computer code EVA)

This procedure was used to increase the contribution of the selected mode in the output signals. To achieve this, the upper flange of the test cylinder was attached to the armature of an electromagnetic shaker (Ⓘ in fig. 3 as well as the detail view in fig. 7) type TA 250-4C-1 (Unholtz-Dickie), operated in the decay mode (the system was shortly driven with a harmonic signal with selected frequency and subsequently disconnected from the energy supply). The vibratory decay of the test cylinder was measured and evaluated in the same manner as described by procedure I. The principal disadvantage of this procedure is the high time consumption - 50 % of experiments needed in the case of procedure I to complete the analysis of all modes in the frequency interval of interest are necessary here to identify one mode.

Typical acceleration and Fourier-transform plots illustrating the procedure are given in fig. 8. They refer to the trial to isolate two different versions of one mode with equal axial and circumferential orders and slightly different eigenfrequencies and orientations in space (doublet). The upper two diagrams were obtained with the excitation frequency f_{ex} = 80.3 Hz, the lower ones with f_{ex} = 80.9 Hz. The diagrams on the right show that both vibration modes participate in both experiments in the response. However, the response in the first case posesses considerably more vibra-

tion energy of the 80.3 Hz mode than of the 80.9 Hz mode, and vice versa. The superposition of the contributions from both modes causes the beatings observable in both diagrams on the left side of fig. 8.

2.3 Procedure III (random excitation and computer code MODAMS)

This procedure is characterized by the stationary random excitation combined with the evaluation of the corresponding response signals using the computer code MODAMS. The excitation was performed in a way similar to that in the preceding case by means of the electrodynamic shaker attached to the upper flange (figures 3 and 7). The stationary, random excitation force and the corresponding acceleration response at each measuring position were simultaneously measured and analysed on-line with the time series analyser type TDA 33 (Genrad). The computer program MODAMS / 2 / was used to perform the calculation of the frequency response functions of each measuring position, their intermediate storing in the computer memory and the consecutive extraction from them of eigenfrequencies, mode shapes and critical damping ratios. The experiments were performed in two series. The first experimental series utilizing the baseband input signal 0-100 Hz and all measuring positions yielded the eigenfrequencies and the corresponding mode shapes of the test cylinder. The critical damping ratios likewise obtained in this experimental series revealed a non-acceptable scatter of values which therefore had to be identified anew in a special test series. This complementary test series was performed with a reduced number of transducers (only those possessing the best signal/noise ratio were used) in the following five selected narrow frequency bands: 51-59, 58.3-66.5, 68.6-76.7, 76.8-93.8, and 92.8-99.2 Hz. The corresponding signal processing was performed with the zoom-subroutine of the computer code MODAMS, utilizing 205 spectral lines and yielding the frequency resolution 0.04-0.08 Hz as well as reproducible critical damping ratios. The principal disadvantage of this procedure turned out to be the great number of individual experiments necessary to identify all modal parameters desired.

Several diagrams illustrating the procedure are presented in fig. 9. The time history plots of the random excitation force F(t) applied on the upper flange ($\psi = 0^{o}$, z = 1615 mm) and of the corresponding acceleration response a(t) measured on the excitation plane in the middle of the shell ($\psi = 0^{o}$, z = 800 mm) are given on the left side of fig. 9. The upper right diagram shows the real part $ReH_{Fa}(f)$ (CO-plot) and the lower one the imaginary part $ImH_{Fa}(f)$ (QUAD-plot) of the corresponding frequency response function $H_{Fa}(f)$. The arrows in these diagrams indicate the eigenfrequencies of one beam mode triplet (its individual eigenfrequencies are located approx. at 20.4, 25.8 and 31 Hz) and of six shell mode doublets. The eigenfrequencies of the beam mode triplet and of three shell mode doublets (located approx. at 54.4, 55.2, 70.7, 72.1, 90.0 and 96.0 Hz) manifest themselves as distinct resonance peaks in the QUAD-plot. By contrast, the eigenfrequencies of the remaining three doublets (located approx. at 57.7, 58.3, 62.7, 63.3, 80.3 and 80.9 Hz) show only single resonance peaks at the corresponding positions. Mutual separation of individual peaks of these three doublets could be obtained using the narrow band excitation combined with the zoom-subroutine mentioned above.

2.4 Procedure IV (impulse excitation and computer code MODAMS)

This procedure is characterized by the utilization of a hand-held impact hammer to excite the test cylinder, combined with the computer code MODAMS to identify the modes of vibration. The transient acceleration response of the test cylinder was systematically measured at one fixed position located in the grid origin ($\psi = 0^{o}$, z = 1000 or (in some redundant experiments) z = 800 mm); the test cylinder was successively excited at different positions identical to those instrumented with accelerometers in the foregoing procedures. We worked with an impact hammer type K 291 A (PCB-Piezotronics), instrumented with a load cell to measure the impact force. The force signal and the corresponding acceleration signal were measured simultaneously and used to calculate the frequency response function. This calculation as well as the subsequent extraction of the modal parameters were performed in the same manner as in the preceding case. The only exception is that this excitation type allows no direct use of the zoom-subroutine of the computer code MODAMS. For that reason, the averaging of

the strongly scattering damping values obtained from individual frequency response functions had to be applied.

Fig. 10 shows the time history plots of the excitation impact force F(t), the corresponding acceleration response a(t) as well as real and imaginary parts of the corresponding frequency response function $H_{Fa}(f)$ illustrating the procedure. The excitation impulse was applied slightly above the reference position on the same generatrix (z = 850 mm, $\psi = 0^{o}$). The plots of the frequency response function illustrate that only several shell modes and no beam mode of the test cylinder could be excited at the given excitation position (absence of resonance peaks at 20.4, 25.8 and 31 Hz). However, the peaks obtained are much sharper than those presented in fig. 9. This indicates that a considerable suppression of leakage was obtained by this type of excitation.

As already mentioned above, the procedure I was used to identify the modes in the whole frequency interval of interest, ranging from 0 to 300 Hz in the case of the test cylinder partially filled with water and from 0 to 355 Hz in the case of the empty cylinder. Alternative procedures II, III and IV used to verify the results of procedure I were applied only in the case of the test cylinder partly filled with water; the corresponding frequency band was reduced to 0-100 Hz. The majority of the results obtained refer to measuring positions 1 through 47 described in paragraphs (a) and (b) at the beginning of section 2; the additional locations on the shell and on the flange were used only in several complementary experiments. All measuring chains were individually calibrated before and after each individual test series.

3. Experimental results

The characteristic features of 25 test series performed are summarized in table II. The columns of this table contain the consecutive number of the test series, the type of the experimental procedure used, the number of individual experiments made in each test series, the accelerometer positions, the coordinates (z, ψ and r) of the point of application of the excitation force (or of the reference accelerometer in case of experimental procedure IV), the direction of excitation force (h = horizontal, v = vertical) and, finally, the type of the fluid charge in the test cylinder

(w = water, a = air). The aim of the majority of the tests performed with the water charge in the test cylinder (tests No. 1, 6, 12, 13, 19, 21, 23, 23, 24, 25 and 26) was to compare the results obtained with each of the four experimental procedures discussed in the proceding section 2. The results obtained for the frequency range 0 - 100 Hz are discussed in section 3.1. The eigenfrequencies, mode shapes and critical damping ratios of the test cylinder shell which are necessary for the verification purposes mentioned in the Introduction, were investigated systematically in the broader frequency range. It extended from 0 to 300 Hz with the test cylinder partly filled with water (test series 6, 7, 12, 13, 16, 18, 19, 21, 23 and 24) and from 0 to 355 Hz in case of the empty test cylinder (test series 5, 8, 11, 14, 15, 17, 20 and 22). These systematic investigations were performed using the experimental procedure I, the results are presented in section 3.2. Several supplementary investigations were carried out on test cylinder flanges and on the non-linear effects observed when the experimental procedure II was applied. The results obtained are presented in section 3.3.

3.1 Comparison of results obtained with different experimental procedures

Typical results obtained with the four experimental procedures described above are represented graphically in figs. 11 through 14. Each of these figures consists of three diagrams. The lower one shows the development of the horizontal section through the shell mode of the first axial and third circumferential orders, identified on the vertical coordinate z = 1000 mm. The abscissa represents the periphery angle ψ of the test cylinder and the ordinate the normed modal amplitude a/a_{max}; symbol○,◇,□ or Δ designates the individual a/a_{max} - values representing the mode shape at the given circumferential position ψ. The upper and the middle diagrams illustrate the values of the natural frequency f and of the critical damping ratio ζ belonging to the given mode shape. For the experimental procedures I and II (figs. 11 and 12) the corresponding f- and ζ-values are represented by horizontal lines. This reflects the fact that the computer code EVA extracts for each mode only one value of the natural frequency and one value of the critical damping ratio, respectively, from the whole number of response signals / 5 /. For the experimental procedures III and IV

(figs. 13 and 14) based on the modal evaluation code MODAMS / 2 /, one f-estimate and one ζ-estimate are obtained from each response data set evaluated. This causes uncertainties due to the scatter of the individual estimates. In case of application of procedure III this scatter can be reduced a little using the zoom-subroutine of the MODAMS-code mentioned in section 2.3. However, the final choice of the "best" eigenvalue estimates must be done by the analyst himself relying on his personal experience and judgement capabilities. To exclude this subjectivism we have averaged all individual eigenvalue estimates obtained - the corresponding mean values are illustrated in fig. 13 by broken horizontal lines. With procedure IV the zoom subroutine is not immediately applicable. However, since the leakage is smaller than in case of procedure III, the scatter of the rough eigenvalue estimates is somewhat narrower (fig. 14).

Representative f- and ζ-estimates obtained in the frequency range 0 - 100 Hz with all four experimental procedures used are summarized in table III. The symbols μ and ν denote the axial and the circumferential orders, respectively, of the given mode; $\overline{f}$ is the mean value of all f-estimates obtained with different experimental procedures and Δ f denotes the maximum deviation from the mean value. The values $\overline{\zeta}$ and $\Delta\ \zeta$ are defined in a similar way. It follows from table III that three different versions of the fundamental beam mode (μ = 1, ν = 1) with slightly different eigenfrequencies (f = 20.42, 25.81 and 31.03 Hz) and critical damping ratios (ζ - 3.83, 1.90 and 1.93 %) have been extracted. The occurrence of this multiple mode (triplet) is most probably caused by the asymmetry of the test cylinder. However, only two procedures - namely II and III - proved to be capable of identifiying all three variantes of the fundamental beam mode triplet in the first attempt. In both cases the vibrational energy was delivered to the test cylinder via its upper flange which had been excited by an electromagnetic shaker. The direct excitation of the shell generally used in procedures I and IV presumably did not provide enough energy - see the upper diagram on the right side of fig. 6 and both diagrams on the right side of fig. 10. Therefore, no variant of the fundamental beam mode triplet was identified by procedure IV (the difficulties arising from the application of procedure IV in the experimental modal analysis of the mixed structures composed of extremely thin and extremely rigid components represent a

generally well known disadvantage of the method). The second mode of the triplet (f = 25.81 Hz) originally not identified by application of procedure I was identified by snapback excitation of the upper flange - see the lower diagram on the right side of fig. 6. The mutual deviations of the fundamental frequency estimates extracted by procedures I, II and III are relatively small - the scatter does not exceed the limits of $\pm$ 1.8 %. This favourable circumstance obviously does not hold in case of the critical damping ratios ξ whose scatter reaches the limits of $\pm$ 13.8 %. The remaining data in table III reveal the existence of six shell mode doublets, centered at approx. 55, 58, 63, 71, 80.3 and 93 Hz. The consistence of the corresponding eigenfrequency estimates is even better than in case of the fundamental beam mode triplet, $(\Delta f/\bar{f})_{max}$ = 0.4 %. By contrast, the scatter of the corresponding ζ-estimates is considerably larger and approaches the limits of $\pm$ 26.6 %.

The scatter of the eigenfrequencies extracted and their comparison with the corresponding theoretical estimates are illustrated graphically in fig. 15. The individual experimental estimates are denoted by the symbols ○, ◇, □ and Δ and plotted over the circumferential order v. The theoretical values precalculated with the computer code SING-S / 7 / are denoted by the symbol - • - . This diagram demonstrates that mutual deviations of eigenfrequency estimates extracted by individual experimental procedures are considerably smaller than the difference between majority of exp. values and the corresponding theoretical predictions. It is evident that the achieved precision of $\pm$ 1.8 % of eigenfrequency estimates extracted by all four experimental procedures used is fully sufficient for the given task.

The extract estimates of the critical damping ratios ζ are plotted over the circumferential order v in fig. 16. A considerable scatter of individual values can be observed, especially by small damping values. This phenomenon is due to two circumstances. One of them is the overwhelming numerical inferiority of the real part $\zeta_j \omega_j$ with respect to the imaginary part $\omega_j \sqrt{1 - \zeta^2_j}$ of the complex eigenvalue

$$\lambda_j = - \zeta_j \omega_j + i\omega_j \sqrt{1 - \zeta^2_j} \qquad (1)$$

extracted from the response signals. In case of extremely small damping

values (ζ_j <<1) this disproportion may lead to numerical difficulties contributing to scatter. Another phenomenon with similar consequences is the strong variability of structural damping caused by variable prestressing of mutually rubbing surfaces, such as flanges. This circumstance deteriorates the reproducibility of modal experiments, especially if individual measurements are performed on different days and at different ambient temperatures.

An inter-comparison of two mode shapes identified with all four experimental procedures used is presented in fig. 17. Both plots represent the development of the horizontal section through the shell modes of the first axial and third circumferential orders, measured on the vertical coordinate z = 1000 mm. The upper plot illustrates the 70.66 Hz-variant of the doublet, the lower plot the 72.11 Hz-variant. A relatively high scatter of individual points filling the band of approx. $\pm$ 30 % of the maximal value can be observed, but the mutual agreement between the individual global mode shapes is acceptable. Another interesting feature of fig. 17 is the occurrence of a distinct phase shift of approx. 23^{o} between the two mode shapes represented. One probable cause of this phenomenon is the presence of the square flanges of the test cylinder, the other the asymmetries produced during manufacturing of the test cylinder shell.

Apart from the scatter of individual points appearing in figures 15 through 17, a good consistency can be observed of the global modal characteristics extracted by all four experimental procedures used. Therefore, all four procedures can be considered as convenient to fulfill the task defined in the Introduction. Indisputable advantages of the relaxation technique in combination with the computer code EVA are the minimum time needed to perform the actual modal experiments and the high frequency resolution necessary to identify the multiple modes. Based on these advantages all remaining modal measurements on the test cylinder were performed with procedure I.

3.2 Review of extracted eigenfrequencies, mode shapes and critical damping ratios of the test cylinder

Ten test series were performed to identify 55 eigenmodes of the test cylinder partly filled with water; the corresponding points of load application

and the directions of the quasi-statical loading force applied to prestress the test cylinder shell in the desired manner are specified in table II. The point of application of the horizontal preloads was sometimes located directly on the shell (z_e = 800 or 1000 mm, $\psi_e = 0^o$) and sometimes on the upper flange (z_e = 1615 mm, $\psi_e = 0^o$). In several additional test series vertical preloading (z_e = 1600 mm, $\psi_e = 45^o$) was applied. The subsequent evaluation showed that a smaller number of tests would also be sufficient to obtain equivalent results. Two types of excitation proved to be particularly effective, namely horizontal preloading applied on the shell (z_e = 800 mm, $\psi_e = 0^o$) and on the upper flange (z_e = 1615 mm, $\psi_e = 0^o$). Typical response signals measured in these tests are presented as examples in the upper part of figs. 18 and 19. The real and the imaginary parts of the Fourier-transform of these signals are plotted versus the frequency f in the lower part of figs. 18 and 19. These plots illustrate the input data sets used by extraction subroutines of the computer code EVA.

The modal characteristies of all 55 eigenmodes identified in the frequency range 0-300 Hz are summarized in table IV. The quantities f, ζ, μ and ν correspond to those already discussed in section 3.1 (table III). The correlation coefficient γ^2_ν given in the sixth column of table IV quantifies the degree of consitency of the circumferential mode shape extracted and of an ideal circumferential cosine wave of the order ν generally obtained in the theoretical solution of the given eigenvalue problem. The congruence of both would yield the value $\gamma^2_\nu = 1$. The majority of modes extracted exhibit the γ^2_ν-values greater than 90 % which indicates good consistency. The phase angle $\psi_{\nu o}$ describes the orientation of the extracted mode shape with respect to origin $\psi = 0$ of the coordinate system used (see fig. 4). The computational procedures used to calculate the quantities γ^2_ν and $\psi_{\nu o}$ are described in the report / 5 /.

The mode shapes of all 55 eigenmodes extracted are illustrated in figs. 20 through 29, presenting one vertical and one horizontal section through the three-dimensional mode shape of each mode. The mode shapes of both types were generally measured in two different experiments, imposed by the restricted number of measuring chains available (see section 2). They are therefore not normed with respect to the amplitude and may reveal opposed polarities. The plots on the left side of each figure represent the axial

mode shapes, measured by accelerometers installed on a constant azimuthal coordinate $\psi = 0^{o}$ and at different height positions z. The plots on the right represent the circumferential mode shapes, measured at a constant height z = 1000 mm and different azimuthal positions ψ. The dashed lines are the auxiliary cosine wave formes calculated with the subroutine MODPLT / 5 /. Diagrams in the first three rows of fig. 20 illustrate three different variants (triplet) of the fundamental beam mode. Mode (1) has the natural frequency f_1 = 20. 75 Hz, the critical damping ratio ζ_1 = 3.3 % and the phase angle $\psi_{vo} = 3^{o}$; the corresponding values of the mode (2) or (3) equal 25.4 or 30.4 Hz, 2.1 or 1.9 % and 45 or - 47,5 ^{o}, respectively. Modes (4) and (5) constitute a shell mode doublet of first axial order and fifth circumferential order. Other doublets are represented for example by the mode pairs (6) and (7) , (8) and (9) or (10) and (11) . With few exceptions (e.g. mode (18) with μ = 2 and ν = 6) nearly every mode was identified in two slightly different variants.

The extracted natural frequency values are compared with the corresponding theoretical values calculated with the computer mode SING-S / 7 / in fig. 30. The calculated natural frequencies are designated by the symbol - • -, the extracted ones by the symbol ◯. The calculated eigenfrequencies of the modes of lower circumferential orders are a little bit higher than the extracted values, indicating the overestimation of the stiffness of the test cylinder flanges. This phenomenon will be discussed once more in the following section. The calculated eigenfrequencies of the higher circumferential order modes are generally underestimated, indicating the overestimation of the virtual modal masses of the coupled fluid. This trend increases with increasing axial order of individual modes.

Critical damping ratios of extracted modes are plotted versus the circumferential order ν in figs. 31 and 32. The majority of them are smaller than 0.2 %. Only three values are greater than 1 %; all of them belong to individual variants of the fundamental beam mode triplet. This indicates the increased contribution to the total energy dissipation of structural damping caused by mutual friction of test cylinder flanges or in the clamping. Similar phenomena were observed also in case of the HDR-core barrel mockup /5, 6/.

To facilitate the quality assessment of the system identification performed, the computer EVA offers the possibility to reconstruct the original input signals, based on the knowledge of the modal parameters f, ζ, C_{rn} and ψ_o (Subroutine REKON / 5 /). A comparison of the original with the reconstructed input signal is given as example in fig. 33. All diagrams refer to the accelerometer position 11 (z = 1000 mm, $\psi = 0^o$); the corresponding snapback excitation was performed 200 mm below (z = 800 mm, $\psi = 0^o$). The diagram on the left of the first row shows the original filtered signal x (t) used for the analysis , the diagram on the right shows the modulus $|\hat{x}(f)|$ of the corresponding Fourier transform. The diagrams in the second row illustrate the reconstructed signal, calculated from the extracted modal parameters by means of the subroutine REKON. The mutual consistence is very good, indicating that all modes making significant contribution to the measured response were correctly identified.

Eight test series in total with four types of snapback excitation were performed to identify 38 eigenmodes of the empty test cylinder in the frequency range 0-355 Hz. The corresponding modal characteristies are summarized in table V. The mode shapes of all 38 eigenmodes extracted are documented in figs. 34 through 40. Comparison of these mode shapes with those documented in figs. 20 through 29 reveals that the majority of them can be found in both sets. However, some of them - for instance the variants (2) and (3) of the fundamental beam mode triplet (fig. 20) or the shell mode of first axial and second circumferential order (mode (2) in fig. 34) can be found in only one set which is an indication of the incompleteness of the eigenmode sets extracted. It is assumed that a denser network of accelerometers on the test cylinder shell is necesswary to obtain the complete sets.

The extracted natural frequencies of the empty test cylinder are compared with the corresponding theoretical values calculated with the computer code ICES-STRUDL / 9 / in fig. 41. The general trend observable here is similar to that in fig. 30 with exception of the coupled fluid phenomena (see discussion of fig. 30). The occurence of additional experimental values at $\nu = 2$ is discussed in the next section. Critical damping ratios ζ of extracted modes are plotted versus the circumferential order ν in figs. 42 and 43. The general trends observable here are again similar to those

observable in figs. 31 and 32. A comparison of the original with the reconstructed response signal calculated with the subroutine REKON is presented in fig. 44. There are nearly no differences observed which suggests that all modes considerably contributing to the test cylinder response were correctly identified.

3.3 Complementary investigations

Three natural frequency values are given in fig. 41, namely 106.43, 189.44 and 221.75 Hz, which clearly disagree with the represented, f-v-pattern, typical of the eigenfrequencies of the cylindrical shells. A complementary series of modal experiments (nos. 2 through 4 in table II) performed with procedure III (based on random excitation of the upper flange in the vertical direction) were carried out to clarify these discrepancies. They revealed a predominant influence of the upper flange on the generation of these particular modes. One typical result of this complementary test series is presented as an example in fig. 45. This figure illustrates the mode shape of the 107.5 Hz mode. The vertical and the horizontal sections through the three-dimensional mode shape, plotted in the lower part of fig. 45, are similar to the mode shape of first axial and second circumferential orders plotted in fig. 34 (mode (2)). The upper part of fig. 45 illustrates the mode shape of the upper flange, revealing displacement maxima at least twice as large as those on the shell. Taking into account the different thicknesses of the corresponding components (thickness of the upper flange/thickness of the test cylinder shell = 20/1), it can be concluded that the given mode shape was generated as a proper mode shape of the upper flange which induced a quasi-forced mode shape of first axial and second circumferential orders of the cylindrical shell. Similar results were obtained from the complementary modal investigations of the remaining two modes mentioned above.

Another similar phenomenon worth mentioning here is the considerable influence of the compliance of the clamping of the test cylinder base on the natural frequency value of the fundamental mode. An additional investigation performed in this field revealed that 36 very rigid clamping claws, used to fix the test cylindder base flange to the mounting plate in our experiments (see fig. 2), were not sufficient to simulate a quasi-rigid

fixing as postulated in the modal calculations. Consequently, both experimental fundamental frequencies are considerably lower than the corresponding calculated values (see figs. 15 or 30 and 41). In contrast to these results, distinctly higher natural frequency values of the fundamental beam mode of the test calinder were measured in the preliminary test series described in / 9 /. In this particular test series the base flange of the test cylinder was embedded in a concrete foundation plate of the experimental hall which resulted in the fundamental frequency of the empty test cylinder being equal to approx. 50 Hz. In case of the test cylinder partly filled with water, the fundamental frequency value of 45.5 Hz was obtained. However, this influence of base flange clamping rapidly decreases with increasing axial and circumferential orders of the shell modes.

The second part of complementary investigations was devoted to non-linear phenomena observed by application of experimental procedure II in the test series no. 25. The harmonic excitation of the upper flange applied in this test series caused a substantially higher acceleration response of the test cylinder shell than application of the remaining excitation techniques. However, despite excellent signal/noise ratios achieved, a considerable scatter of eigenfrequencies and critical damping ratios had been observed. An additional analysis of extraordinarily long portions of the response signals yielded a splitting of the corresponding eigenfrequency and critical damping ratio into two or three distinct values, depending on the length of the signal sample evaluated. The mode shapes, associated with individual eigenvalue pairs, were identical. This result contradicts theoretical expectations based on linear models. To explain this contradiction, the occurrence of non-linear phenomena was postulated and a systematic analysis was performed of the response signals, divided into several, very short-time intervals. Typical results obtained are presented in figs. 46 and 47. Figure 46 shows as an example the natural frequency value of the shell mode of first axial and seventh circumferential orders, extracted in each short time interval, plotted versus an initial acceleration reference value $C_{4,\ 13}$ (the first subscript denotes the accelerometer position, the second the mode number - see / 5 /). Figure 47 presents the critical damping ratios, extracted in the same time intervals. Both diagrams reveal considerable scatter which is due to the reduced size of the data samples evaluated. However, the trend to decrease of the natural frequency values

plotted in fig. 46 is incontestable, suggesting the appearance of a slight nonlinearity. To verify the possibility of the extraction of the split f - and ζ-values in such a case, a trial evaluation of several artificial signals was performed. These signals were constructed in accordance with equation

$$x_r(t) = C_{r,13} \exp(-\zeta_{13} 2\pi f_{13} t) \cos 2\pi \left[f_{13} - q \exp(-\zeta_{13} \pi f_{13} t) \right] t, \quad (2)$$

comprising the increase of natural frequency with the decreasing vibration level (r denotes different accelerometer positions). Evaluation of a 2 sec long data sample of this type yielded two natural frequency values, f_{13} = 80.817 and 80.873 Hz, and two corresponding critical damping ratios, ζ_{13} = 1.286 and 0.311 %. Similarly, evaluation of a 5 sec long portion of the same data sample yielded three natural frequency values, f_{13} = 80.828, 80.881 and 80.885 Hz, and three critical damping ratios, ζ = 1.940, 0.459 and 1.1155 %. These results confirm the hypothesis postulated above.

4. Concluding remarks

The comparative modal survey described in section 3.1 revealed good consistency of the modal data extracted by all four experimenal procedures used. A tentative application of the modified relaxation procedure involving a preselected excitation frequency and a very high initial vibration level yielded a perceptible decrease with increasing amplitude of the natural frequencies of the test cylinder. Evaluation of the corresponding relaxation signals with the EVA computer code furnished a set of multiple modes with multiple natural frequencies and critical damping ratios and identical mode shapes. This phenomenon offers a possibility to discover the slight nonlinearities of the tested structure. Indisputable advantages of the relaxation technique in combination with the EVA computer code are the minimum test requirements regarding duration and vibrational excitation as well as the high resolution capability necessary to separate and identify the multiple modes frequently occuring in case of the shell structures.

A comparison of the calculated and extracted natural frequencies of the test cylinder yielded a very good mutual agreement in the case of the shell modes of first and second axial orders and 3rd through 7th circumferential orders. With increasing axial and circumferential orders, systematic deviations between calculated and extracted eigenfrequencies have been observed in case of the test cylinder partly filled with water. Max. deviation of approx. 14 % exhibit the shell modes of 12th circumferential order, which was the highest circumferential order examined in our experiments. The natural frequency values of the fundamental beam mode of the test cylinder exhibit still greater deviations. However, it was stated that this disagreement was primarily caused by an insufficient experimental simulation of the quasi-rigid fixation of the base plate of the test cylinder, postulated in the modal calculations. The critical damping ratios of the shell modes extracted were generally of the order of several per mills and did not attain 1 %. Only the fundamental beam mode revealed the ζ-values within the range of 1.9 - 3.3 %.

References

/1/ Beátrix, Ch.: Experimental Determinaton of the Vibratory Characteristics of Structures.
ONERA Technical Note No. 212E, Chatillon, 1974

/2/ Peterson, E.L., Klosterman, A.L.: Obtaining good results from an experimental modal survey. Journal of the Society of Environmental Engineers, March 1978, 17-1, p. 3-10

/3/ Vold, H., Kundrat, J., Rocklin, G.T., Russel, R.: A Multi-Input Modal Estimation Algorithm for Mini-Computers. SAE Int. Congress & Exposition, Detroit, Michigan, February 22-26, 1982, Paper No. 820194

/4/ Lang, G.F.: Understanding Vibration Measurements, Sound and Vibration, 1976, 29,3, 26-37

/5/ Eberle, F., Kadlec, J.: Extraction of Eigenfrequencies, Mode Shapes and Critical Damping Ratios of HDR Core Barrel Mockup from Step Relaxation Response Signals Measured in the Snapback Test Series V59, KfK 3408, Kernforschungszentrum Karlsruhe, Oct. 1982

/6/ Eberle, F., Kadlec, J: Experimental modal analysis of the HDR core barrel. Transactions Seventh Int. Conf. on Structural Mechanics in Reactor Technology, Chicago 22-26 Aug. 1983, Paper B7/4

/7/ Krieg, R., Göller, B., Hailfinger, G.: Transient, three-dimensional potential flow problems and dynamic response of surrounding structures. Part II: Simultaneous coupling between fluid and structural dynamics (computer code SING-S). Journal of computational Physics 34, 164-183, 1980

/8/ Rittirsch, G.: Dezentrales gekoppeltes Mehrrechnersystem zur breitbandigen Meßdatenerfassung und Auswertung. KfK-Nachrichten 1-2, Kernforschungszentrum Karlsruhe, 1980

/9/ Eberle, F., Göller, B., Hailfinger, G., Kadlec, J.: Eigenoscillations of a fluid filled cylindrical shell - comparison between theoretical and experimental results. Transactions Sixth Int. Conf. on Structural Mechanics in Reactor Technology, Paris 17 - 21 Aug. 1981, Paper B5/4

List of tables

List of figures

Fig. 11: Typical modal characteristics obtained by application of experimental procedure I (Snapback excitation + computer code EVA).

Fig. 12: Typical modal characteristics obtained by application of experimental procedure II (transient sine-wave excitation + computer code EVA).

Fig. 13: Typical modal characteristics obtained by application of experimental procedure III (stationary random excitation + computer code MODAMS).

Fig. 14: Typical modal characteristics obtained by application of experimental procedure IV (impulse excitation + computer code MODAMS).

Fig. 15: Calculated and extracted natural frequency values of the test cylinder partly filled with water. Comparison of results obtained by application of four different experimental procedures.

Fig. 16: Critical damping ratios extracted. Comparison of results obtained by application of four different experimental procedures.

Fig. 17: Comparison of two typical mode shapes identified by four different experimental procedures.

Fig. 18: Typical time history and Fourier-transform of the measured acceleration response (test cylinder partly filled with water, excitation location z_e = 800 mm, $\psi_e = 0^o$; accelerometer position z_a = 1000 mm, $\psi_a = 0^o$).

Fig. 19: Typical time history and Fourier-transform of the measured acceleration response (test cylinder partly filled with water, excitation location z_e = 1615 mm, $\psi_e = 0^o$; accelerometer position z_a = 1000 mm, $\psi_a^e = 0^o$).

Fig. 20: Extracted mode shapes of the test cylinder partly filled with water.

Figs. 21 - through 29: Extracted mode shapes of the test cylinder partly filled with water (cont.).

Fig. 30: Comparison of the calculated and measured natural frequencies of the test cylinder partly filled with water.

Fig. 31: Critical damping ratio ξ of extracted modes of the test cylinder partly filled with water (μ = 1).

Fig. 32: Critical damping ratio ξ of extracted modes of the test cylinder partly filled with water (μ = 2,3 and 4).

Fig. 33: Comparison of the original input signal with the reconstructed input signal (test cylinder partly filled with water, excitation location z_e= 800 mm, ψ_e = 0°; accelerometer position z_a= 1000 mm, ψ_a = 0°).

Fig. 34: Extracted mode shapes of empty test cylinder.

Fig. 35 through 40: Extracted mode shapes of empty test cylinder (cont.).

Fig. 41: Comparison of the calculated and measured natural frequencies of the empty test cylinder.

Fig. 42: Critical damping ratio ξ of extracted modes of the empty test cylinder (μ = 1).

Fig. 43: Critical damping ratio ξ of extracted modes of the empty test cylinder (μ = 2,3 and 4).

Fig. 44: Comparison of the original input signal with the reconstructed input signal (test cylinder empty, excitation location z_e= 800 mm, ψ_e = 0°; accelerometer position z_a= 1000 mm, ψ_a = 0°).

Fig. 45: Mode shape f_2 = 107.5 Hz

Fig. 46: Decrease of eigenfrequency f_{13} with increasing initial value of acceleration $C_{4,\,13}$

Fig. 47: Variation of critical damping ratio ξ_{13} with increasing initial value of acceleration $C_{4,\,13}$

Position No.	z [mm]	ψ [grad]	r [mm]	measurement direction v=vertical h=horizontal	Position No.	z [mm]	ψ [grad]	r [mm]	measurement direction v=vertical h=horizontal	Position No.	z [mm]	ψ [grad]	r [mm]	measurement direction v=vertical h=horizontal
1	20	360	503	h	28	1000	60	503	h	55	1740	135	560	v
2	100	360	503	h	29	1000	48	503	h	56	1660	135	865	v
3	200	360	503	h	30	1000	36	503	h	57	1660	180	508	v
4	300	360	503	h	31	1000	24	503	h	58	1660	180	620	v
5	400	360	503	h	32	1000	12	503	h	59	1740	225	560	v
6	500	360	503	h	33	1000	360	503	h	60	1660	225	865	v
7	600	360	503	h	34	1000	348	503	h	61	1660	270	508	v
8	700	360	503	h	35	1000	336	503	h	62	1660	270	620	v
9	800	360	503	h	36	1000	324	503	h	63	1740	315	560	h
10	900	360	503	h	37	1000	312	503	h	64	1660	315	865	h
11	1000	360	503	h	38	1000	300	503	h	65	20	225	503	h
12	1100	360	503	h	39	1000	288	503	h	66	100	225	503	h
13	1200	360	503	h	40	1000	276	503	h	67	200	225	503	h
14	1300	360	503	h	41	1000	264	503	h	68	300	225	503	h
15	1400	360	503	h	42	1000	252	503	h	69	400	225	503	h
16	1500	360	503	h	43	1000	240	503	h	70	500	225	503	h
17	1570	360	503	h	44	1000	228	503	h	71	600	225	503	h
18	1000	180	503	h	45	1000	216	503	h	72	700	225	503	h
19	1000	168	503	h	46	1000	204	503	h	73	800	225	503	h
20	1000	156	503	h	47	1000	192	503	h	74	900	225	503	h
21	1000	144	503	h	48	1000	180	503	h	75	1000	225	503	h
22	1000	132	503	h	49	1660	360	508	v	76	1100	225	503	h
23	1000	120	503	h	50	1660	360	620	v	77	1200	225	503	h
24	1000	108	503	h	51	1740	45	560	v	78	1300	225	503	h
25	1000	96	503	h	52	1660	45	865	v	79	1400	225	503	h
26	1000	84	503	h	53	1660	90	508	v	80	1500	225	503	h
27	1000	72	503	h	54	1660	90	620	v	81	1570	225	503	h

KfK IRE

Table I : Accelerometer locations

Test No.	Procedure	Number of measurements	Measuring locations used	Location and direction of excitation force				Medium
				z [mm]	ψ [grad]	r [mm]	v≡vertical h≡horizontal	w≡water a≡air
1	III	48	1-48	1600	45	875	v	w
2	III	17	65-81	1600	45	875	v	a
3	III	31	18-48	1600	45	875	v	a
4	III	16	49-64	1600	45	875	v	a
5	I	6	1-17 and 20,22,24,26,28,30,32,35 37,39,40,42,44,46,47,48	1000	0	503	h	a
6	I	6		1000	0	503	h	w
7	I	9		800	0	503	h	w
8	I	6		800	0	503	h	a
9	I	3	1-17	800	0	503	h	w+50mm
10	IV	48	11(33)	Locations 1-48		503	h	w
11	I	3	20,22,24,26,28,30,32,35	1600	45	875	v	a
12	I	3	37,39,40,42,44,46,47,48	1600	45	875	v	w
13	I	3	1-17	1600	45	875	v	w
14	I	3	1-17	1600	45	875	v	a
15	I	3	49-64	1600	45	875	v	a
16	I	3	49-64	1600	45	875	v	w
17	I	3	49-64	1615	0	625	h	a
18	I	3	49-64	1615	0	625	h	w
19	I	3	1-17	1615	0	625	h	w
20	I	3	1-17	1615	0	625	h	a
21	I	3	20,22,24,26,28,30,32,35	1615	0	625	h	w
22	I	3	37,39,40,42,44,46,47,48	1615	0	625	h	a
23	I	3	1-17	1615	0	625	h	w
24	I	3	20,22,24,26,28,30,32,35	1615	0	625	h	w
25	II	12	37,39,40,42,44,46,47,48	1615	0	625	h	w
26	III	5	9,11,18,27	1615	0	625	h	w

KfK

Table II : Test matrix

		Natural frequencies f extracted with all four experimental procedures						Critical damping ratio ζ extracted with all four experimental procedures					
μ	v	I (Hz)	II (Hz)	III (Hz)	IV (Hz)	f (Hz)	Δ f/f (%)	I (%)	II (%)	III (%)	IV (%)	ζ (%)	Δ ζ/ζ (%)
1	1	20.75	20.3	21.2	-	20.42	1.6	3.3	4.2	4.0	-	3.83	13.8
1	1	-	26.23	25.4	-	25.81	1.6	-	2.1	-	-	1.90	10.5
1	1	30.40	31.58	31.1	-	31.03	1.8	1.9	2.1	1.8	-	1.93	8.8
1	5	54.26	54.34	54.42	54.50	54.38	0.22	0.52	0.50	0.50	0.56	0.52	7.7
1	5	55.20	55.20	55.25	55.20	55.21	0.07	0.11	0.10	0.12	0.13	0.115	13.0
1	4	57.67	57.75	57.80		57.74	0.12	0.22	0.24	0.23	-	0.23	4.3
1	4	58.21	58.26	58.34	58.50	58.32	0.31	0.16	0.13	0.14	0.14	0.143	11.9
1	6	62.52	62.67	62.70	62.70	62.65	0.21	0.55	0.54	0.54	0.58	0.553	4.9
1	6	63.18	63.22	63.41	63.50	63.32	0.28	0.045	0.069	0.071	0.06	0.0613	26.6
1	3	70.56	70.70	70.76	70.63	70.66	0.14	0.09	0.086	0.090	0.087	0.0883	2.0
1	3	71.89	72.23	72.31	72.00	72.11	0.28	0.14	0.14	0.125	0.13	0.134	6.5
1	7	80.26	80.33	80.36	80.31	80.32	0.08	0.29	0.29	0.27	0.29	0.285	5.3
1	7	80.81	80.83	80.91	80.90	80.86	0.06	0.045	0.045	0.062	0.07	0.0555	26.2
1	2	90.05	90.75	90.73	90.10	90.41	0.40	0.31	0.33	0.27	0.4	0.327	22.2
1	2	96.07	96.20	96.34	96.10	96.18	0.17	0.11	0.145	0.18	0.15	0.146	24.8

Table III Review of natural frequencies and critical damping ratios of the test cylinder, extracted with all four experimental procedures used (test cylinder partly filled with water)

Mode No.	f (Hz)	ζ (%)	μ	ν	γ^2_ν (%)	Ψ (grad)
1	20.75	3.3	1	1	93.9	3.0
2	26.29	2.1	1	1	96.6	45.0
3	30.40	1.9	1	1	95.5	-47.5
4	54.26	0.52	1	5	92.2	10.0
5	55.20	0.11	1	5	96.2	-8.6
6	57.67	0.22	1	4	91.6	14.1
7	58.21	0.16	1	4	95.6	-6.6
8	62.52	0.55	1	6	92.0	1.5
9	63.18	0.045	1	6	96.6	13.1
10	70.56	0.09	1	3	91.7	25.3
11	71.89	0.14	1	3	96.5	0.2
12	80.26	0.29	1	7	93.5	-3.1
13	80.81	0.045	1	7	98.9	9.9
14	90.05	0.31	1	2	80.8	45.1
15	96.07	0.11	1	2	92.1	2.5
16	105.80	0.045	1	8	86.7	11.1
17	106.19	0.083	1	8	94.8	-2.5
18	110.62	0.13	2	6	91.5	15.3
19	112.89	0.31	2	7	94.3	15.3
20	113.64	0.078	2	7	93.2	-2.9
21	121.63	0.18	2	5	89.6	9.1
22	123.25	0.32	2	5	94.4	9.7
23	127.99	0.081	2	8	93.3	-9.8
24	128.37	0.045	2	8	96.2	4.2
25	136.44	0.118	1	9	94.9	-7.8
26	136.95	0.028	1	9	98.6	2.1
27	147.02	0.080	2	4	65.8	16.5
28	149.28	0.30	2	4	69.0	-4.6
29	153.40	0.040	2	9	95.7	0.5
30	154.02	0.042	2	9	87.7	-8.7
31	172.33	0.055	1	10	97.4	6.2
32	173.47	0.028	1	10	95.2	-3.0
33	174.70	0.052	3	8	88.5	17.5
34	186.38	0.057	2	10	87.9	-5.3
35	186.93	0.034	2	10	97.2	1.5
36	190.53	0.057	2	3	72.0	-26.2
37	190.96	0.042	3	9	58.9	1.4
38	193.46	0.086	2	3	86.3	-3.0
39	211.98	0.036	3	10	94.0	-5.2
40	213.14	0.047	3	10	74.5	3.9
41	215.23	0.033	1	11	98.2	13.6
42	226.65	0.036	2	11	98.5	-7.0
43	227.07	0.038	2	11	96.9	0.7
44	239.53	0.045	4	8	90.0	17.7
45	244.13	0.095	4	9	88.7	13.4
46	250.27	0.048	3	11	90.7	-15.1
47	250.77	0.037	4	7	84.5	-8.3
48	258.46	0.035	4	10	90.6	-7.9
49	261.85	0.045	1	12	93.6	-0.5
50	263.38	0.134	1	12	88.3	7.3
51	271.49	0.082	2	12	97.3	0.1
52	273.06	0.039	2	12	96.5	7.8
53	279.75	0.126	4	6	75.5	-4.3
54	286.65	0.058	4	11	85.9	5.6
55	292.51	0.166	3	12	96.5	0.4

Table IV: Extracted modal characteristics of test cylinder partly filled with water

Mode No.	f [Hz]	ζ [%]	μ	ν	γ_ν^2 [%]	Ψ [grad]
1	32.10	n.i.	1	1	64.6	89.2
2	106.43	0.84	1	2	68.7	46.0
3	116.05	0.11	1	5	98.0	9.8
4	117.23	0.21	1	5	98.6	-9.6
5	125.92	0.105	1	6	96.7	5.8
6	126.45	0.095	1	6	98.8	-9.5
7	132.24	0.36	1	4	94.6	19.8
8	134.14	0.87	1	4	91.8	-8.5
9	153.20	0.043	1	7	98.0	-3.8
10	153.70	0.036	1	7	99.1	9.9
11	178.06	0.32	1	3	94.6	-25.0
12	181.41	0.60	1	3	96.7	5.7
13	189.44	0.84	1	2	63.5	-1.5
14	193.12	0.036	1	8	96.9	-1.0
15	209.75	0.061	2	7	97.8	-3.8
16	211.00	0.13	2	7	98.7	-11.7
17	215.20	0.065	2	6	95.4	3.0
18	216.77	0.071	2	6	98.4	-13.8
19	221.75	0.48	2	2	84.8	42.5
20	228.26	0.037	2	8	97.6	4.9
21	229.20	0.048	2	8	98.6	-7.0
22	240.61	0.02	1	9	99.0	6.1
23	240.74	0.023	2	9	99.3	-3.8
24	249.27	0.087	2	5	90.5	10.4
25	252.64	0.032	2	5	84.7	-10.5
26	264.16	0.032	2	9	98.3	1.4
27	265.42	0.041	2	9	97.3	8.8
28	295.05	0.022	1	10	99.2	5.7
29	295.53	0.018	1	10	99.3	-3.5
30	297.27	0.075	3	8	58.0	4.5
31	301.30	0.046	3	8	78.3	-7.1
32	311.59	0.14	2	10	91.3	-7.1
33	313.08	0.070	2	10	91.1	0.9
34	317.37	0.046	3	9	90.4	-8.4
35	321.37	0.29	2	4	87.1	-2.0
36	347.05	0.097	3	6	73.3	2.7
37	351.67	0.031	3	10	74.6	5.0
38	353.91	0.091	3	6	64.7	-9.1

Table V: Extracted modal characteristics of empty test cylinder
(n.i. ≡ not identified in this test series)

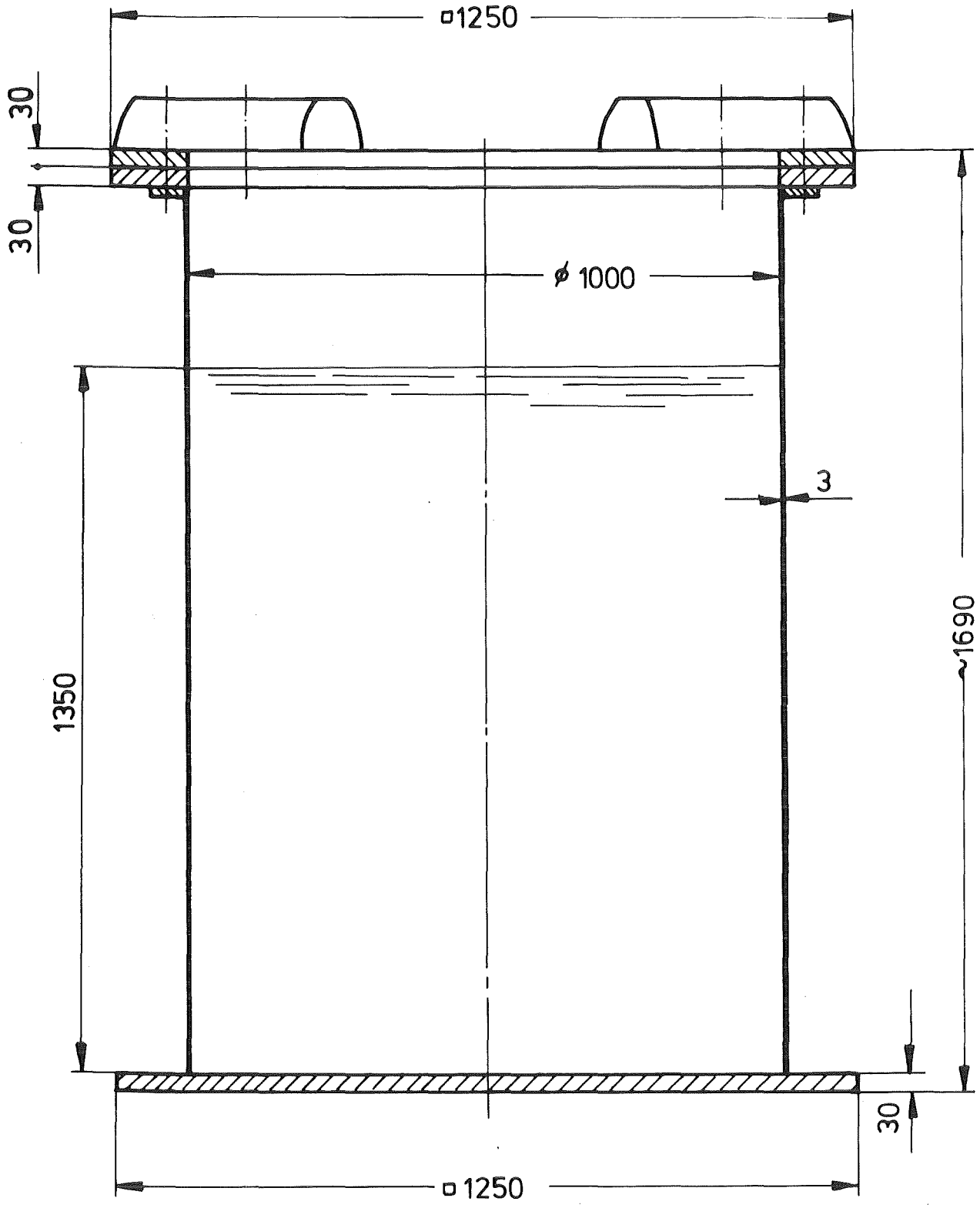

KfK IRE

Fig. 1: Test cylinder

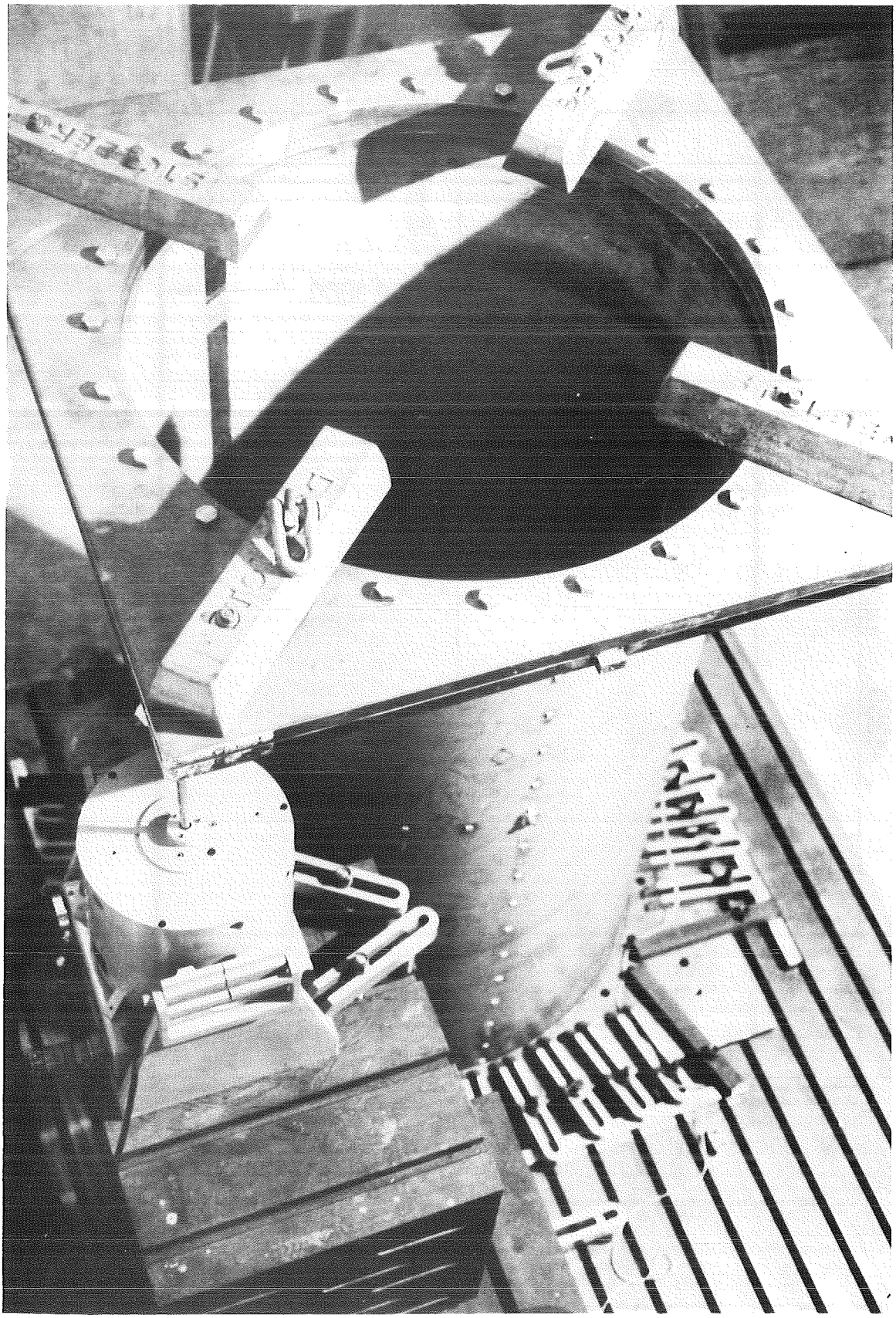

Fig. 2: Test bench

Procedure I : snapback excitation + computer code EVA
Procedure II : transient sine-wave excitation + computer code EVA
Procedure III : stationary random excitation + computer code MODAMS
Procedure IV : impulse excitation + computer code MODAMS

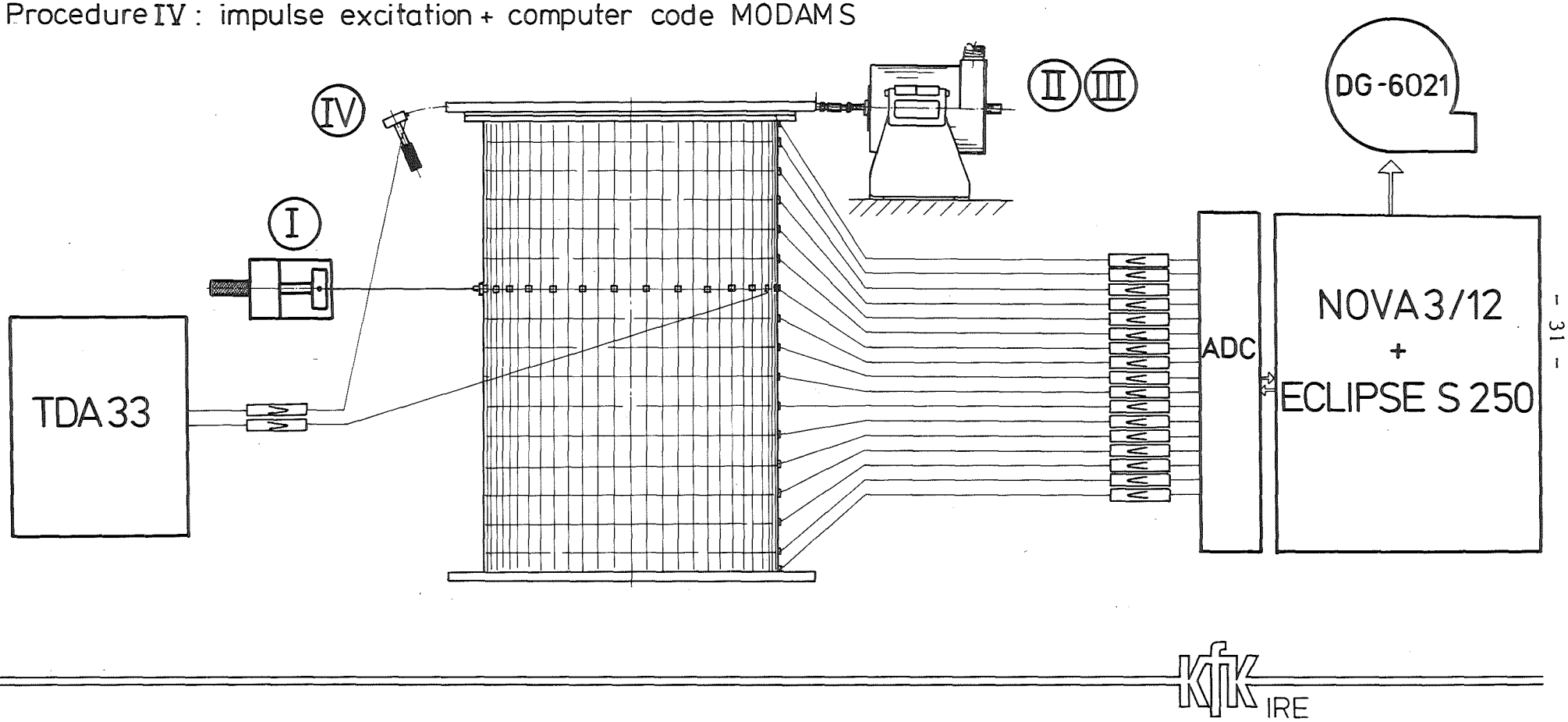

Fig.3 : Experimental setup

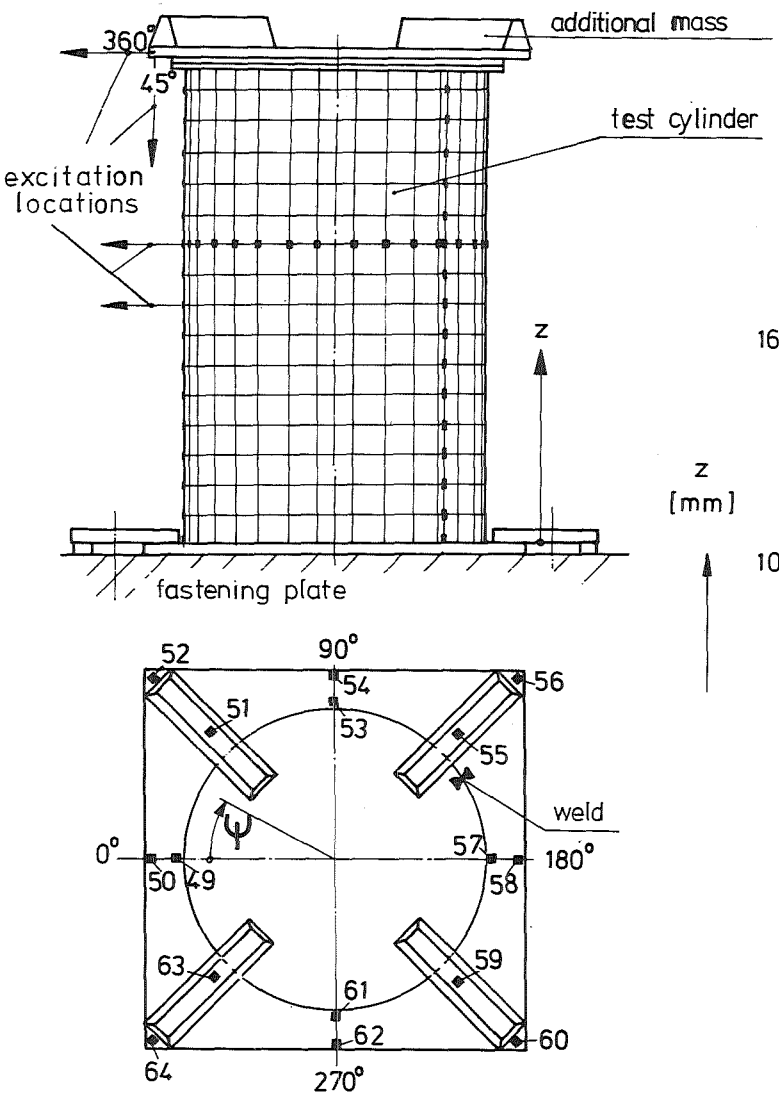

development of the cylinder surface

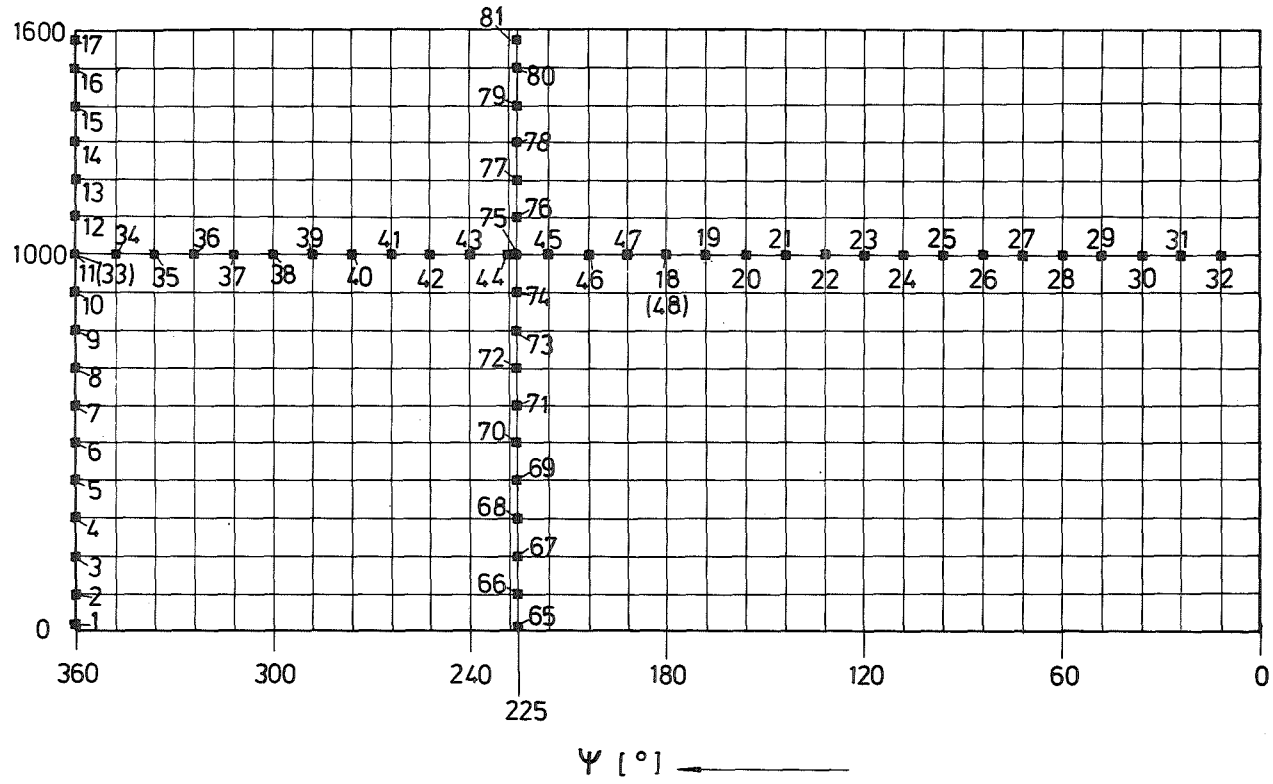

KfK IRE

Fig. 4: Plan of measuring and excitation locations on the test cylinder

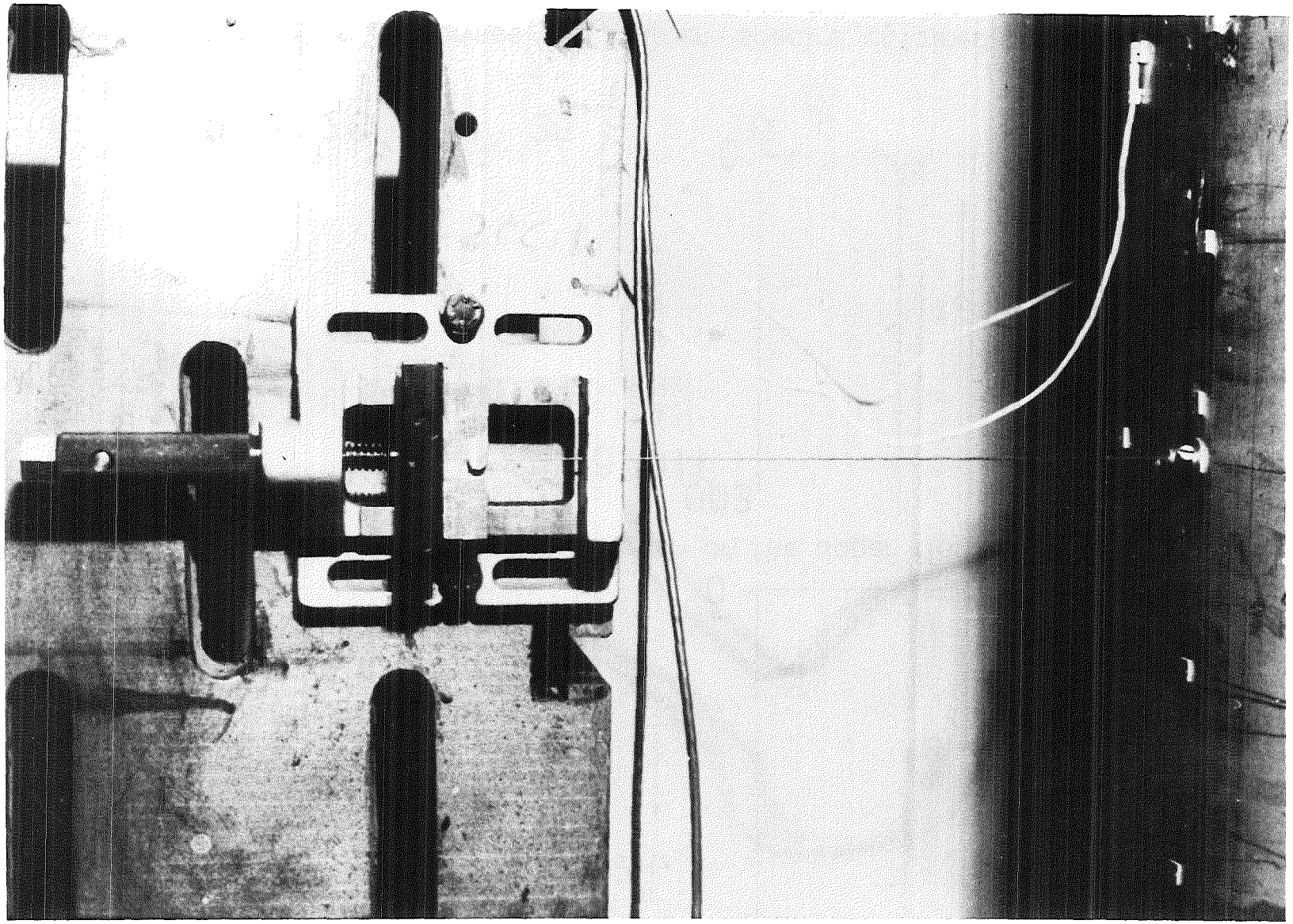

KfK IRE

Fig.5: Snapback device

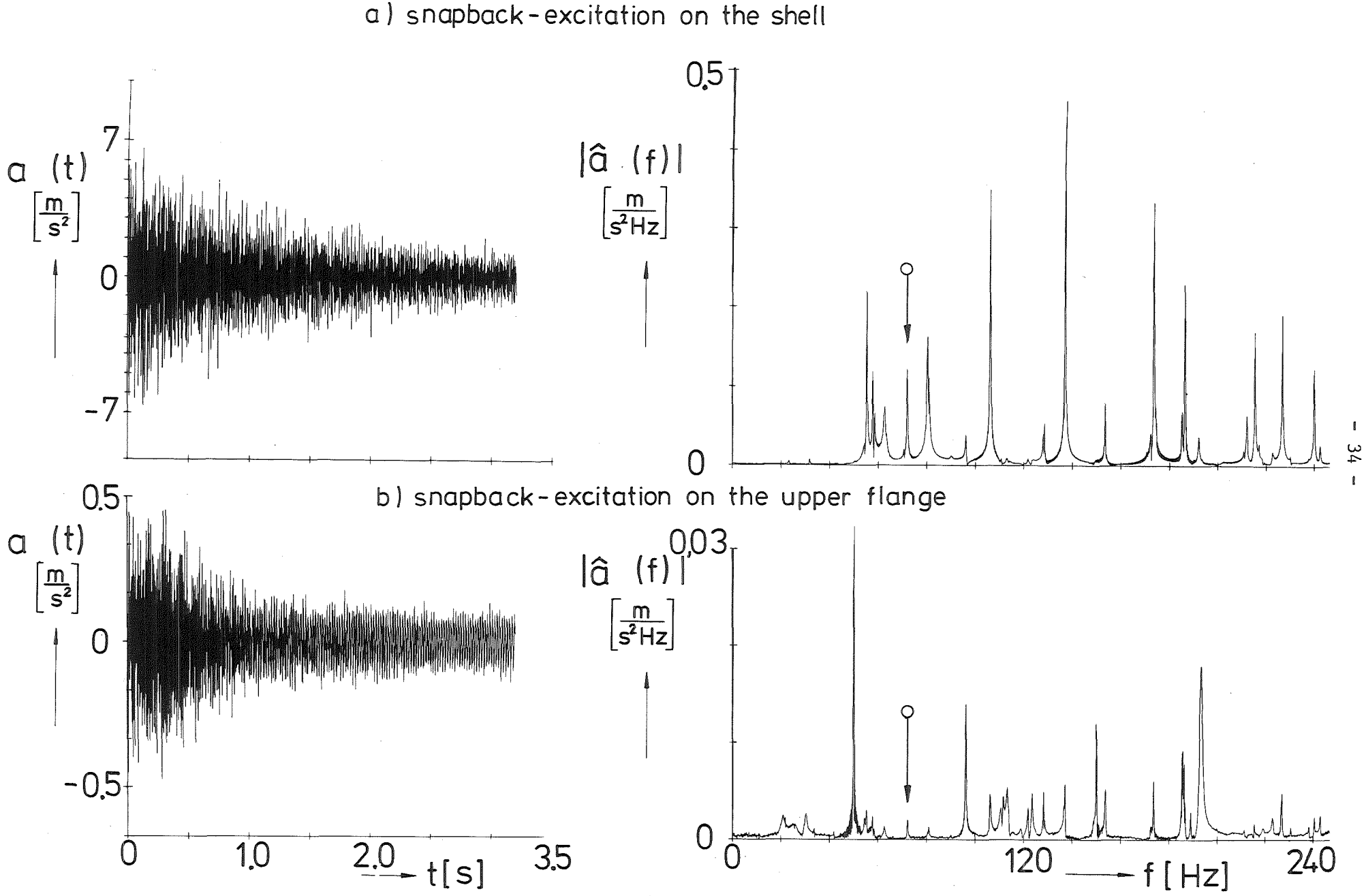

Fig. 6 : Typical acceleration responses and Fourier-spectra obtained by snapback excitation (procedure I)

KfK IRE

Fig. 7: Shaker excitation

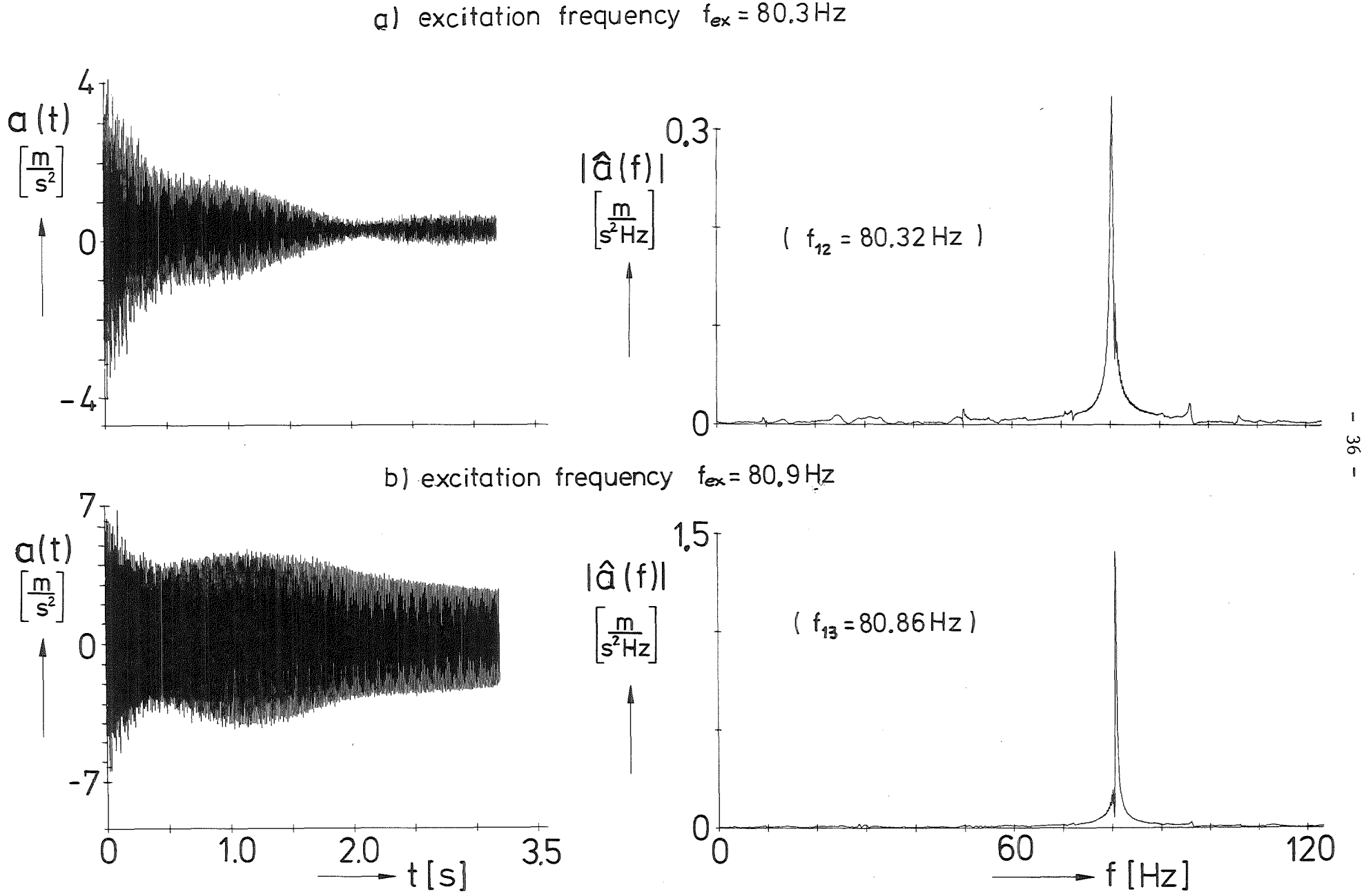

Fig. 8 : Typical acceleration responses and Fourier-spectra obtained by transient sine-wave excitation (procedure II)

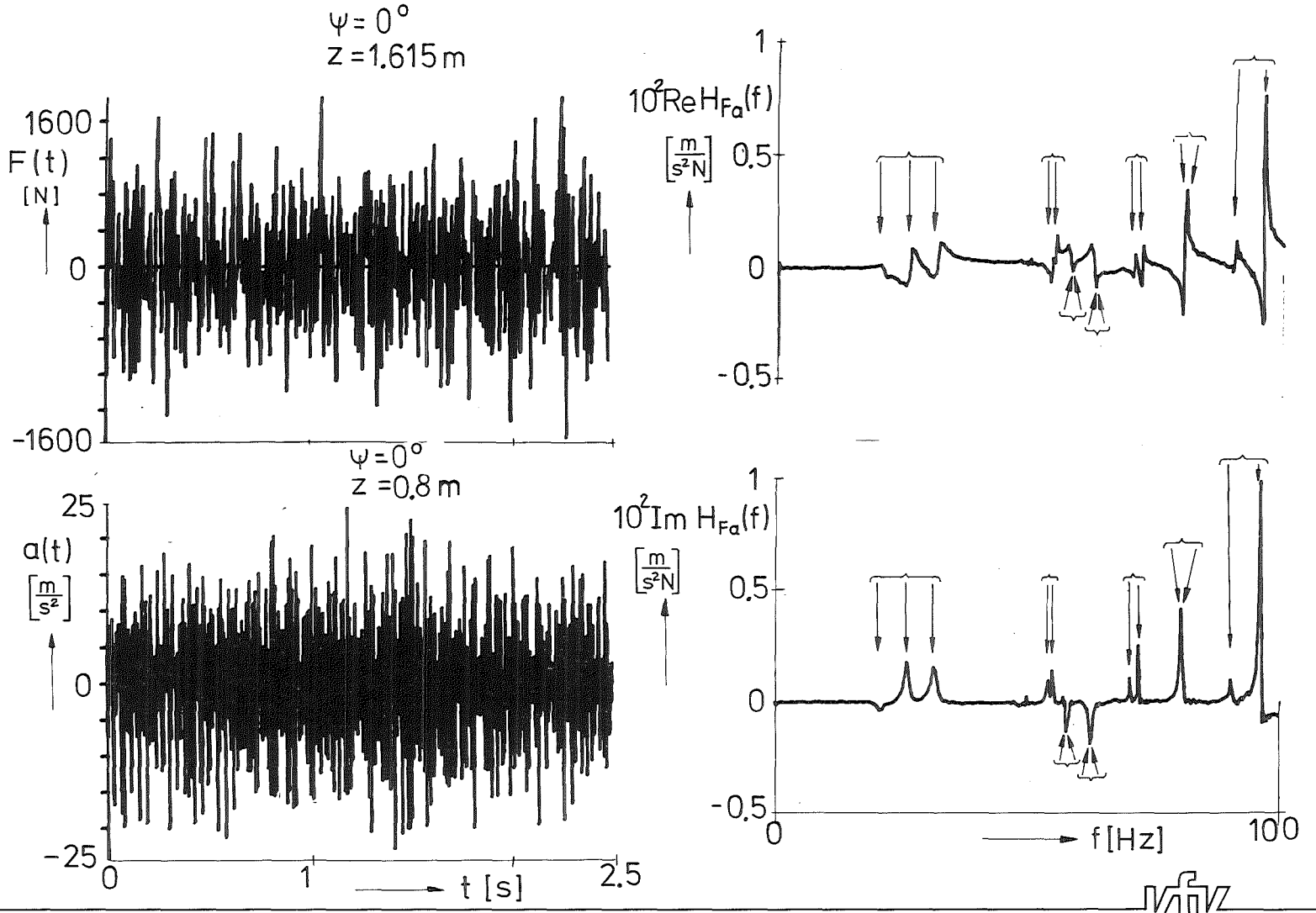

Fig. 9 : Typical time histories of random excitation force F(t) and of acceleration response a(t) and components of the corresponding frequency response function $H_{Fa}(f)$ (procedure III)

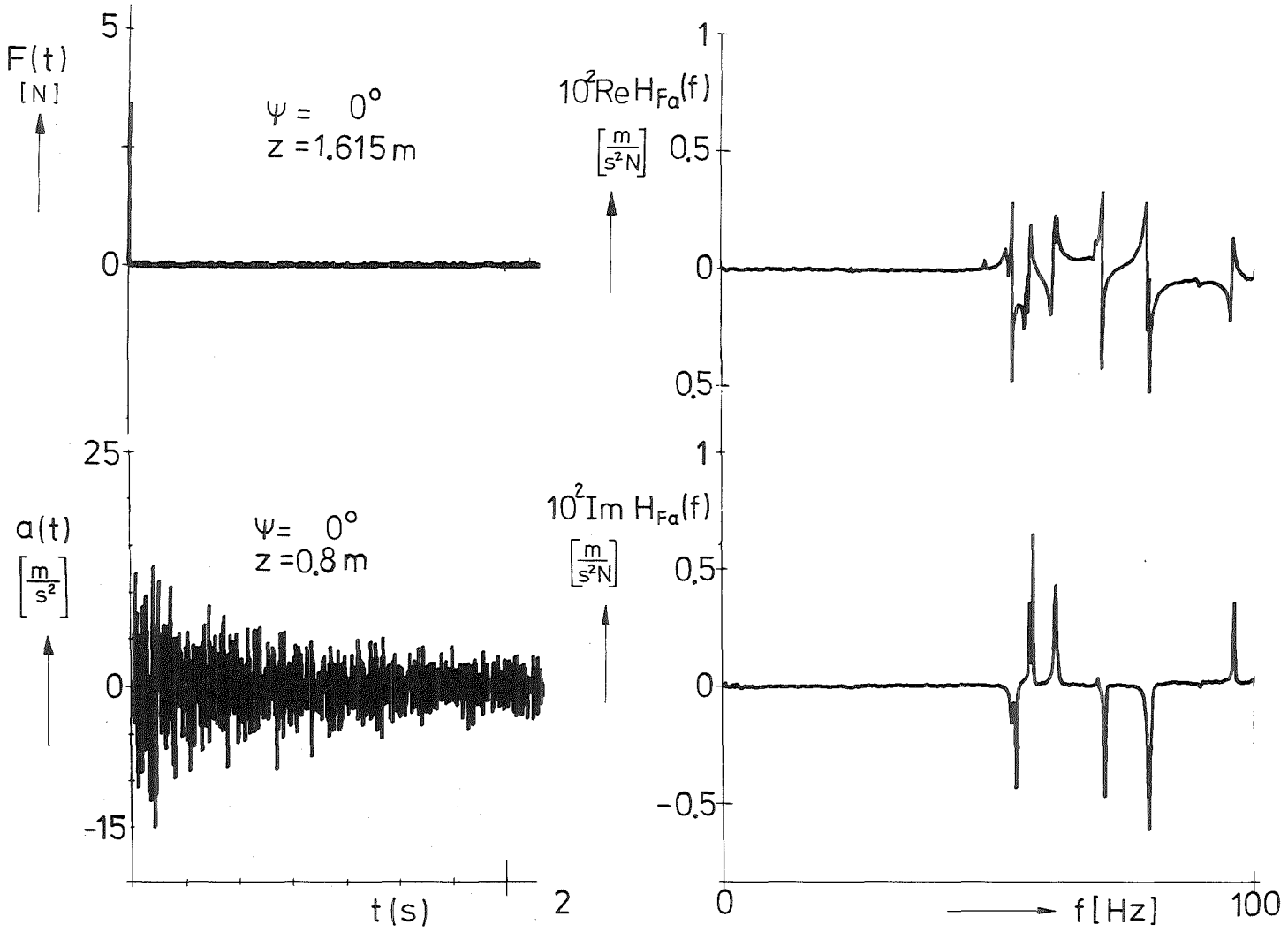

Fig.10: Typical time histories of excitation impulse F(t) and of acceleration response a(t) and components of corresponding frequency response function $H_{Fa}(f)$ (procedure IV)

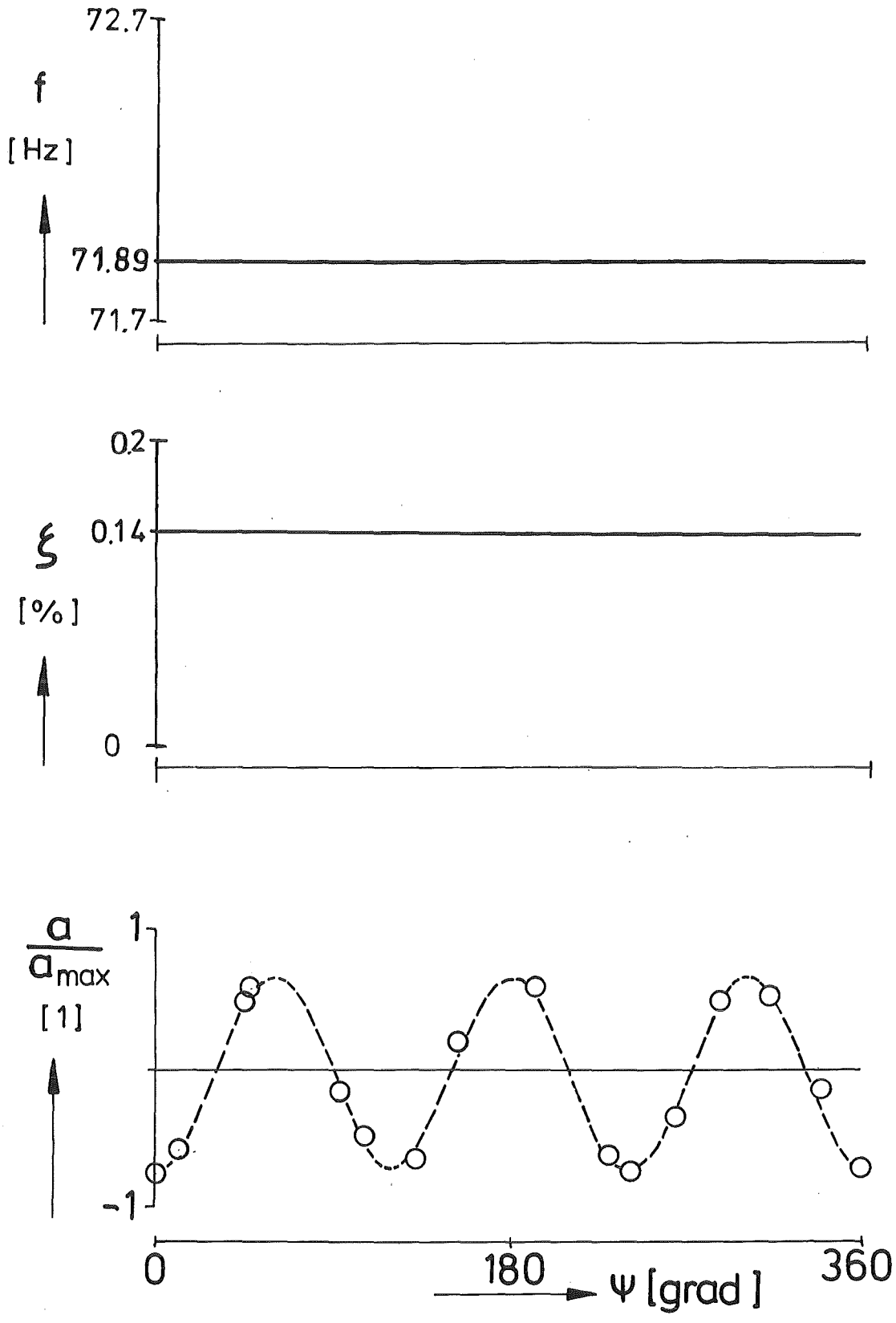

Fig.11: Typical modal characteristics obtained by application of experimental procedure I (snapback excitation + computer code EVA)

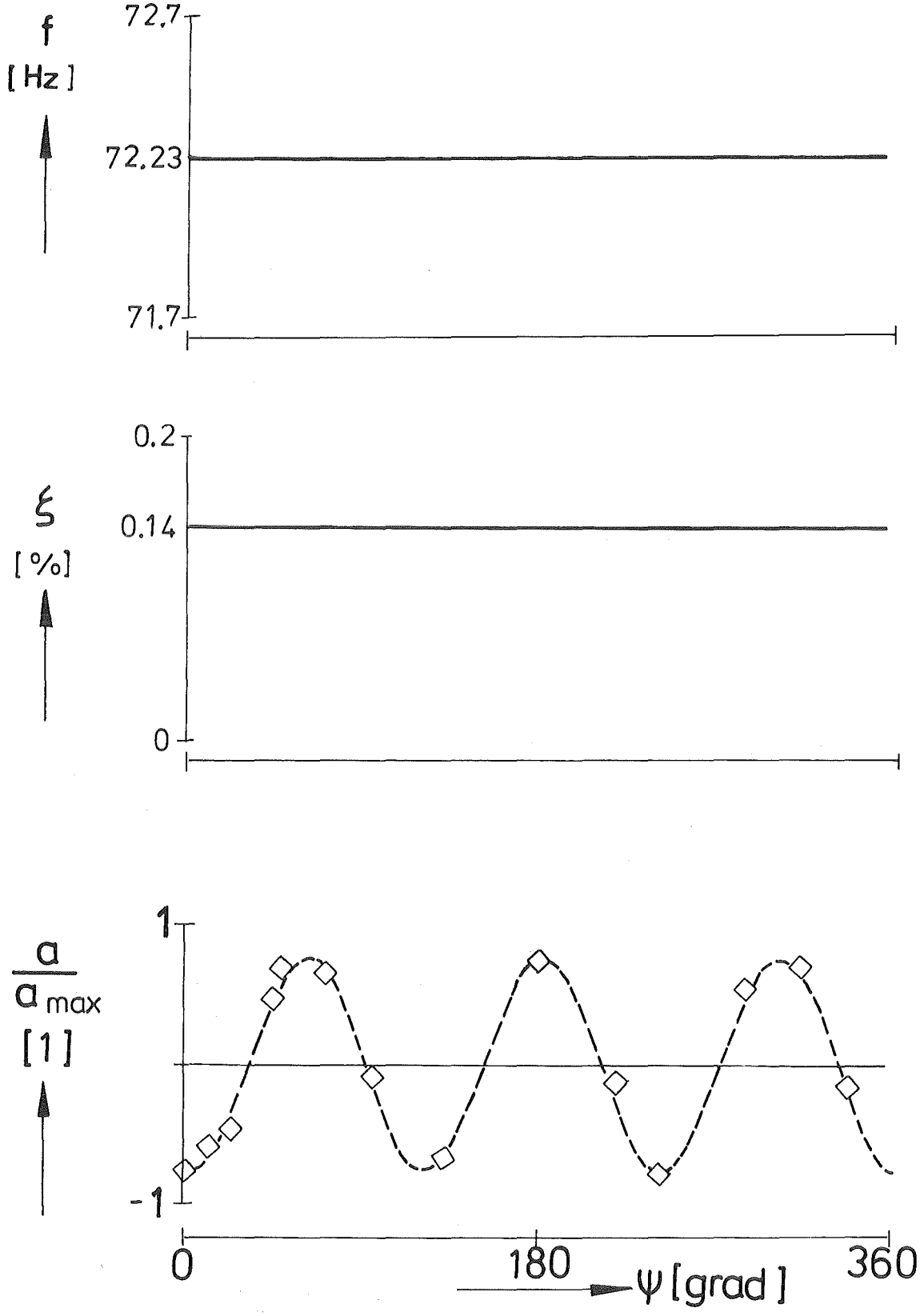

Fig. 12: Typical modal characteristics obtained by application of experimental procedure II (transient sine-wave excitation + computer code EVA)

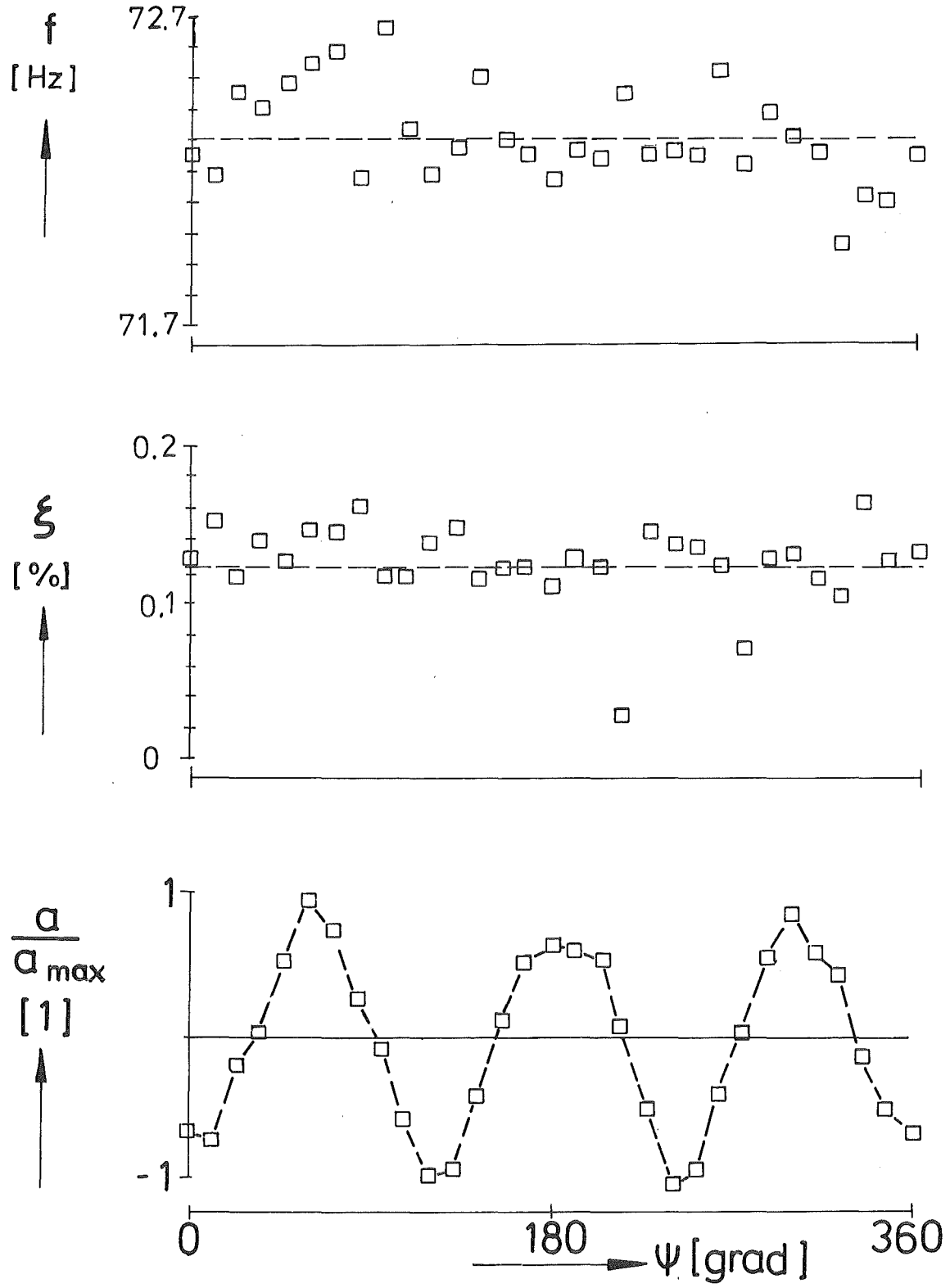

Fig.13: Typical modal characteristics obtained by application of experimental procedure III (stationary random excitation + computer code MODAMS)

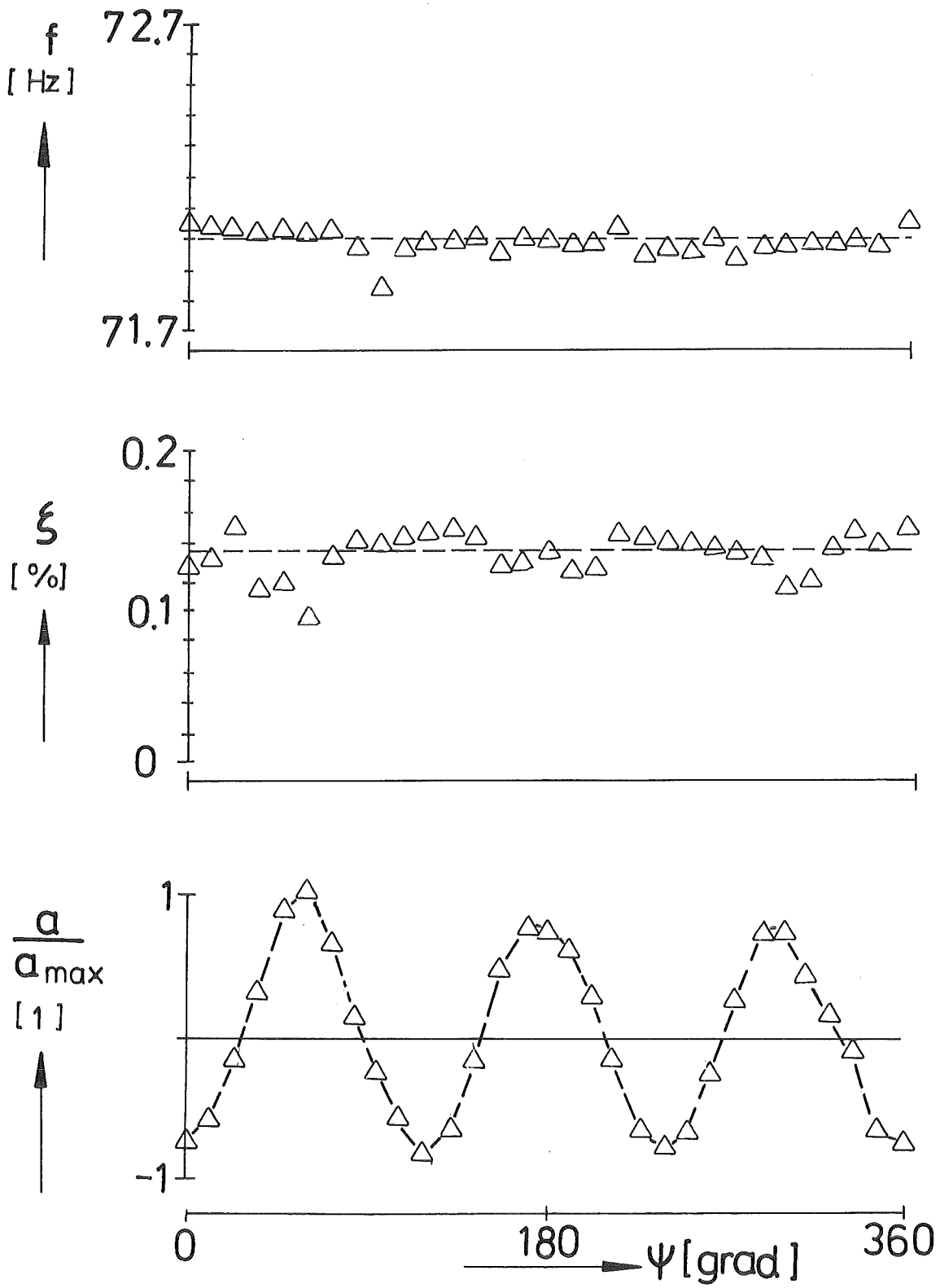

Fig. 14 : Typical modal characteristics obtained by application of experimental procedure IV (Impulse excitation + computer code MODAMS)

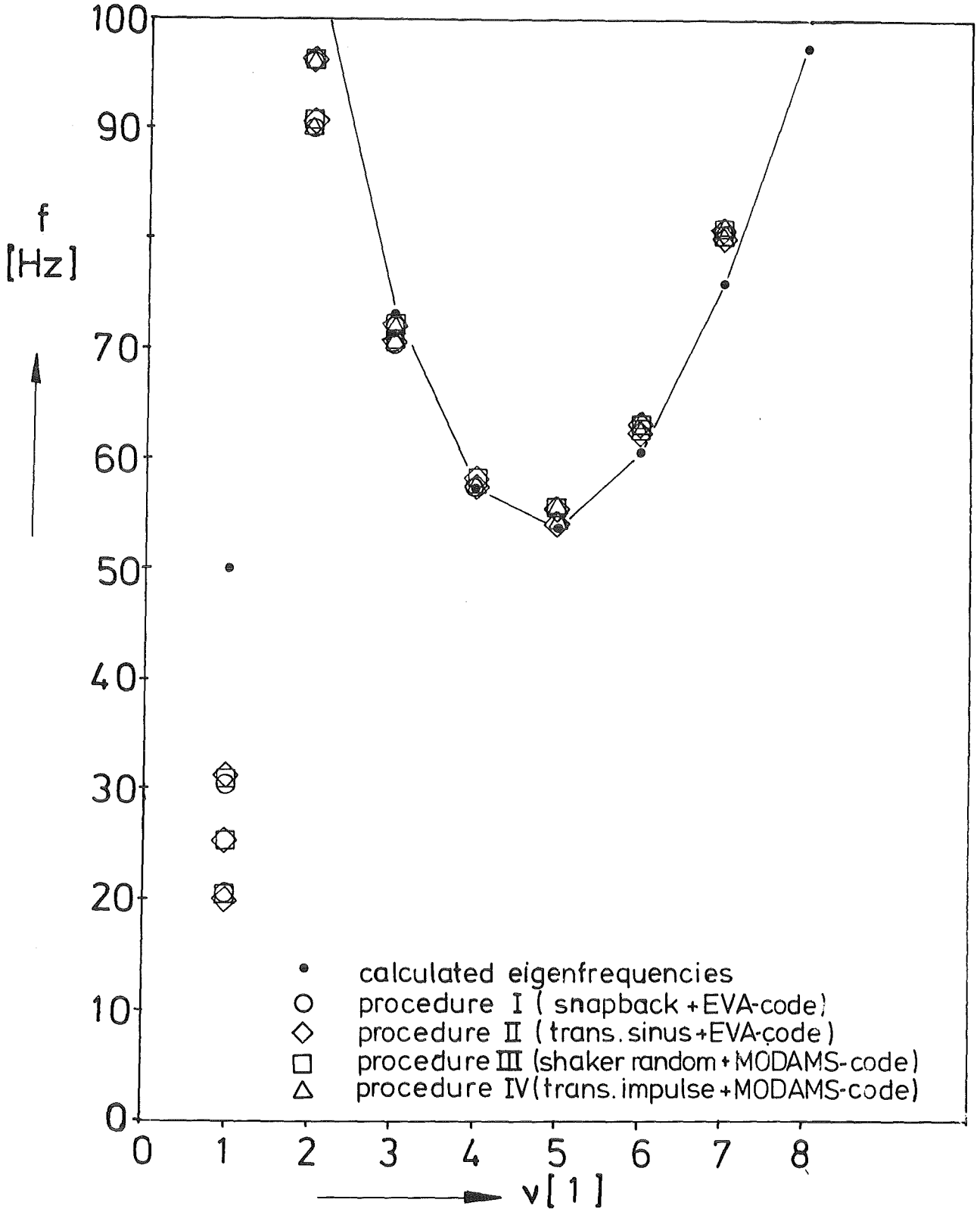

Fig. 15: Calculated and extracted natural frequency values of the test cylinder partly filled with water. Comparison of results obtained by application of four different experimental procedures

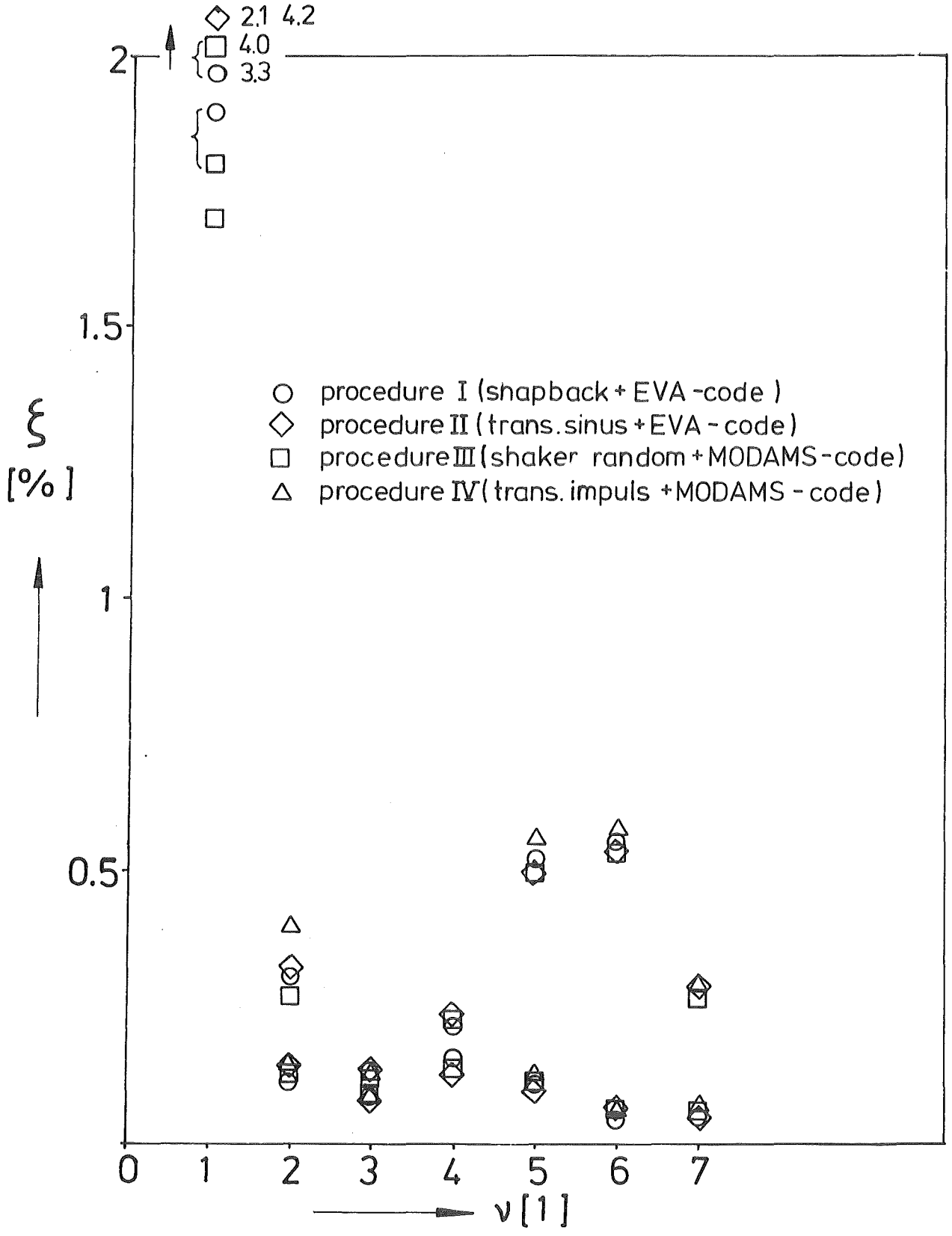

KfK IRE

Fig. 16: Critical damping ratios extracted. Comparison of results obtained by application of four different experimental procedures

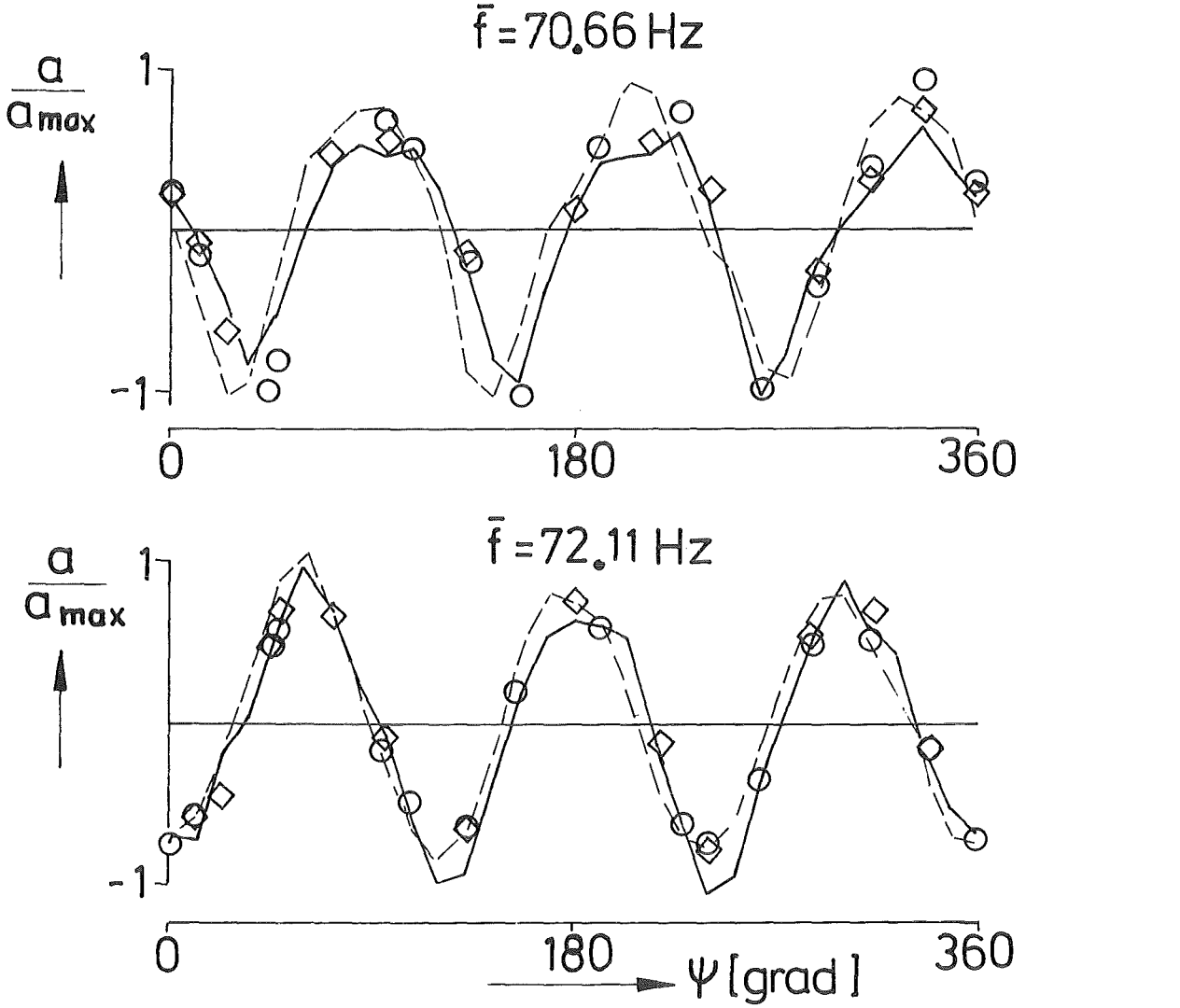

○ procedure I (snapback + EVA-code)
◇ procedure II (trans. sinus + EVA-code)
—— procedure III (shaker random + MODAMS-code)
--- procedure IV (trans. impuls + MODAMS-code)

KfK IRE

Fig. 17: Comparison of two typical mode shapes identified by four different experimental procedures

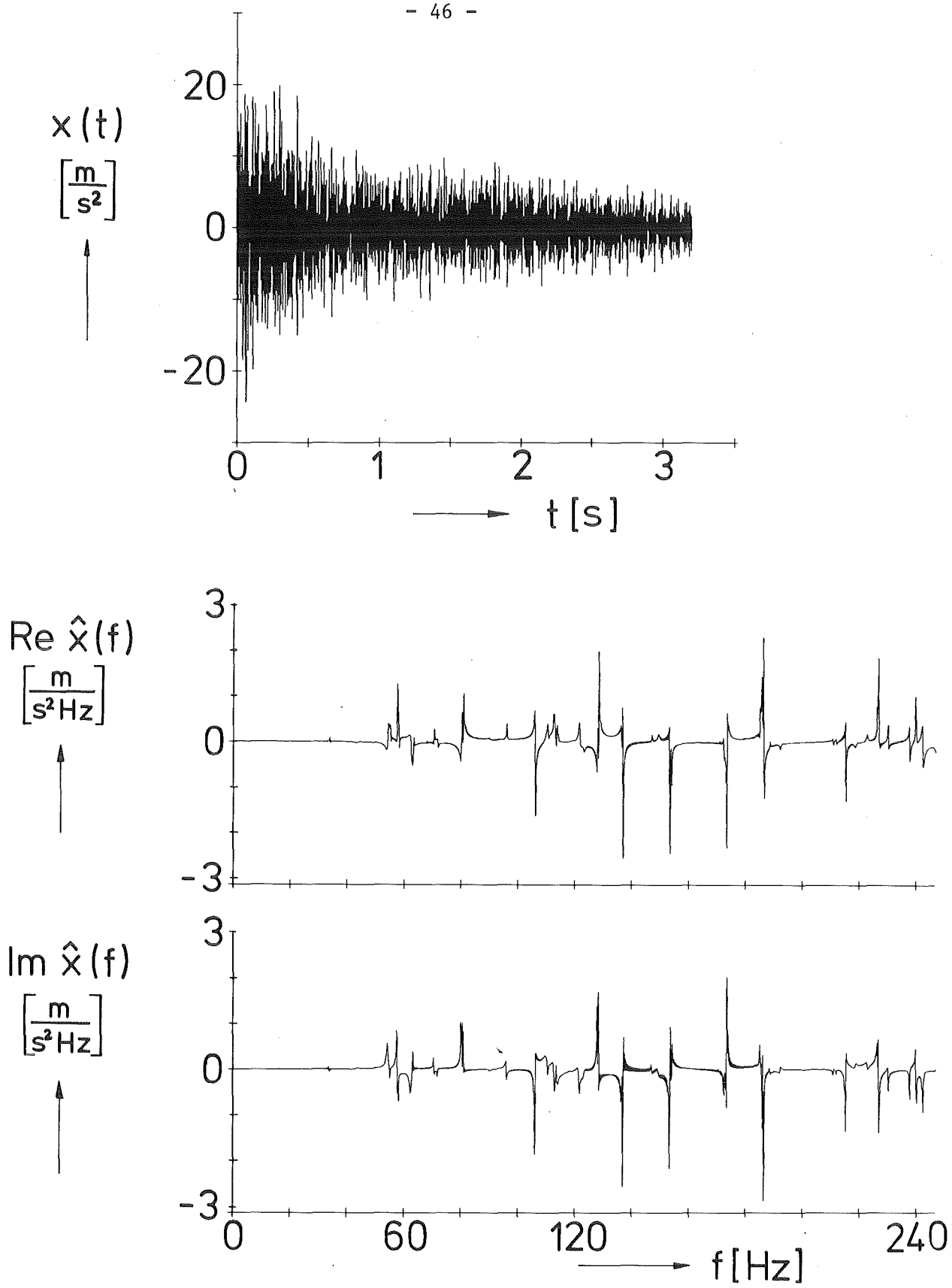

KfK IRE

Fig. 18: Typical time history and Fourier-transform of the measured acceleration response (test cylinder partly filled with water, excitation location $z_e = 800$mm, $\psi_e = 0°$; accelerometer position $z_a = 1000$ mm, $\psi_a = 0°$

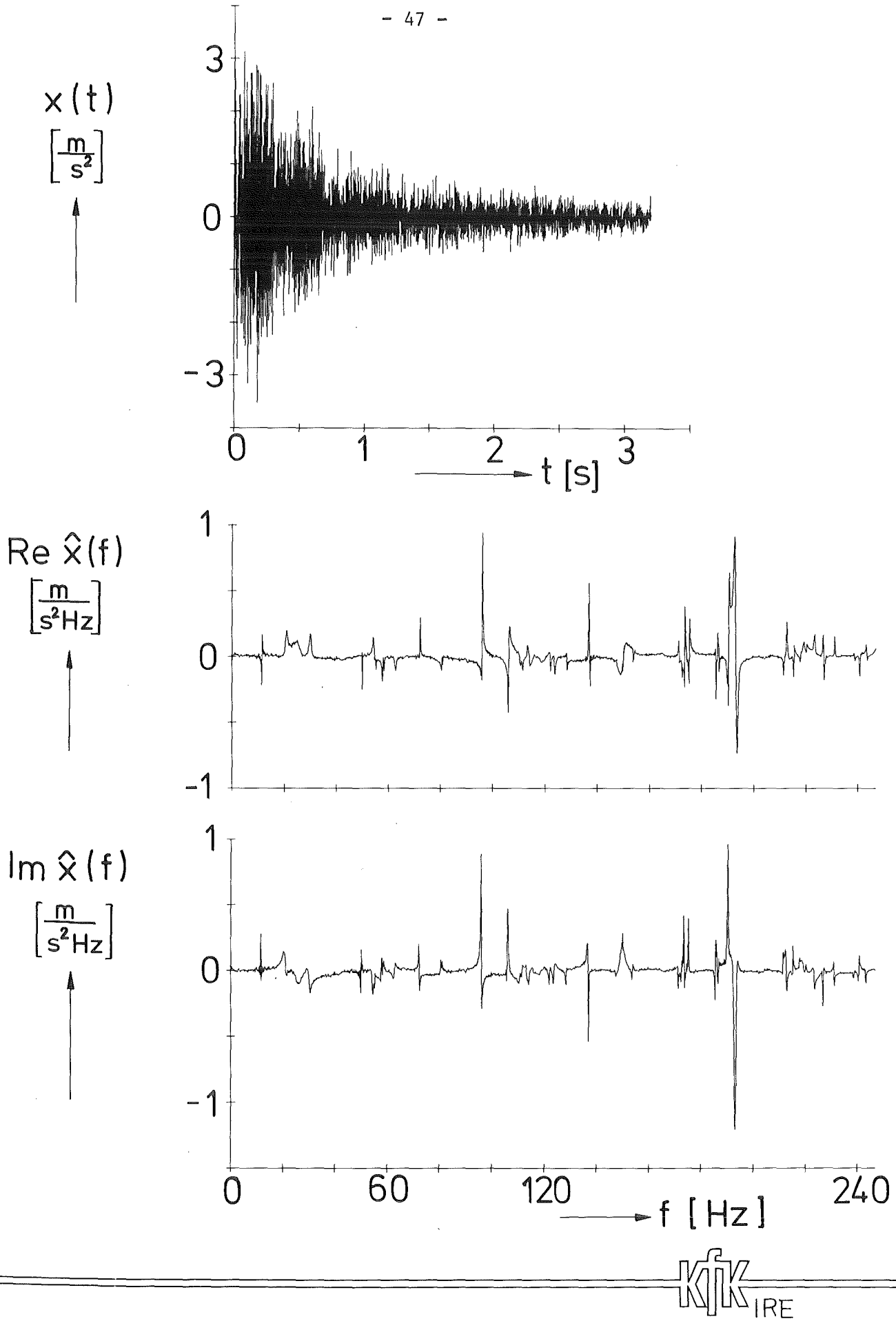

Fig. 19: Typical time history and Fourier-transform of the measured acceleration response (test cylinder partly filled with water, excitation location $z_e = 1615\,mm$, $\psi_e = 0°$; accelerometer position $z_a = 1000\,mm$, $\psi_a = 0°$)

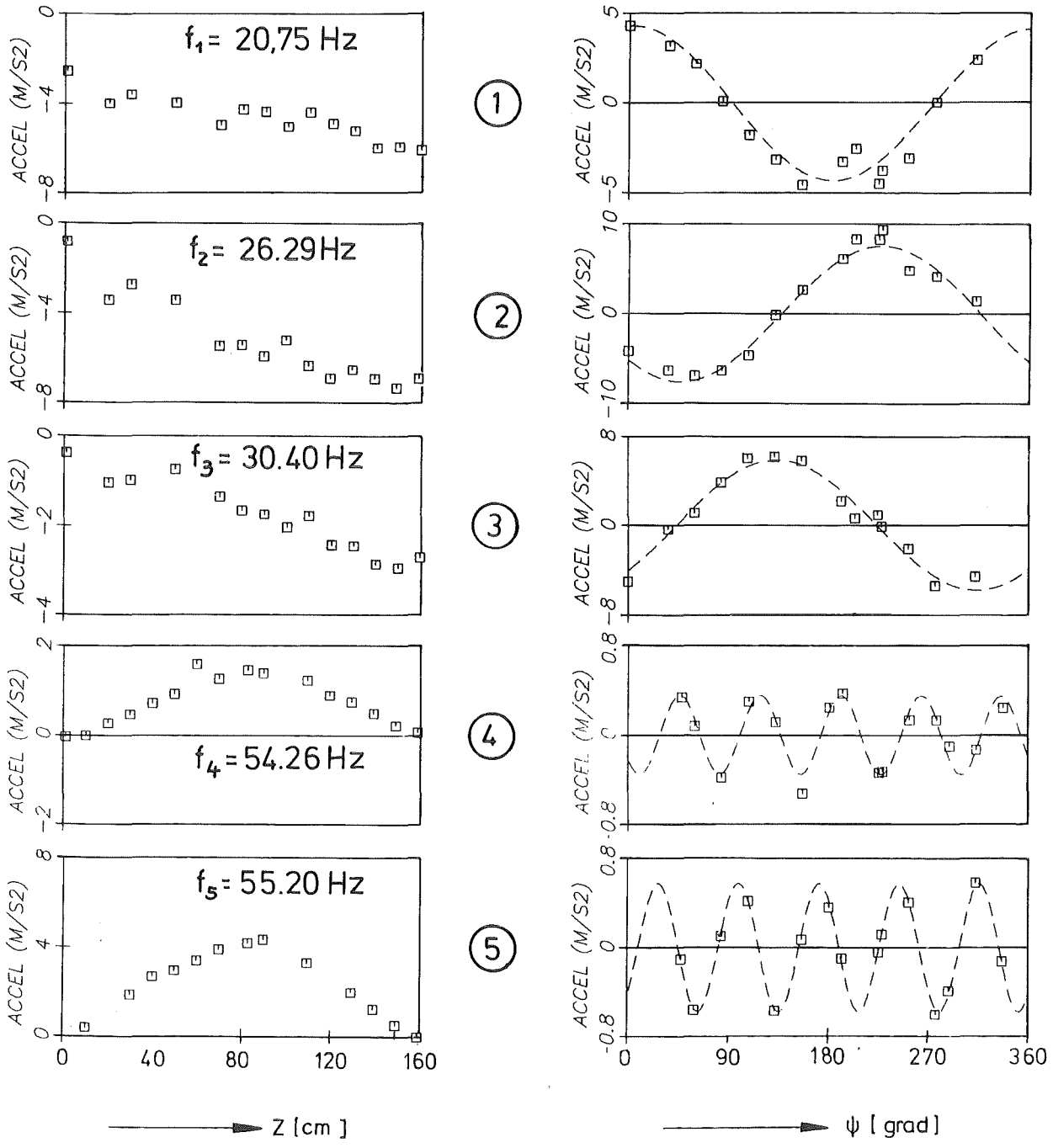

KfK IRE

Fig. 20 : Extracted mode shapes of the test cylinder partly filled with water

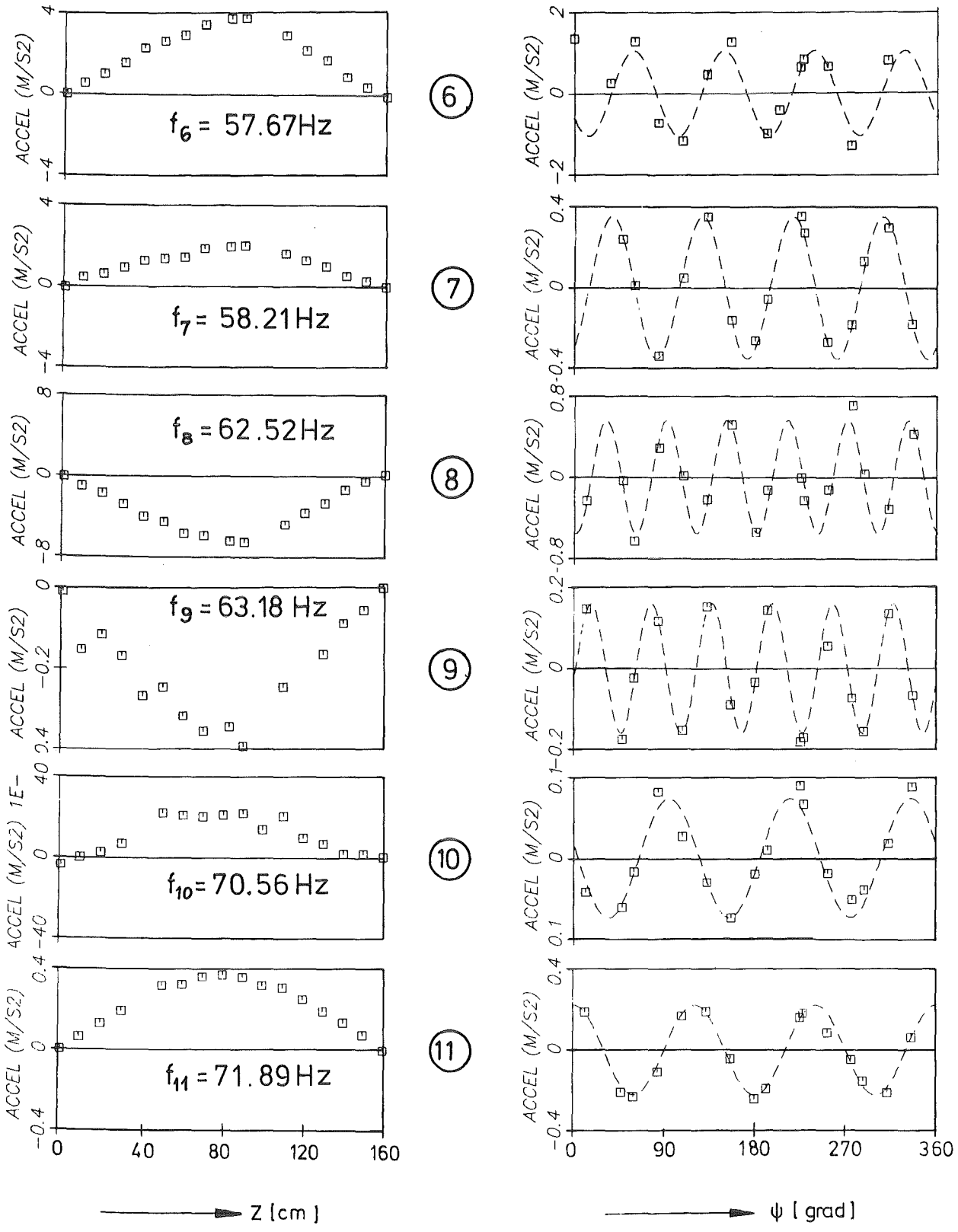

Fig.21 : Extracted mode shapes of the test cylinder partly filled with water (cont)

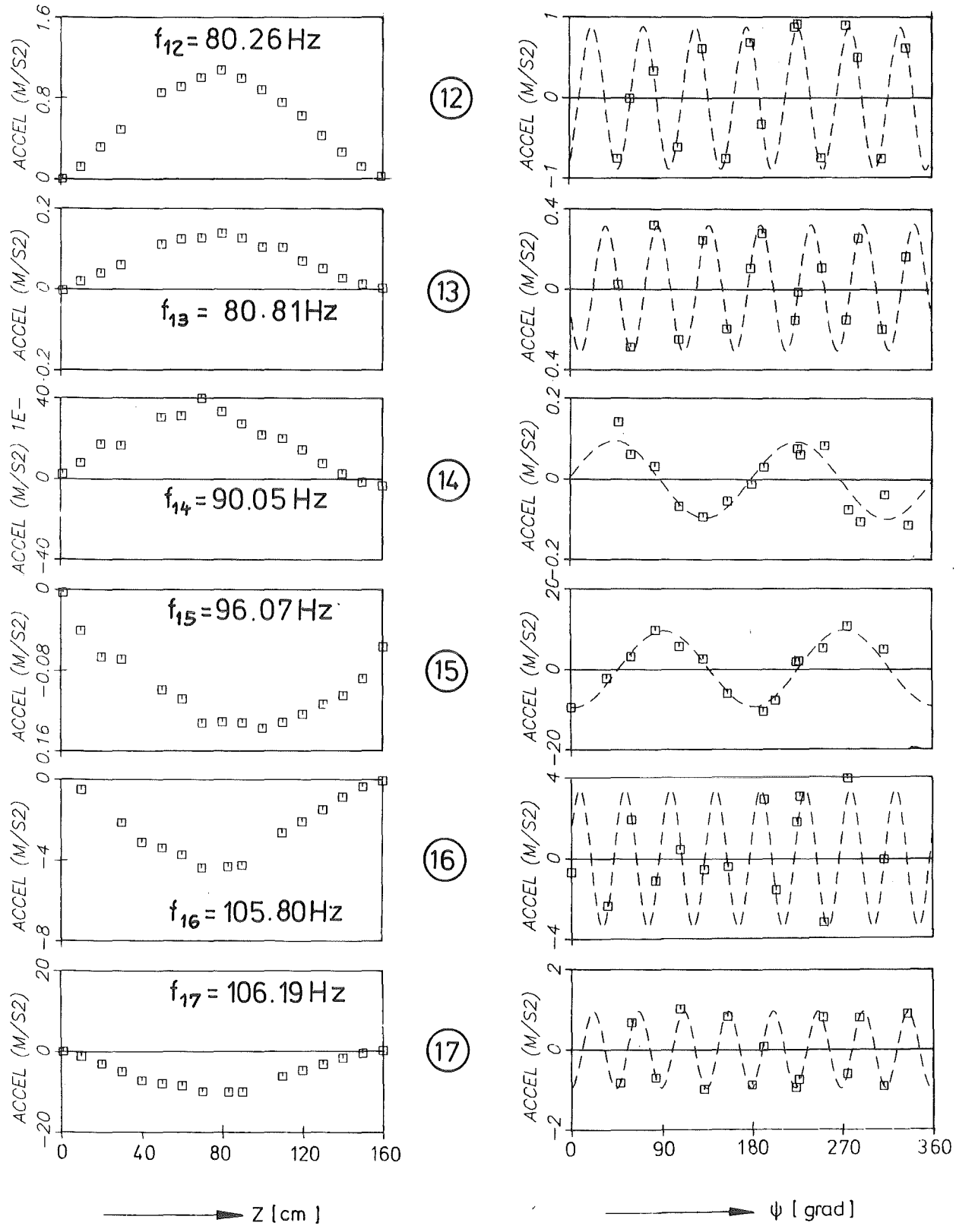

KfK IRE

Fig. 22: Extracted mode shapes of the test cylinder partly filled with water (cont.)

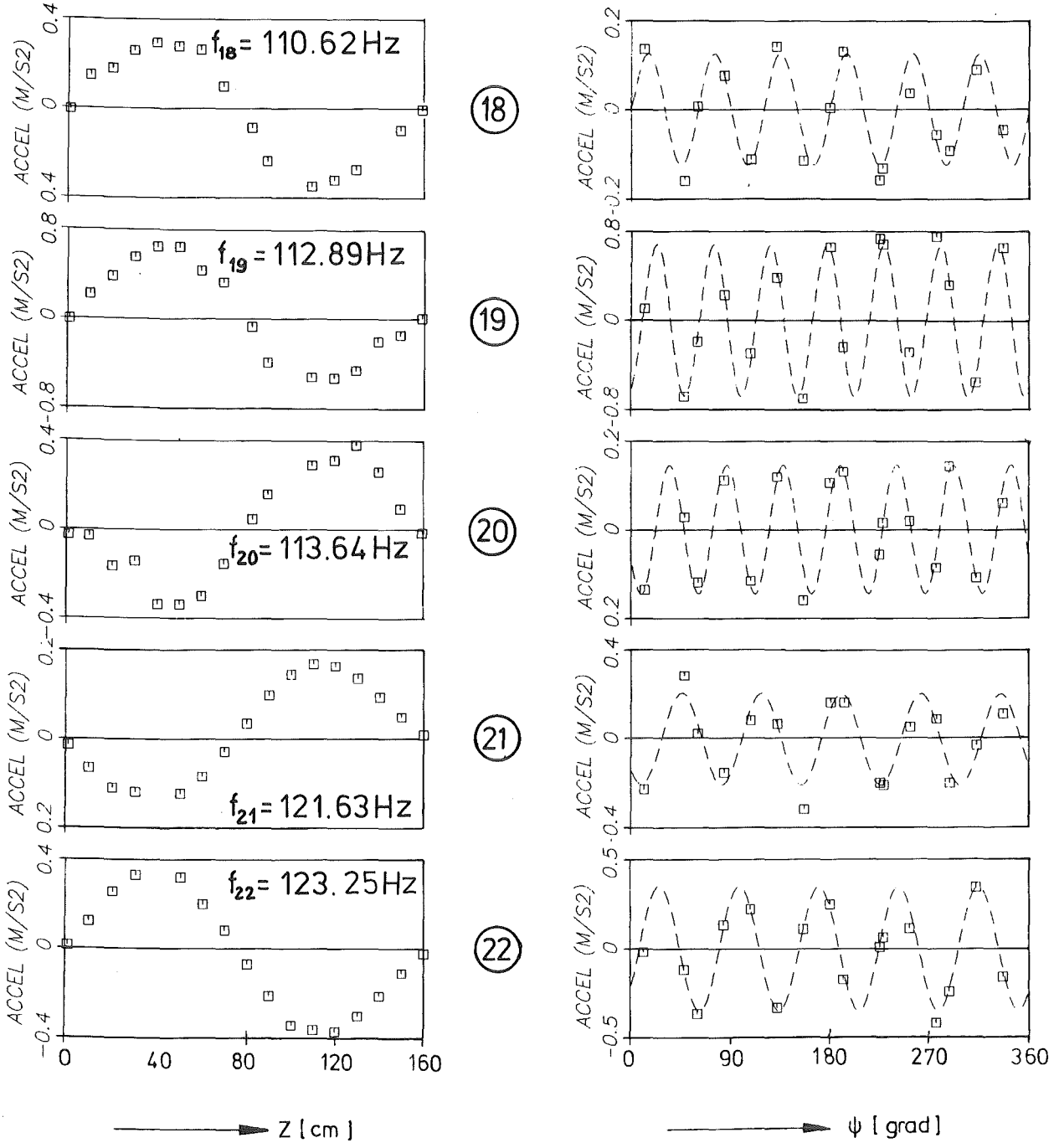

Fig. 23: Extracted mode shapes of the test cylinder partly filled with water (cont.)

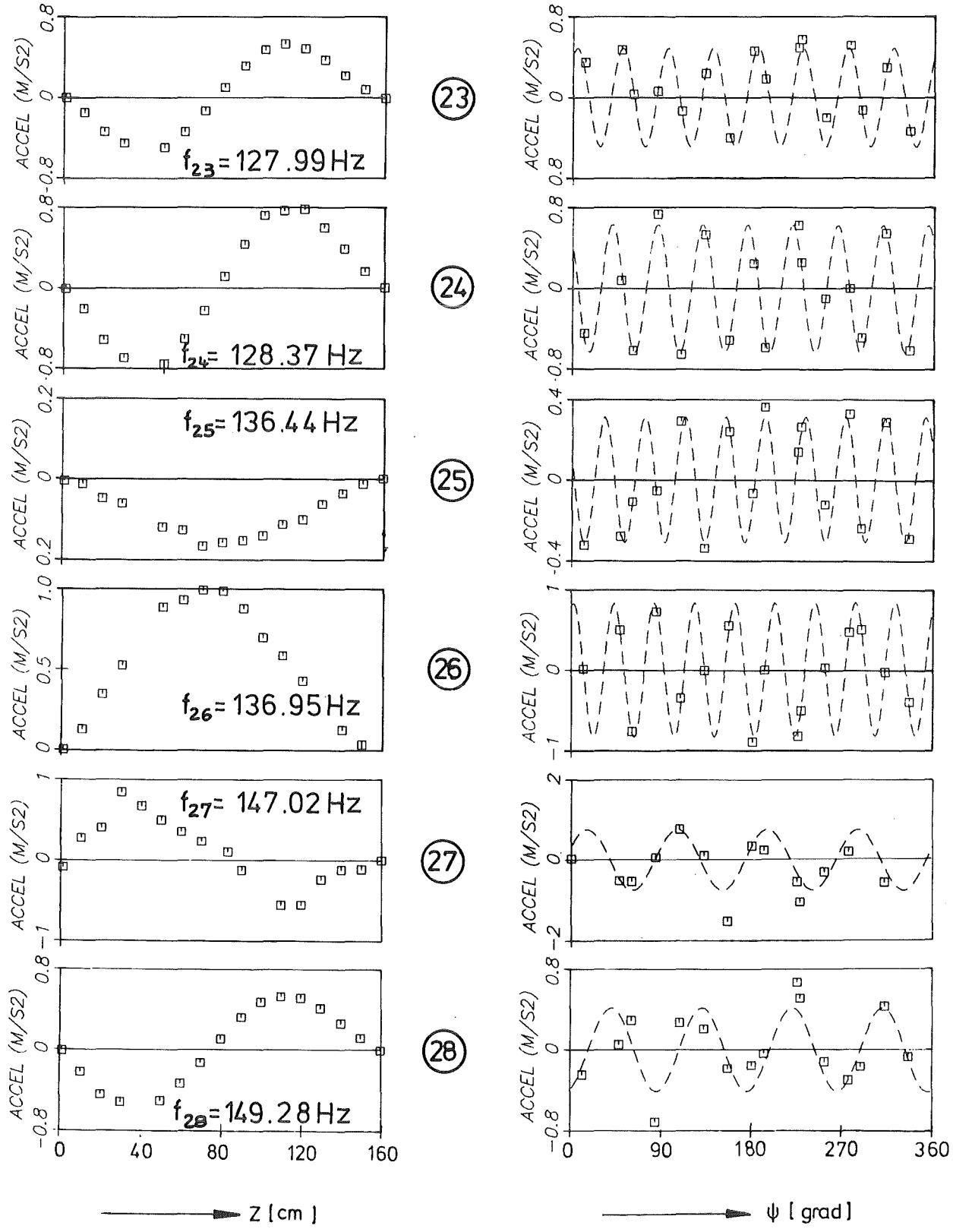

KfK IRE

Fig. 24: Extracted mode shapes of the test cylinder partly filled with water (cont.)

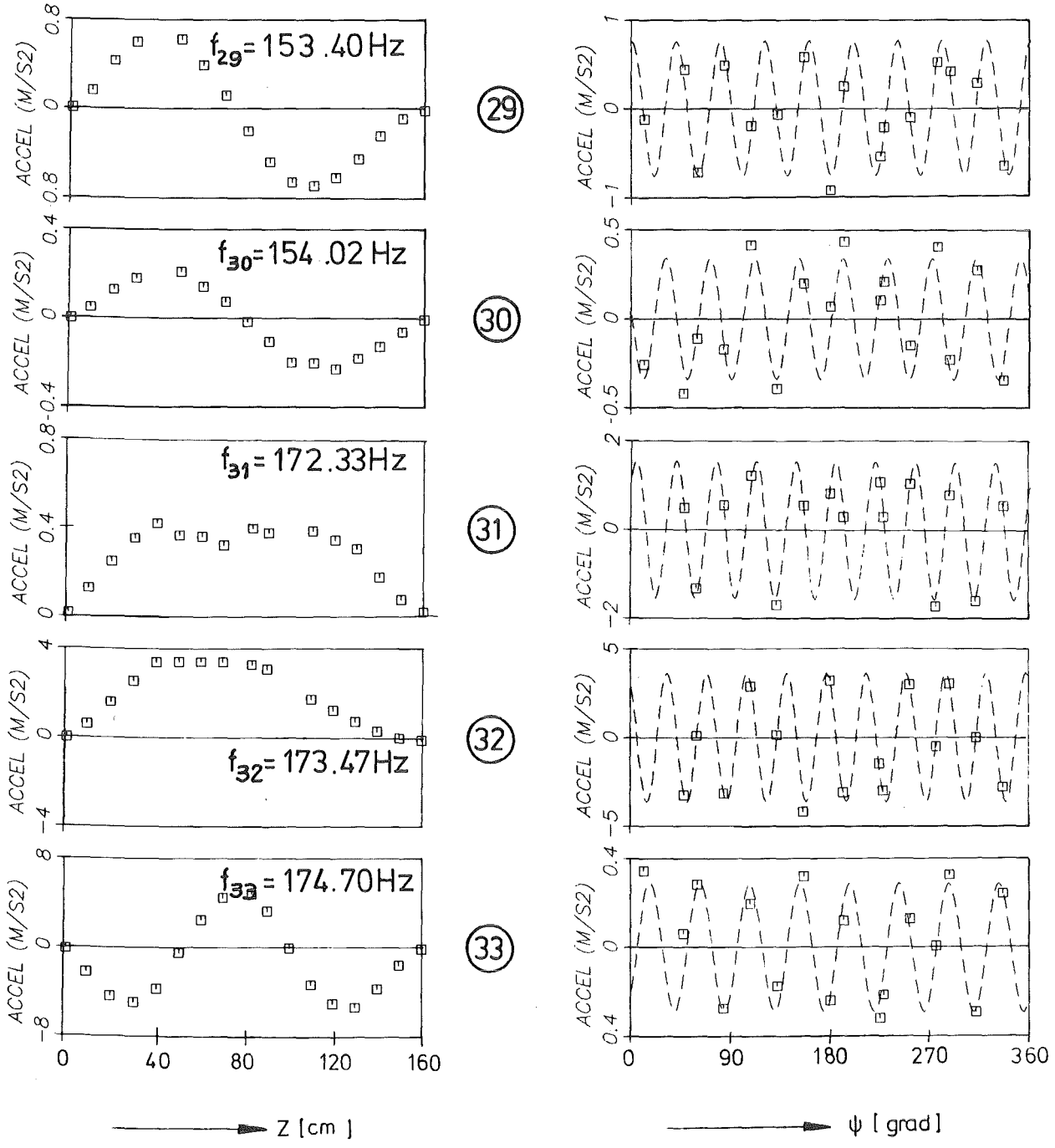

KfK IRE

Fig. 25: Extracted mode shapes of the test cylinder partly filled with water (cont.)

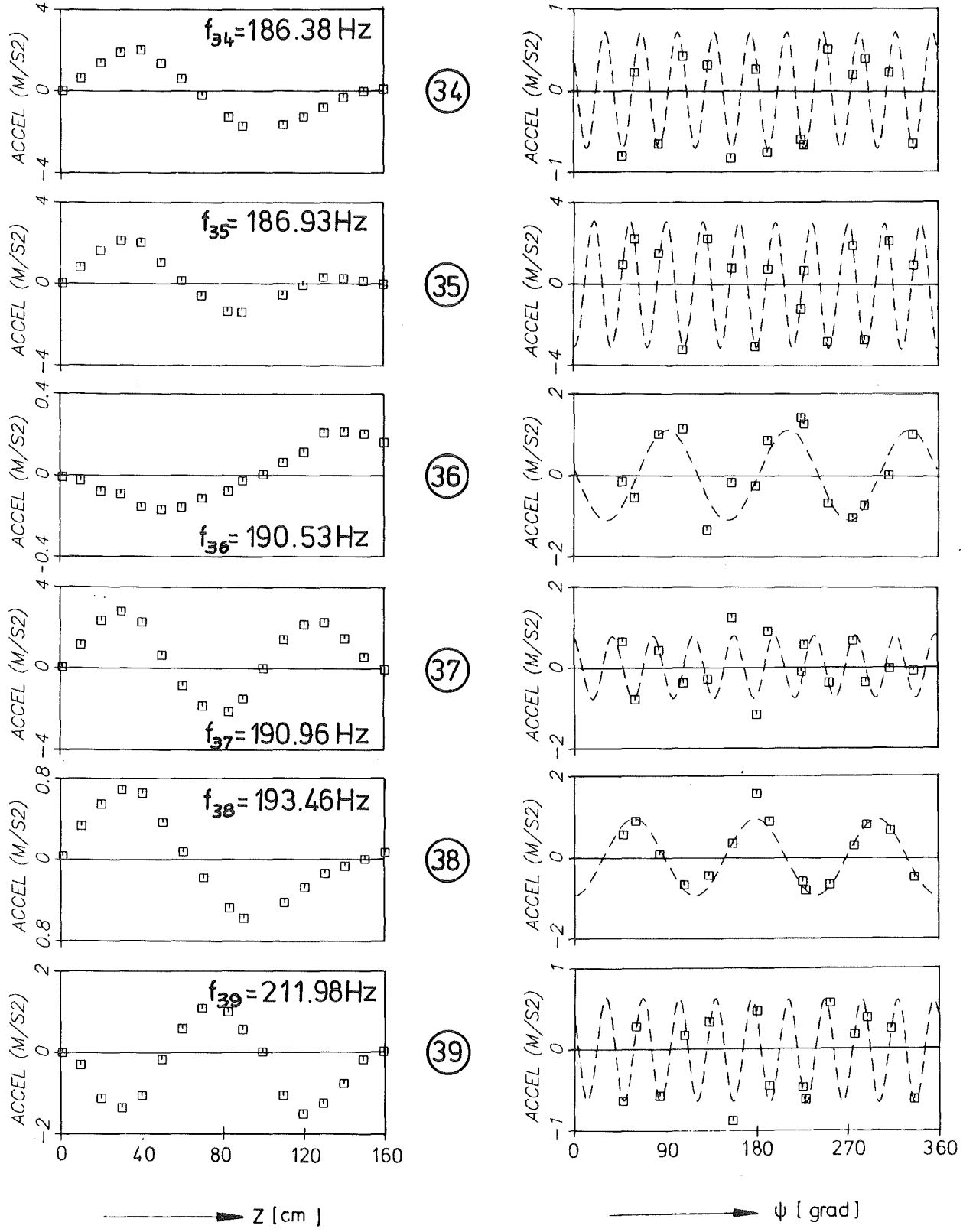

Fig. 26: Extracted mode shapes of the test cylinder partly filled with water (cont.)

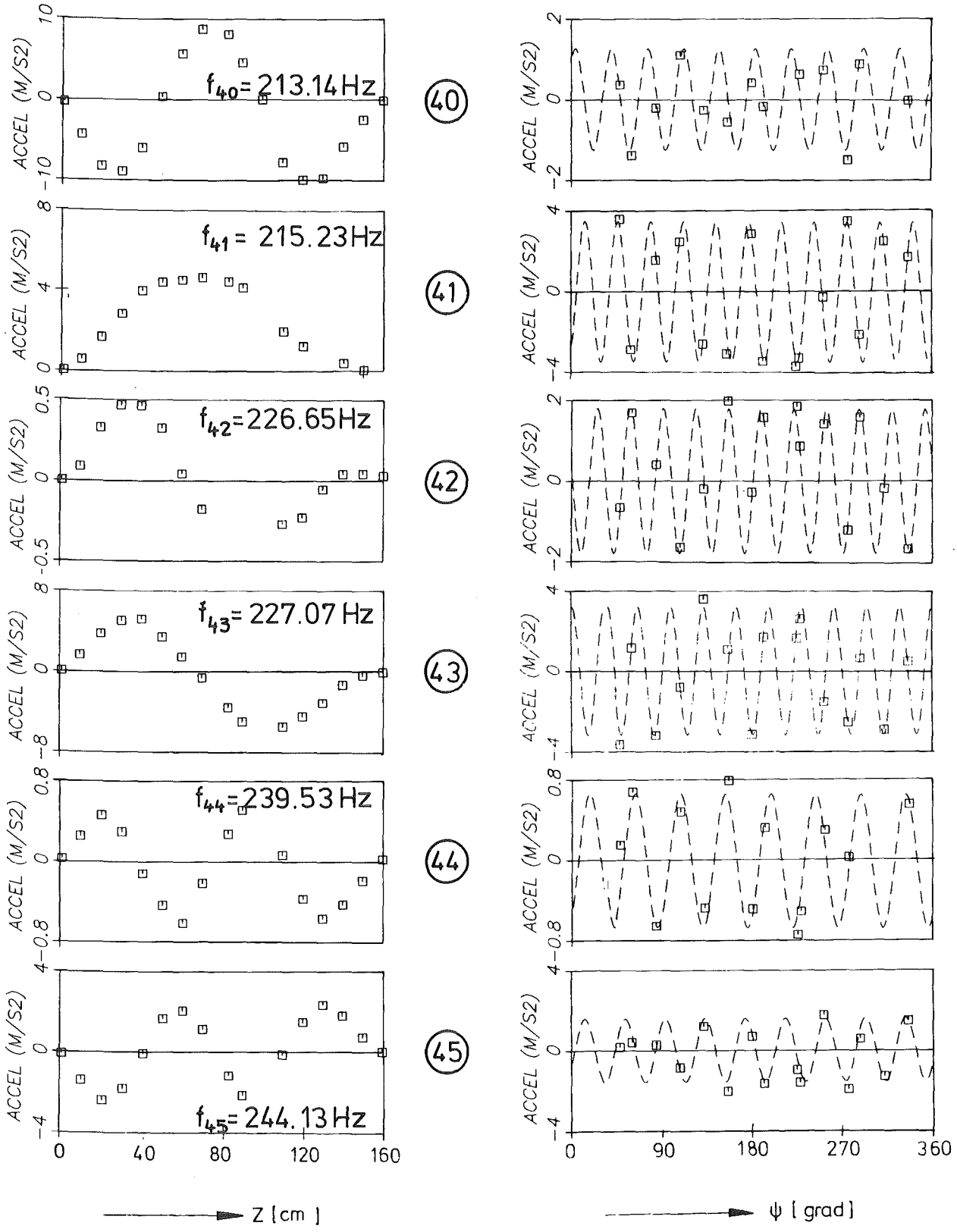

KfK IRE

Fig. 27 : Extracted mode shapes of the test cylinder partly filled with water (cont.)

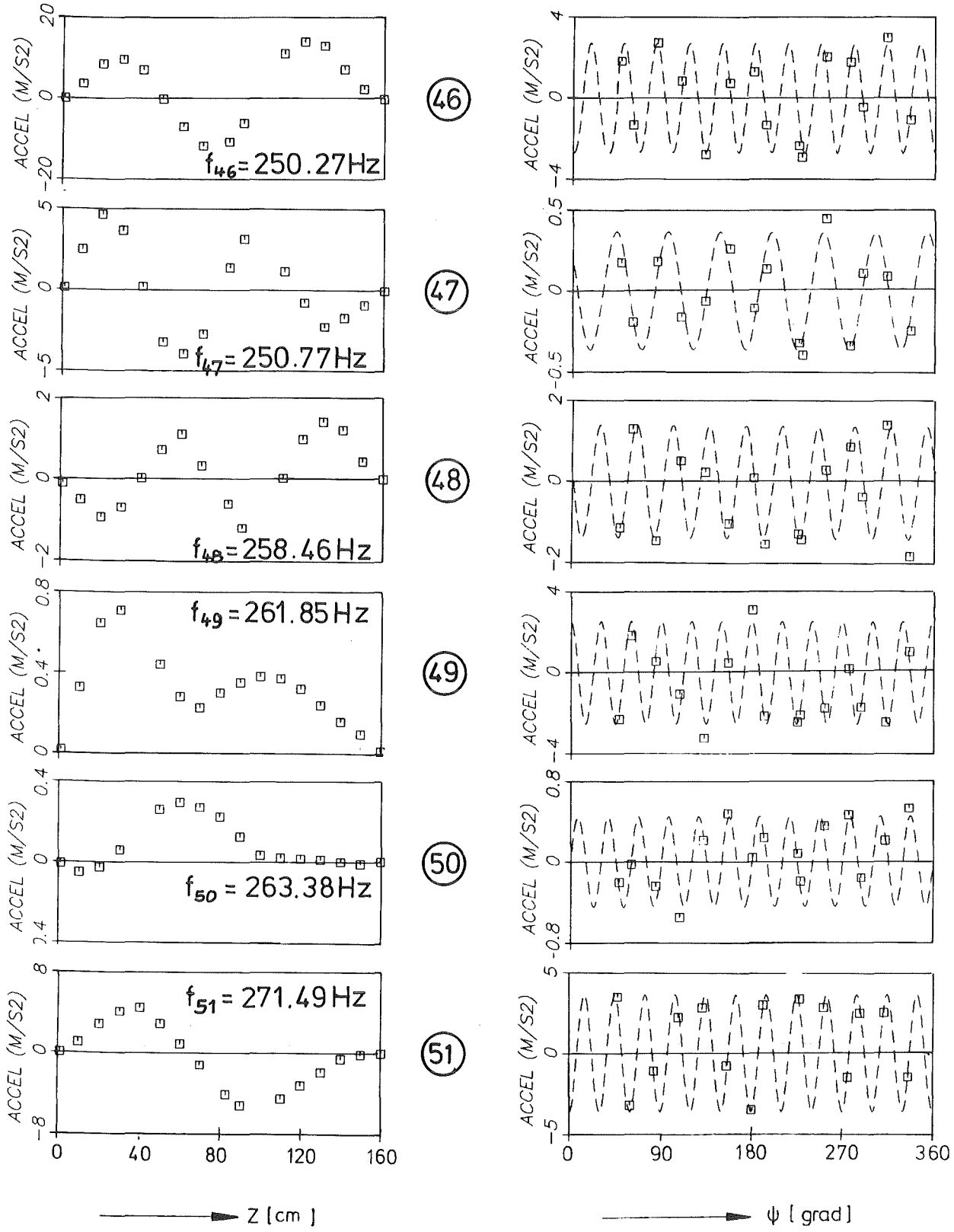

KfK IRE

Fig. 28 : Extracted mode shapes of the test cylinder partly filled with water (cont.)

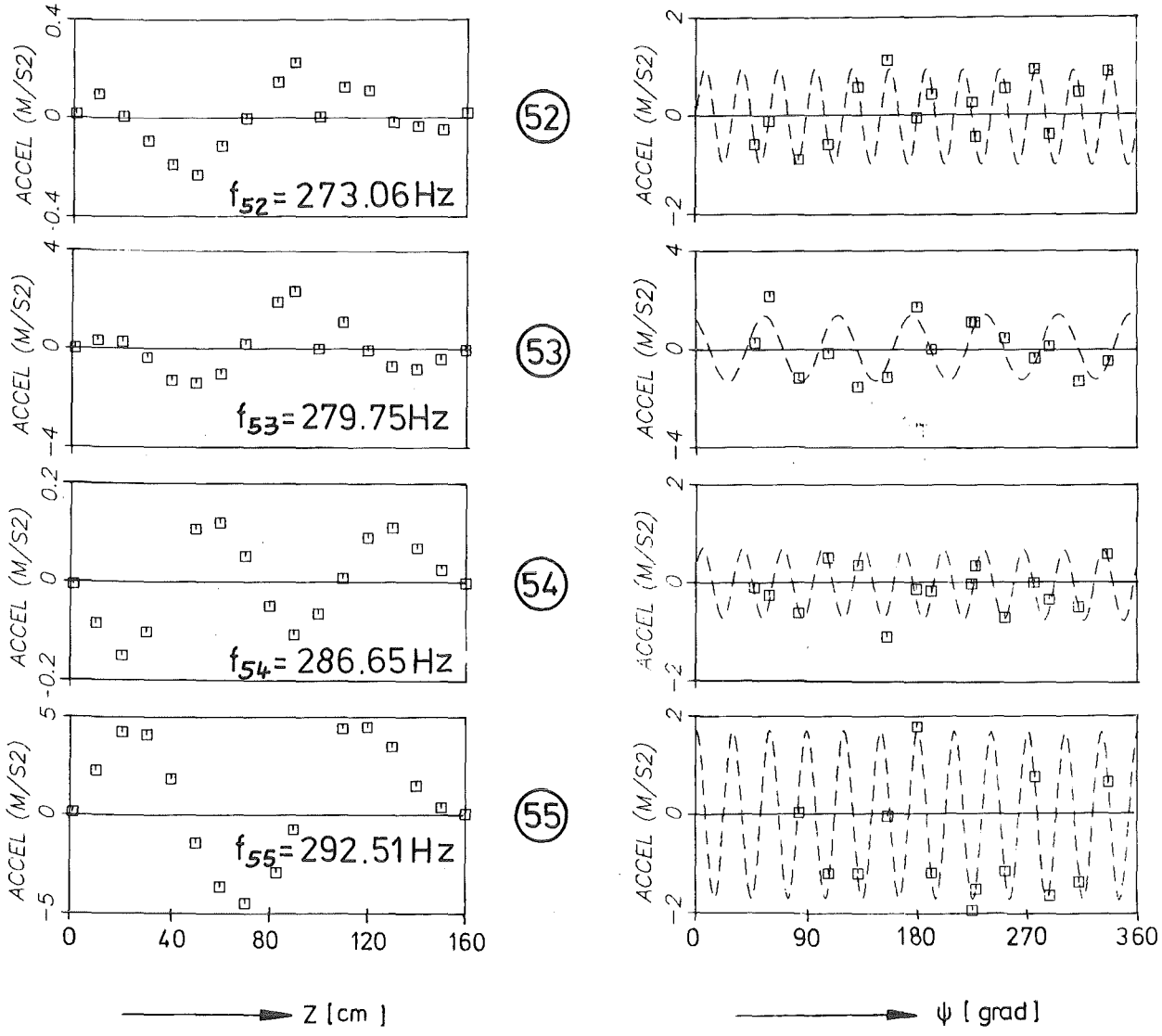

KfK IRE

Fig. 29 : Extracted mode shapes of the test cylinder partly filled with water (cont.)

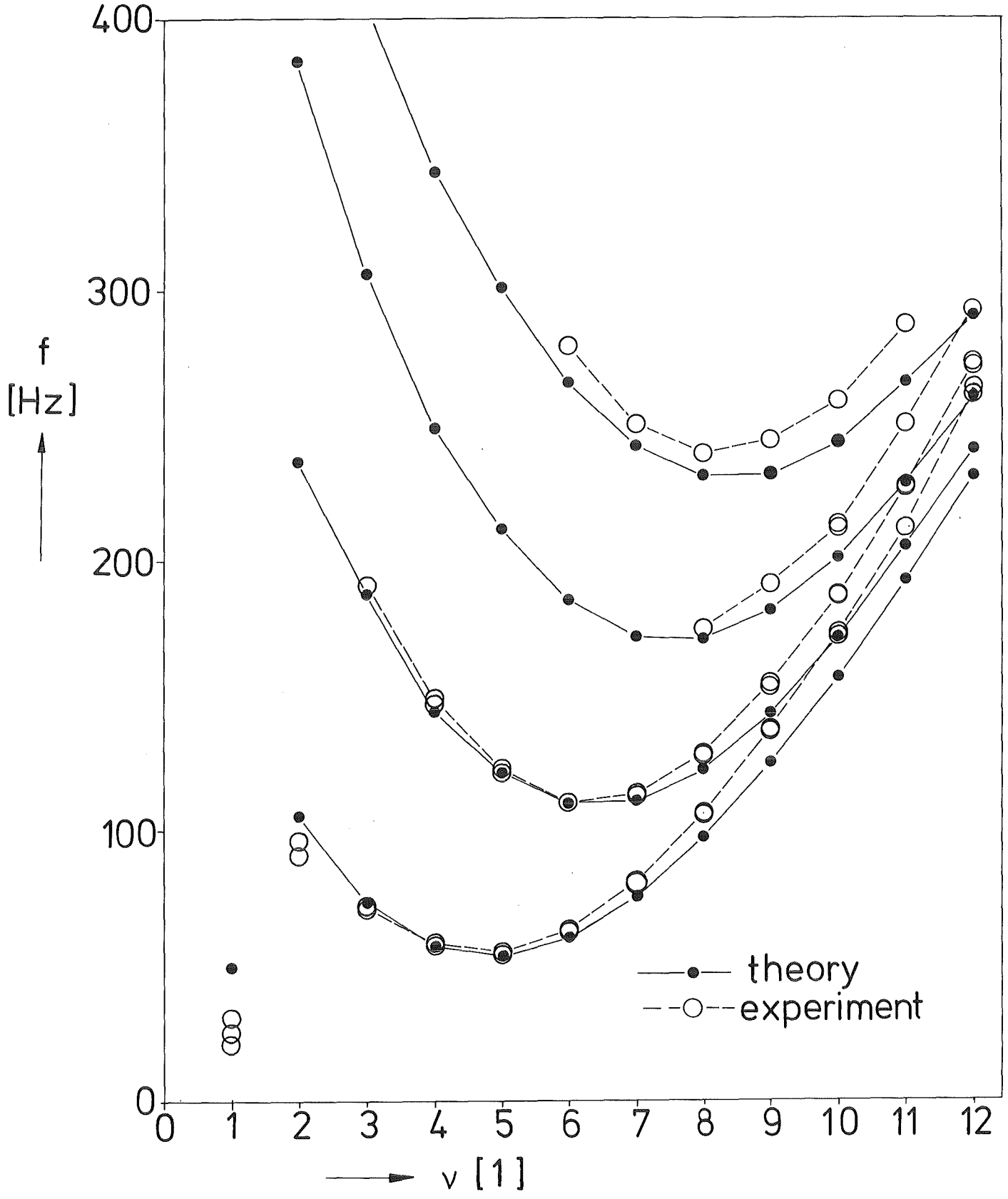

Fig. 30: Comparison of the calculated and measured natural frequencies of the test cylinder partly filled with water

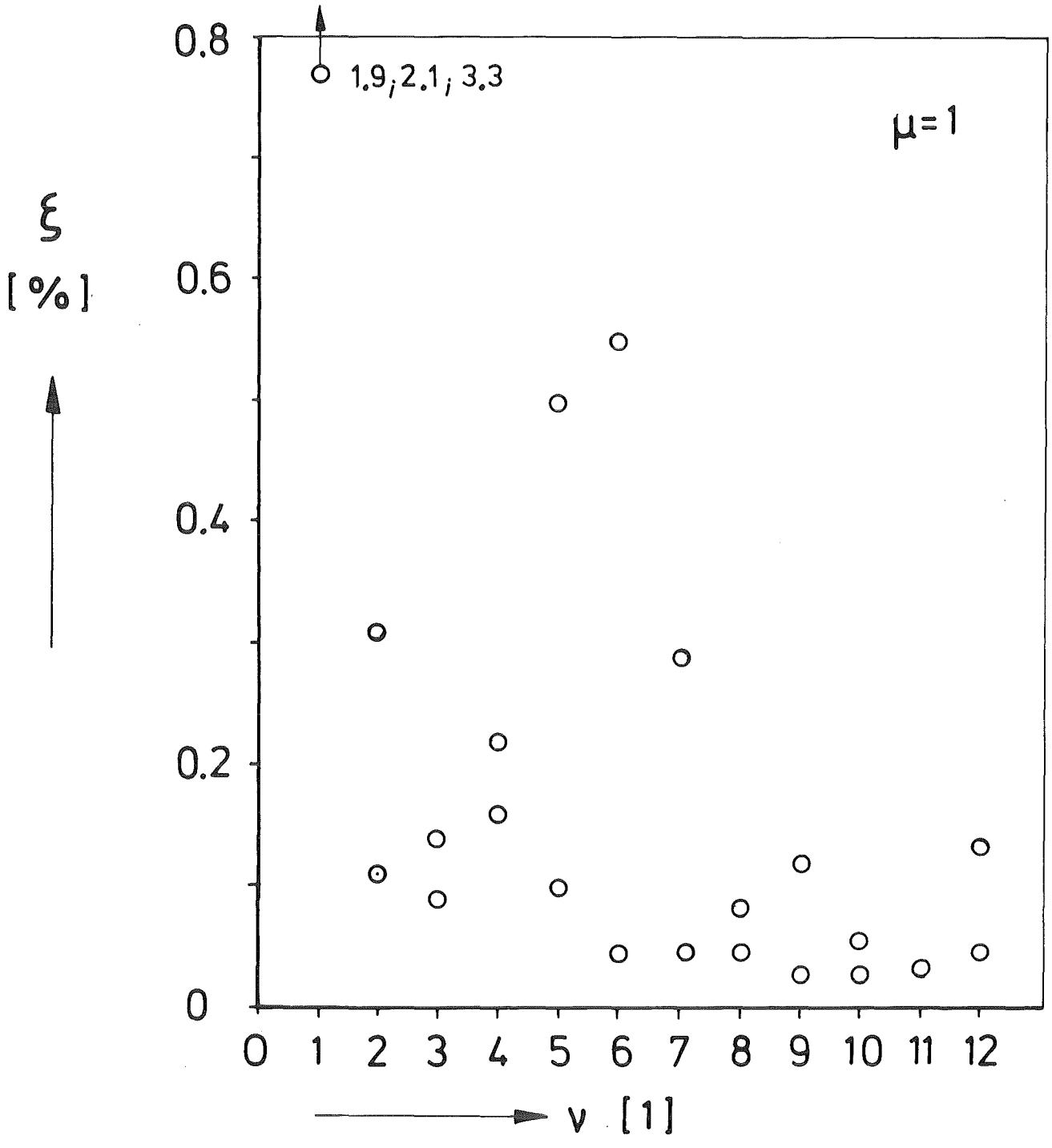

KfK IRE

Fig.31: Critical damping ratio ξ of extracted modes of the test cylinder partly filled with water ($\mu = 1$)

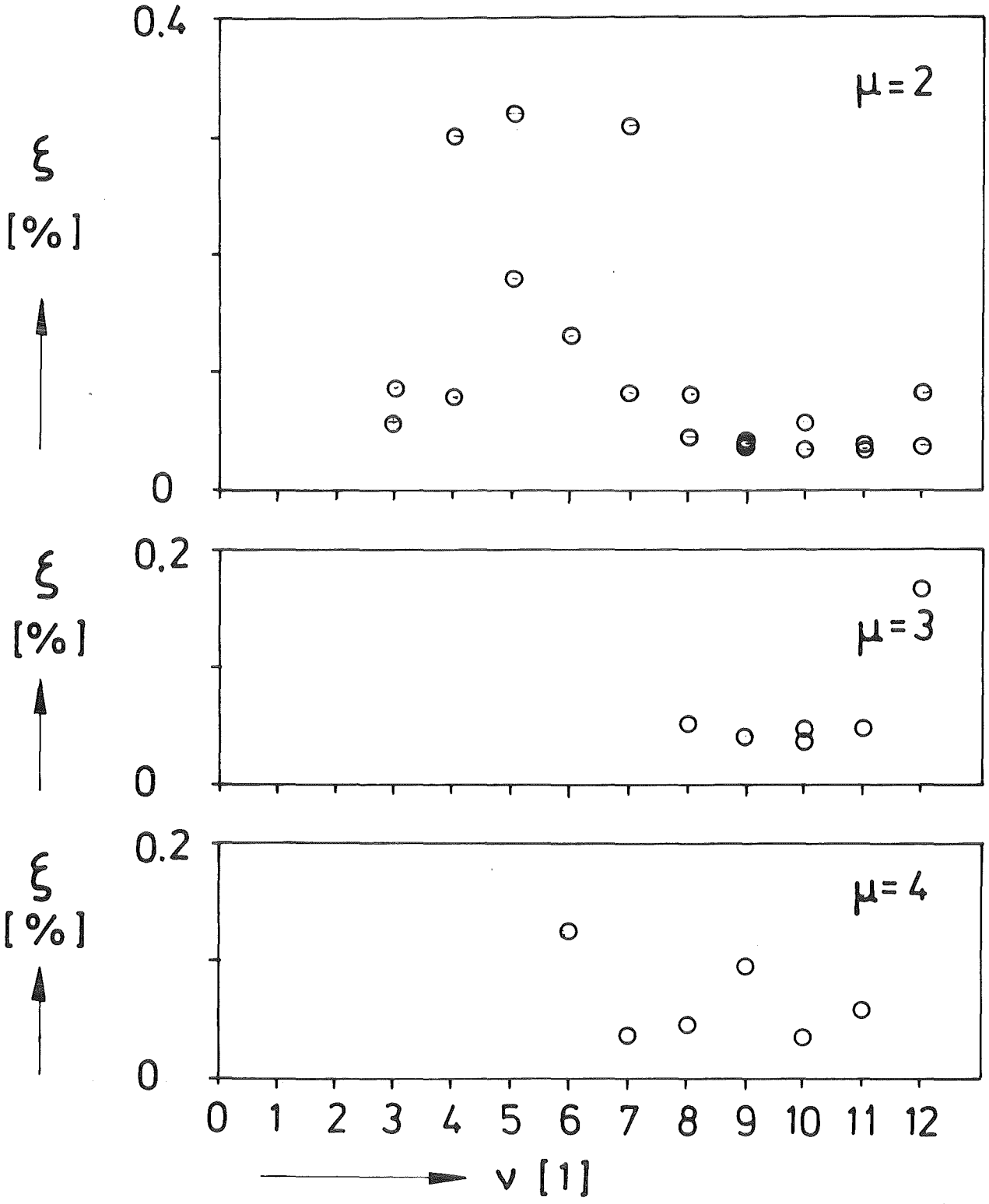

KfK IRE

Fig.32: Critical damping ratio ξ of extracted modes of the test cylinder partly filled with water (μ=2,3 and 4)

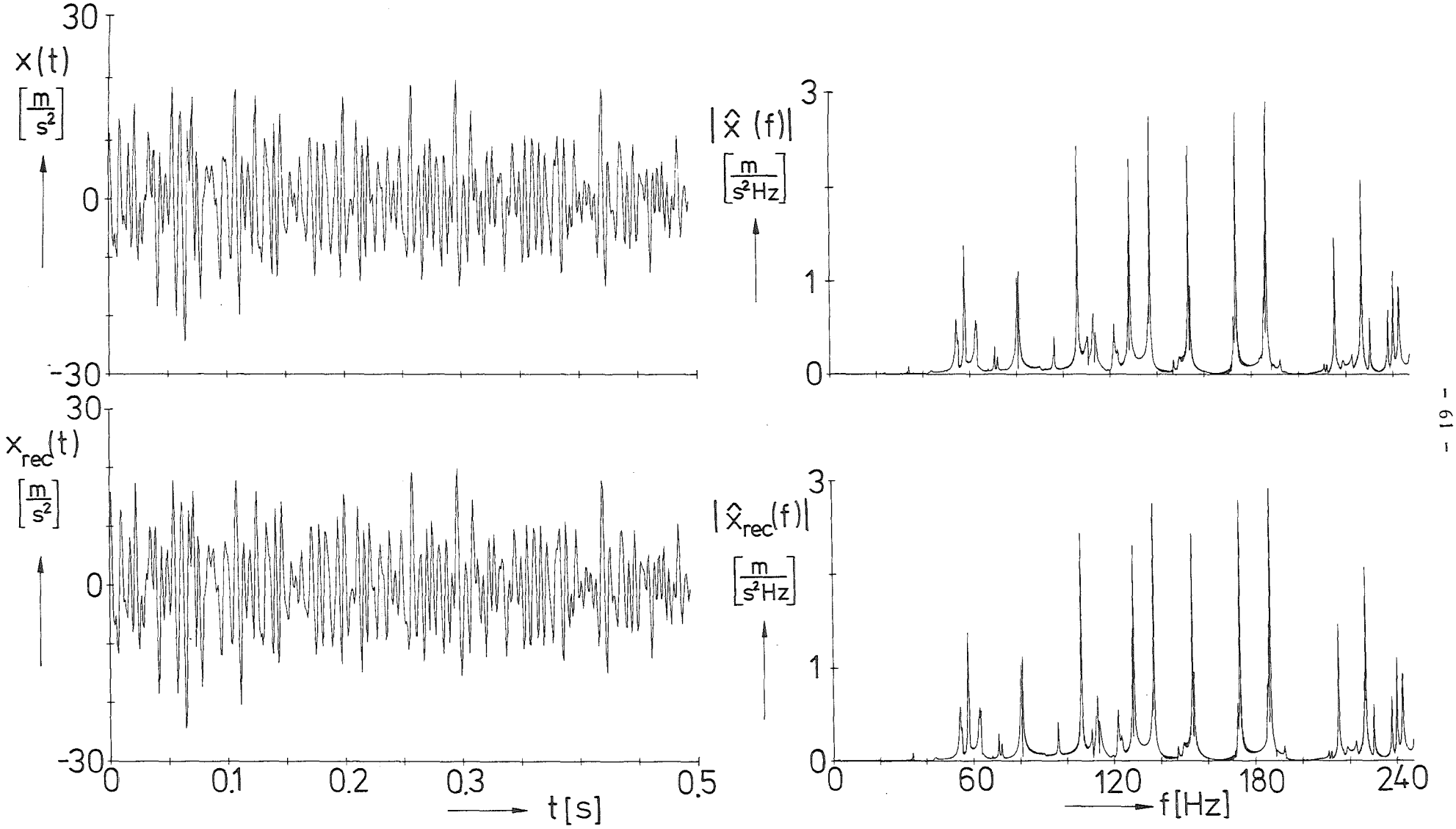

Fig. 33: Comparison of the original input signal with the reconstructed input signal (test cylinder partly filled with water, excitation location z_e=800mm, ψ_e=0°; accelerometer position z_a=1000mm, ψ_a= 0°)

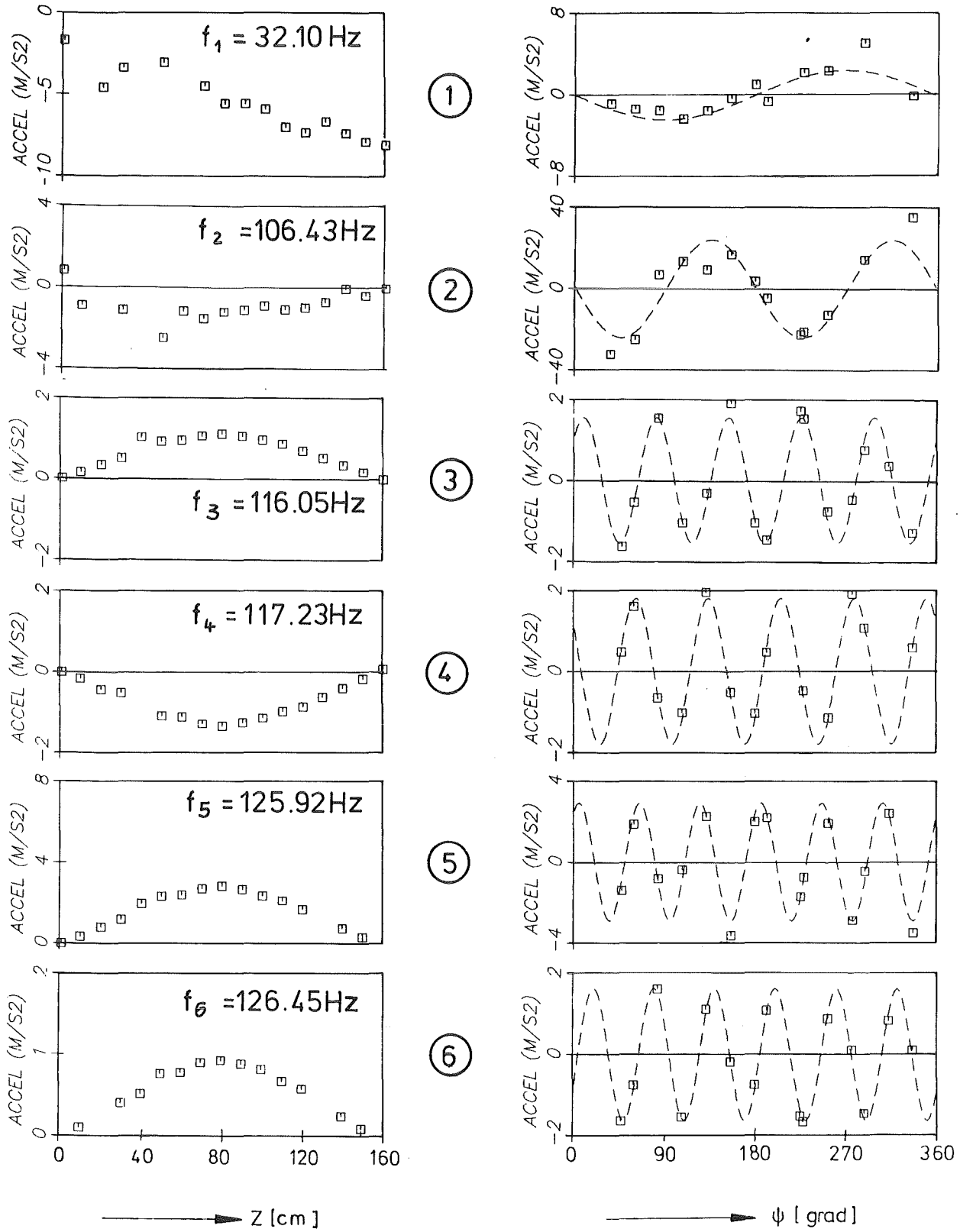

KfK IRE

Fig. 34: Extracted mode shapes of empty test cylinder

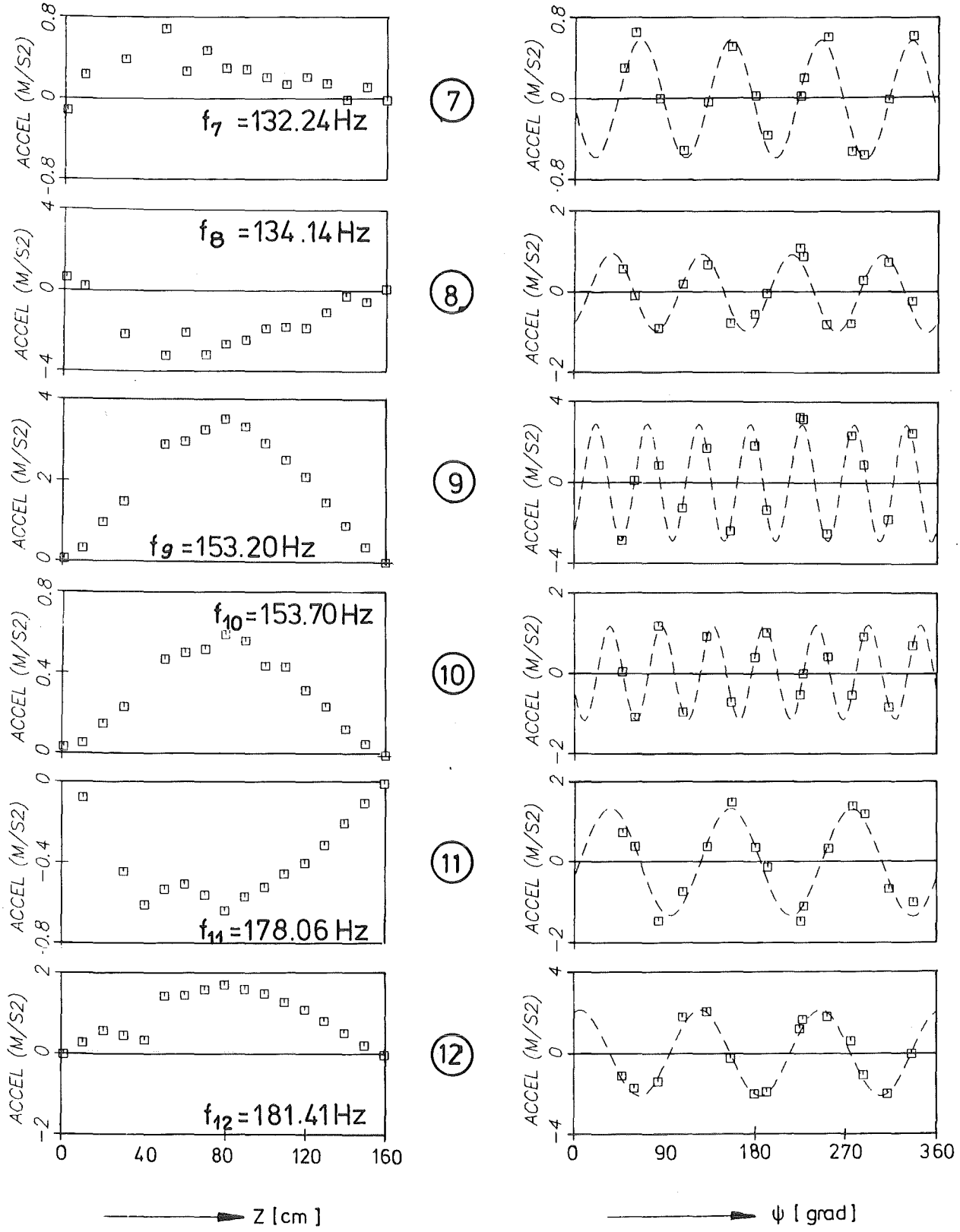

KfK IRE

Fig. 35: Extracted mode shapes of empty test cylinder (cont.)

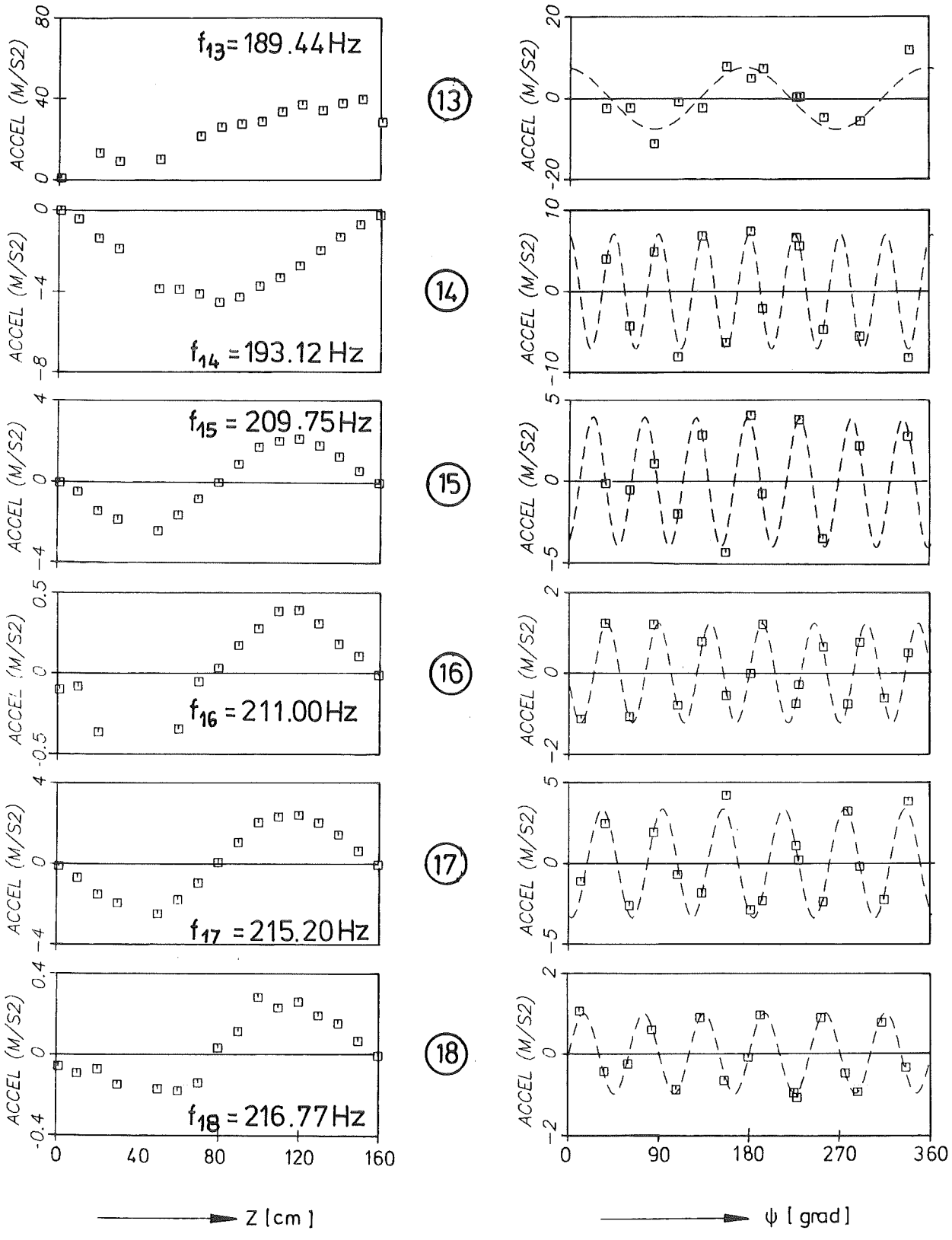

KfK IRE

Fig.36: Extracted mode shapes of empty test cylinder (cont.)

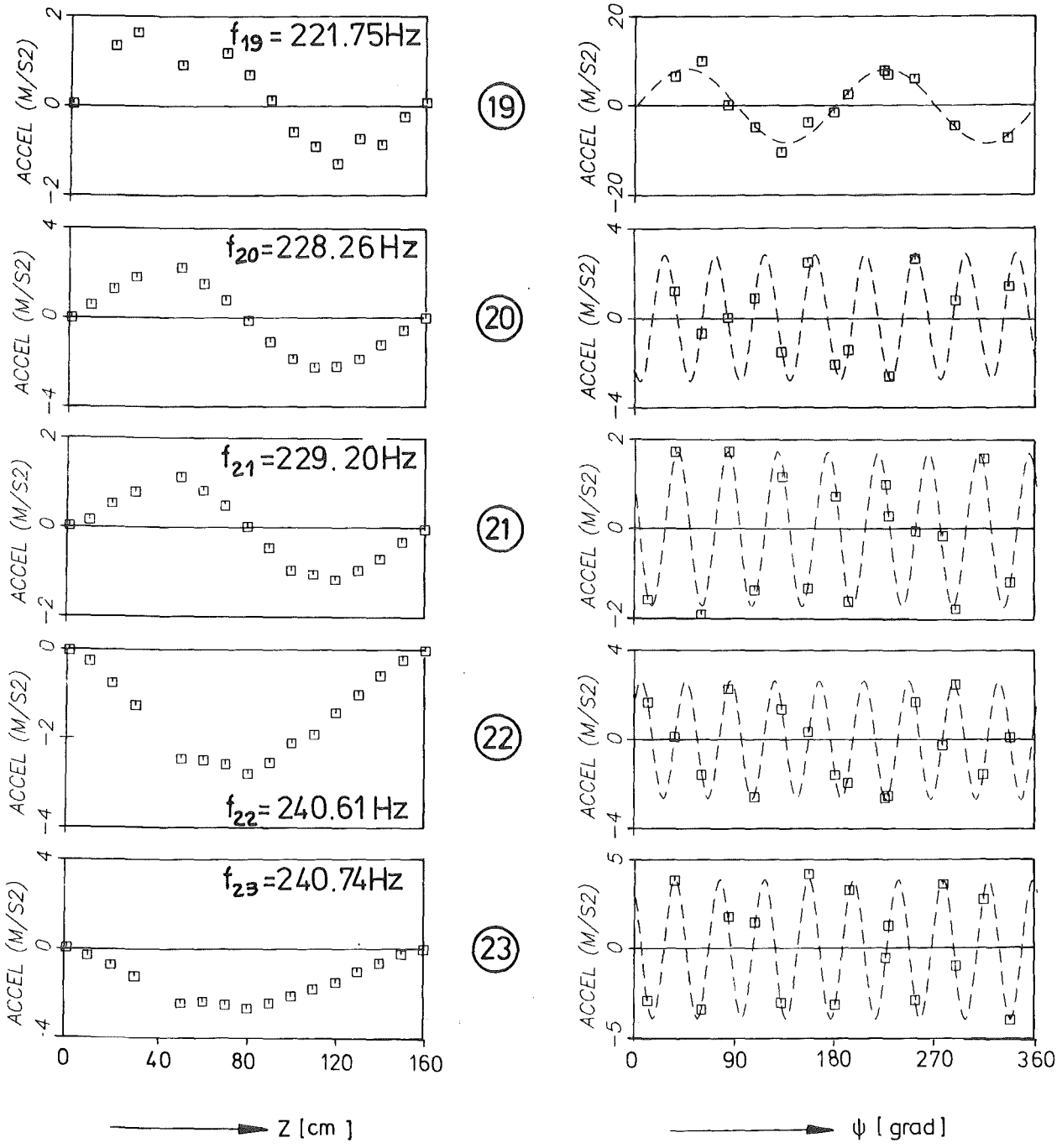

Fig. 37: Extracted mode shapes of empty test cylinder (cont.)

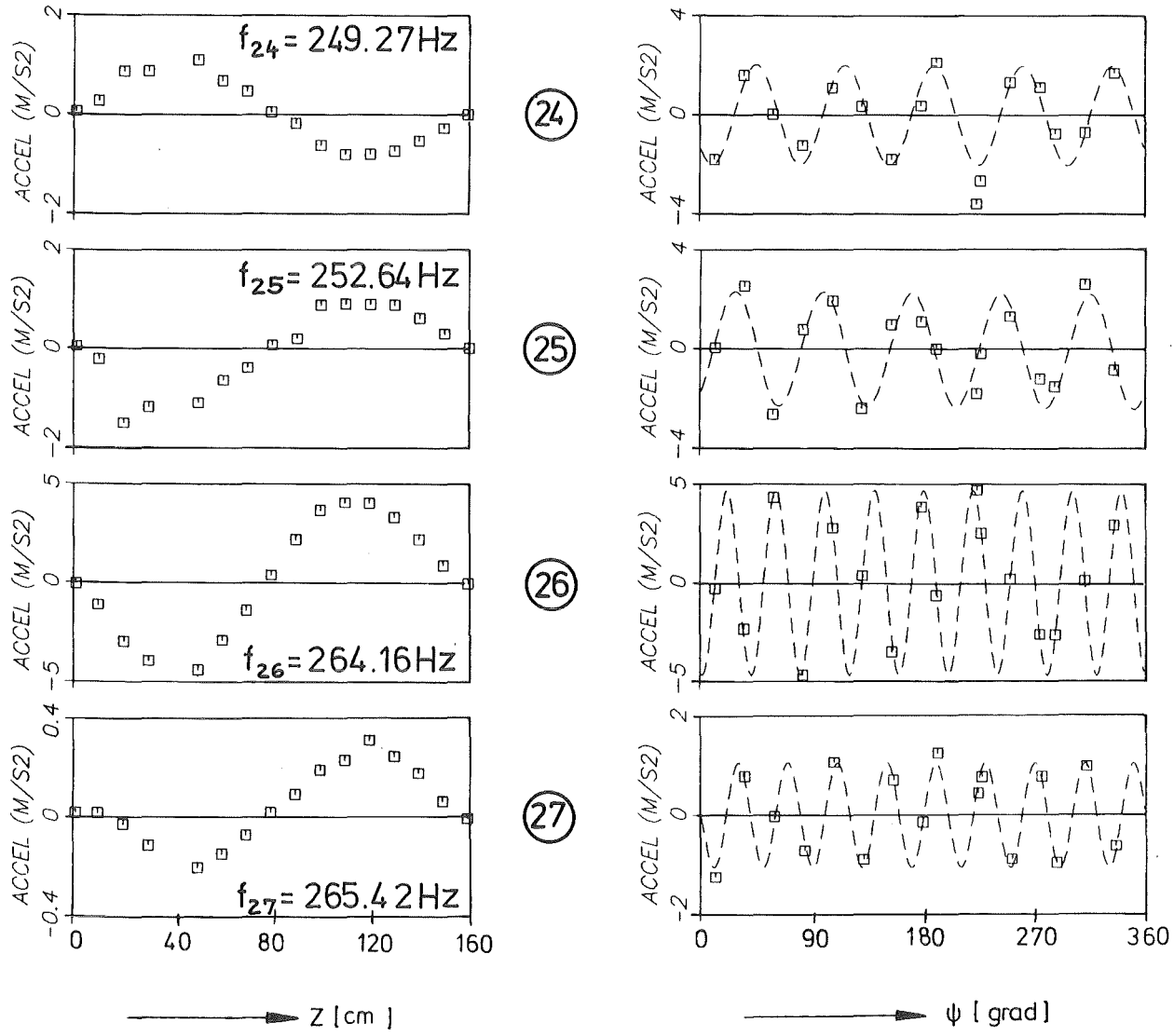

KfK IRE

Fig. 38: Extracted mode shapes of empty test cylinder (cont.)

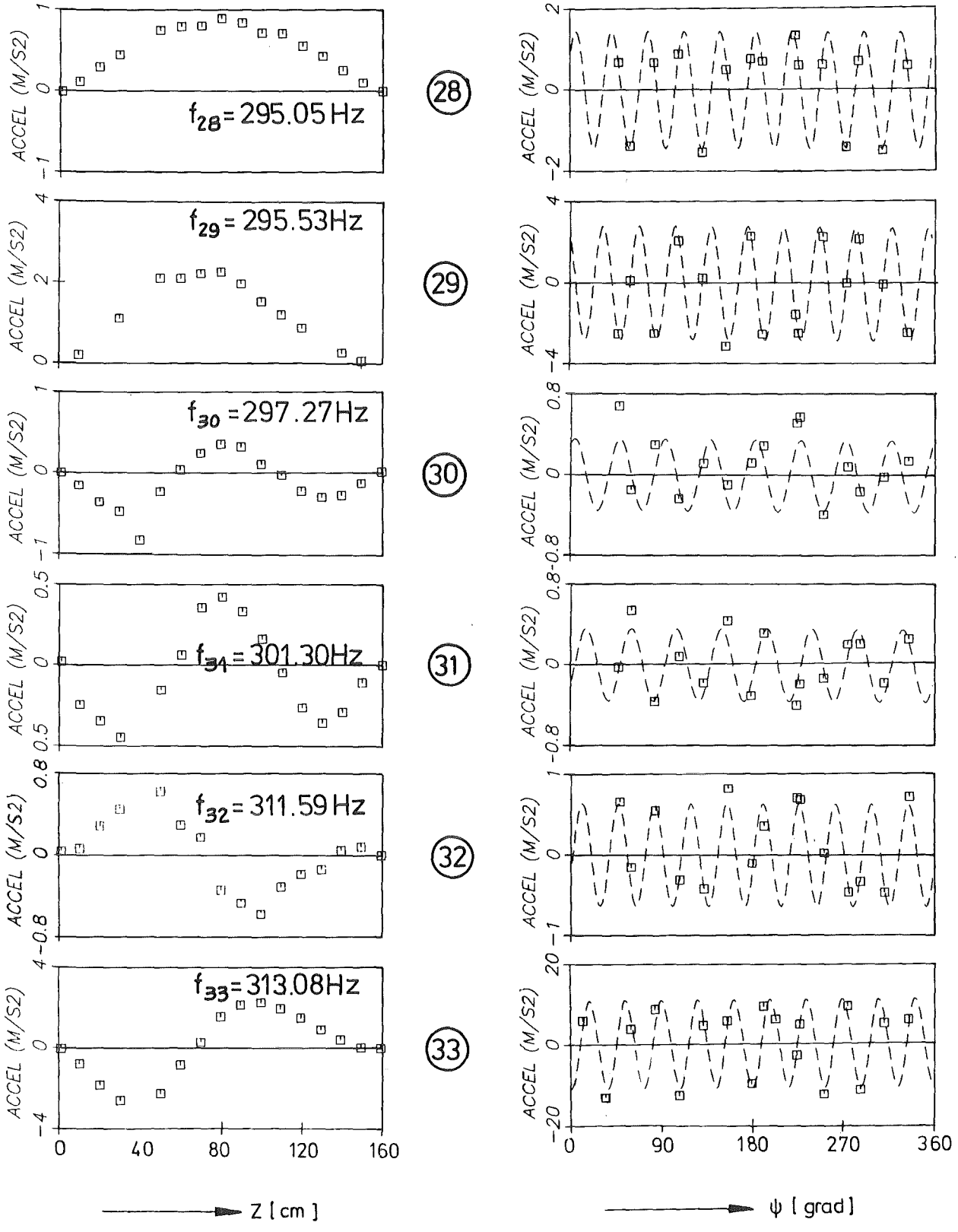

Fig. 39: Extracted mode shapes of empty test cylinder (cont.)

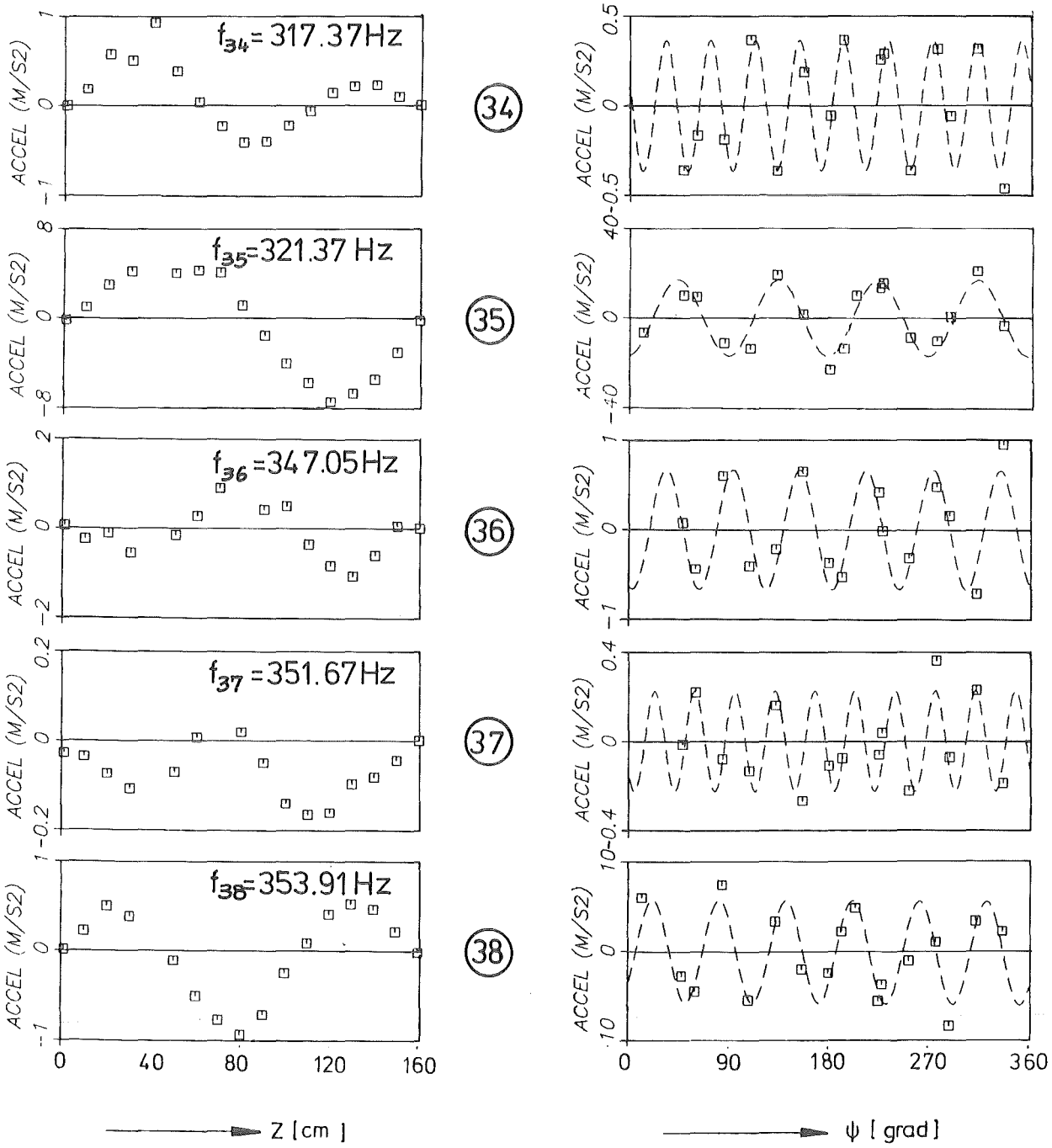

Fig. 40: Extracted mode shapes of empty test cylinder (cont.)

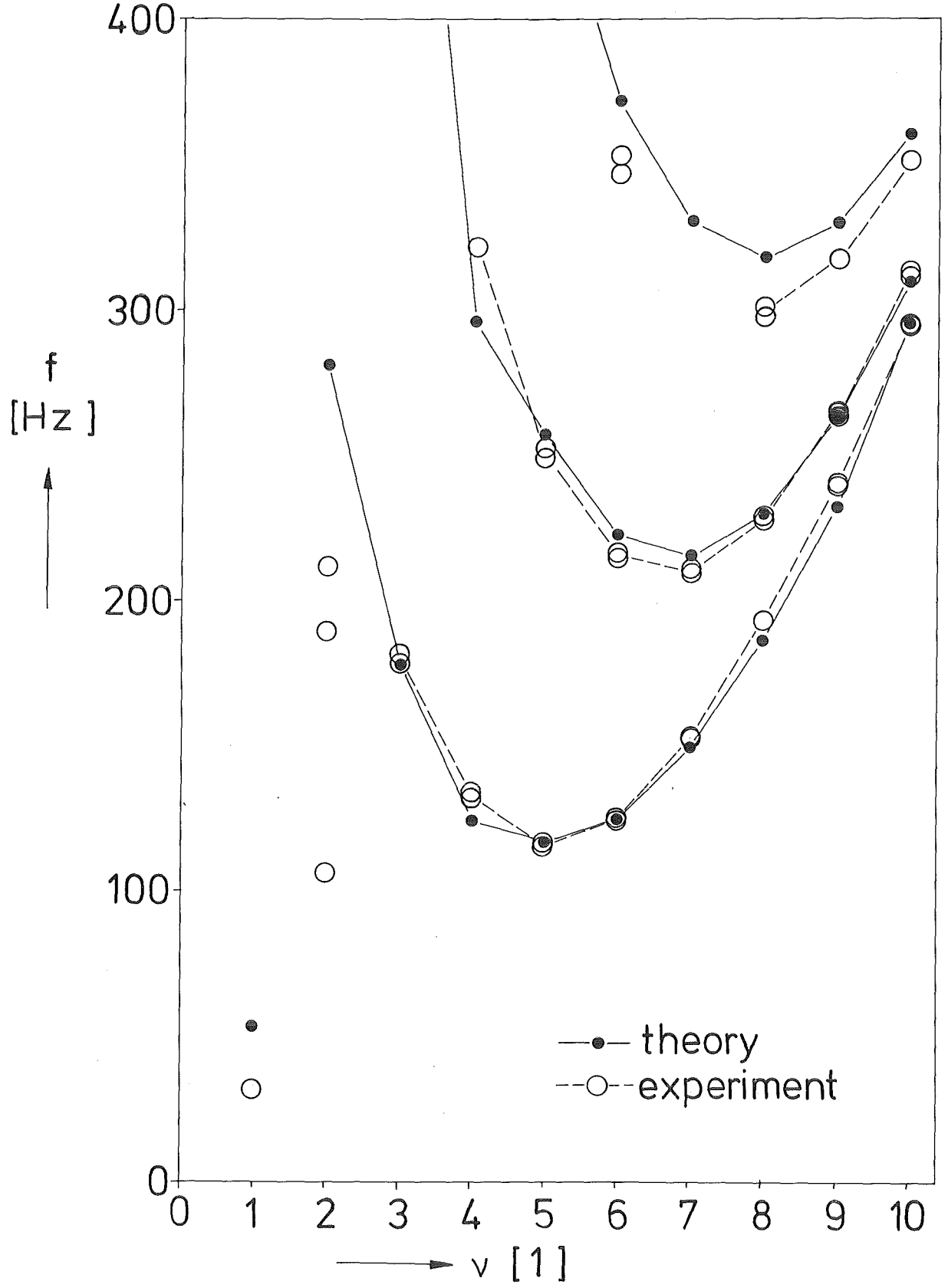

Fig. 41: Comparison of the calculated and measured natural frequencies of the empty test cylinder

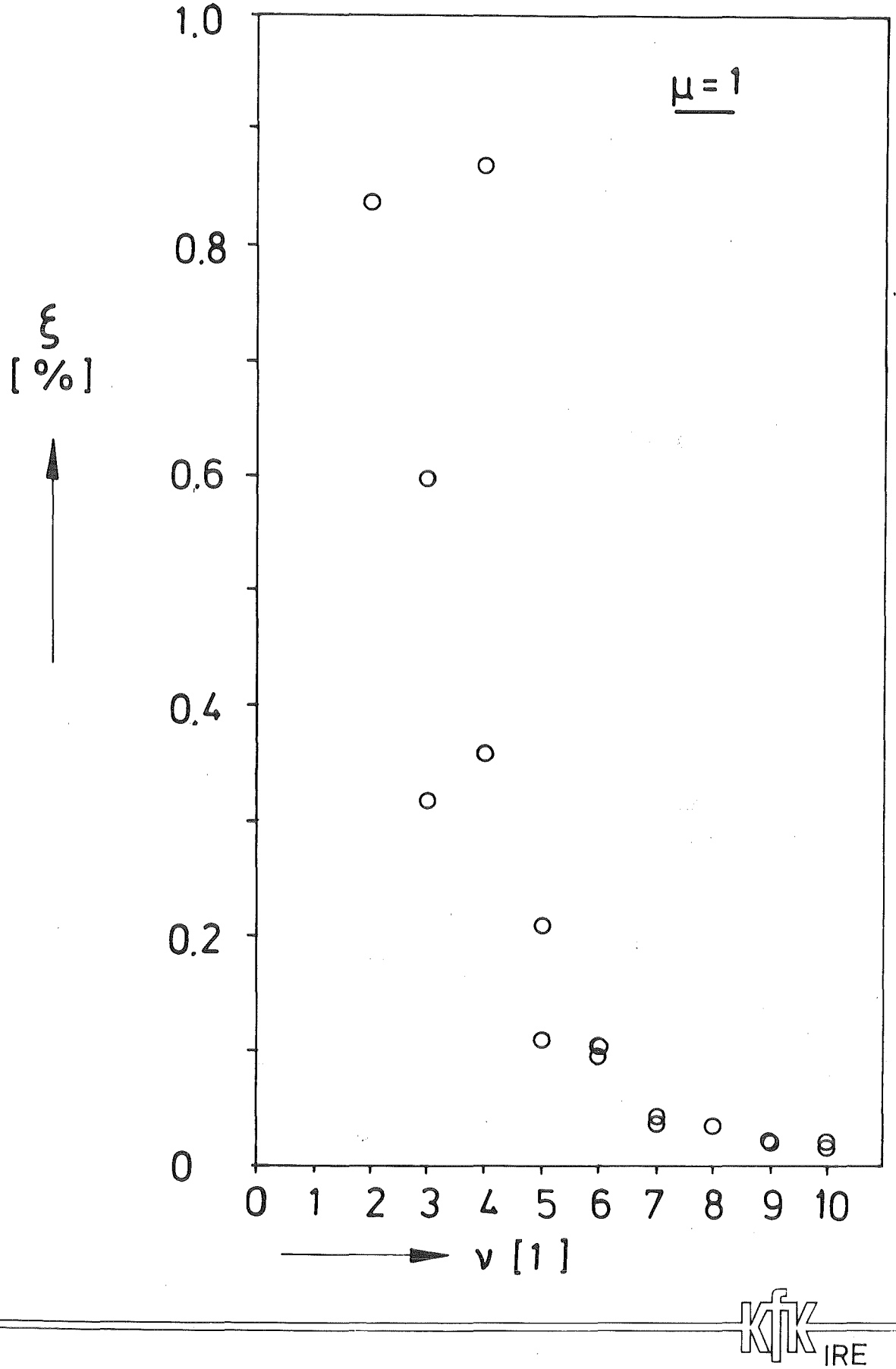

KfK IRE

Fig. 42: Critical damping ratio ξ of extracted modes of the empty test cylinder ($\mu = 1$)

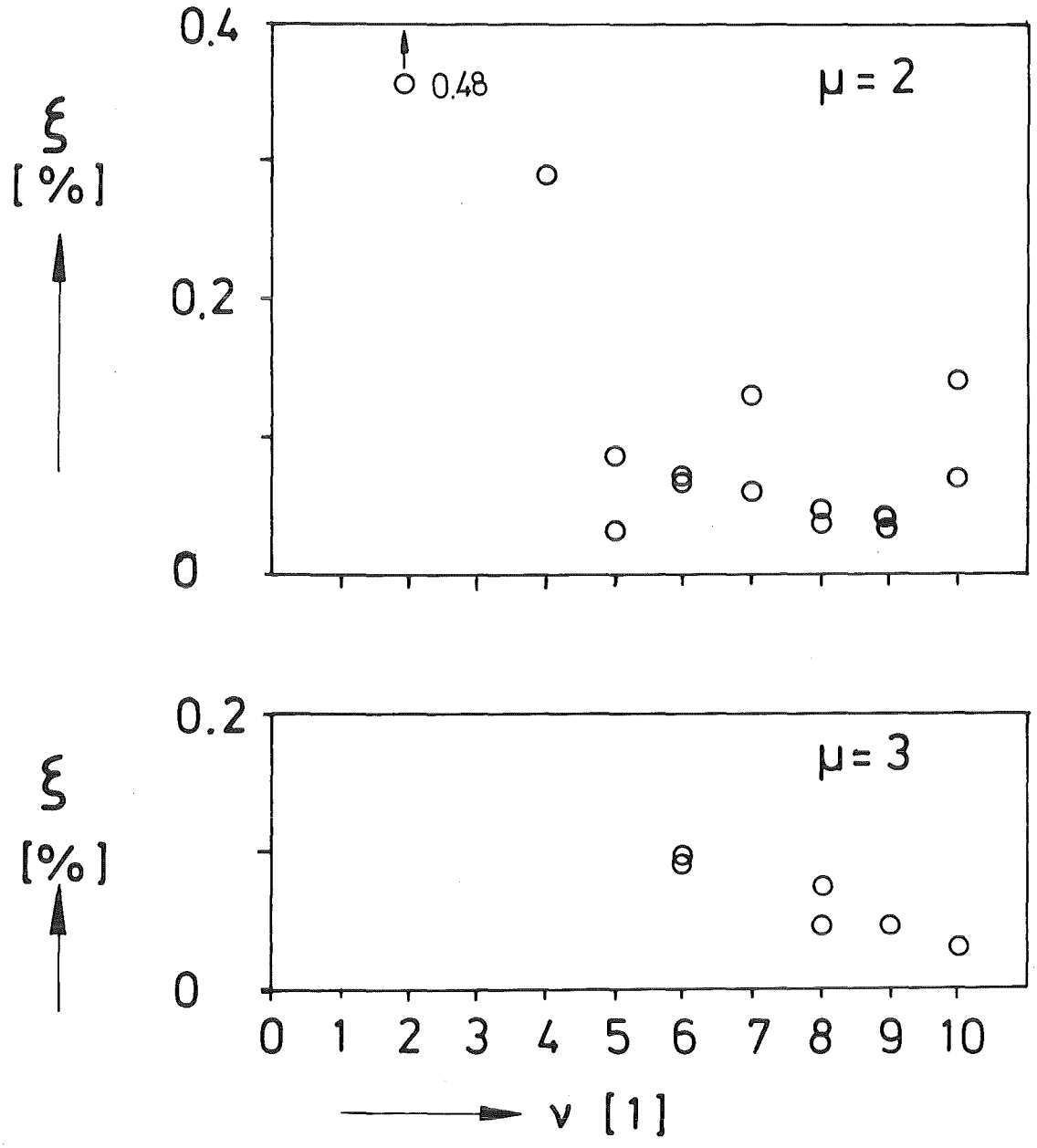

Fig. 43: Critical damping ratio ξ of extracted modes of empty test cylinder (μ = 2, 3 and 4)

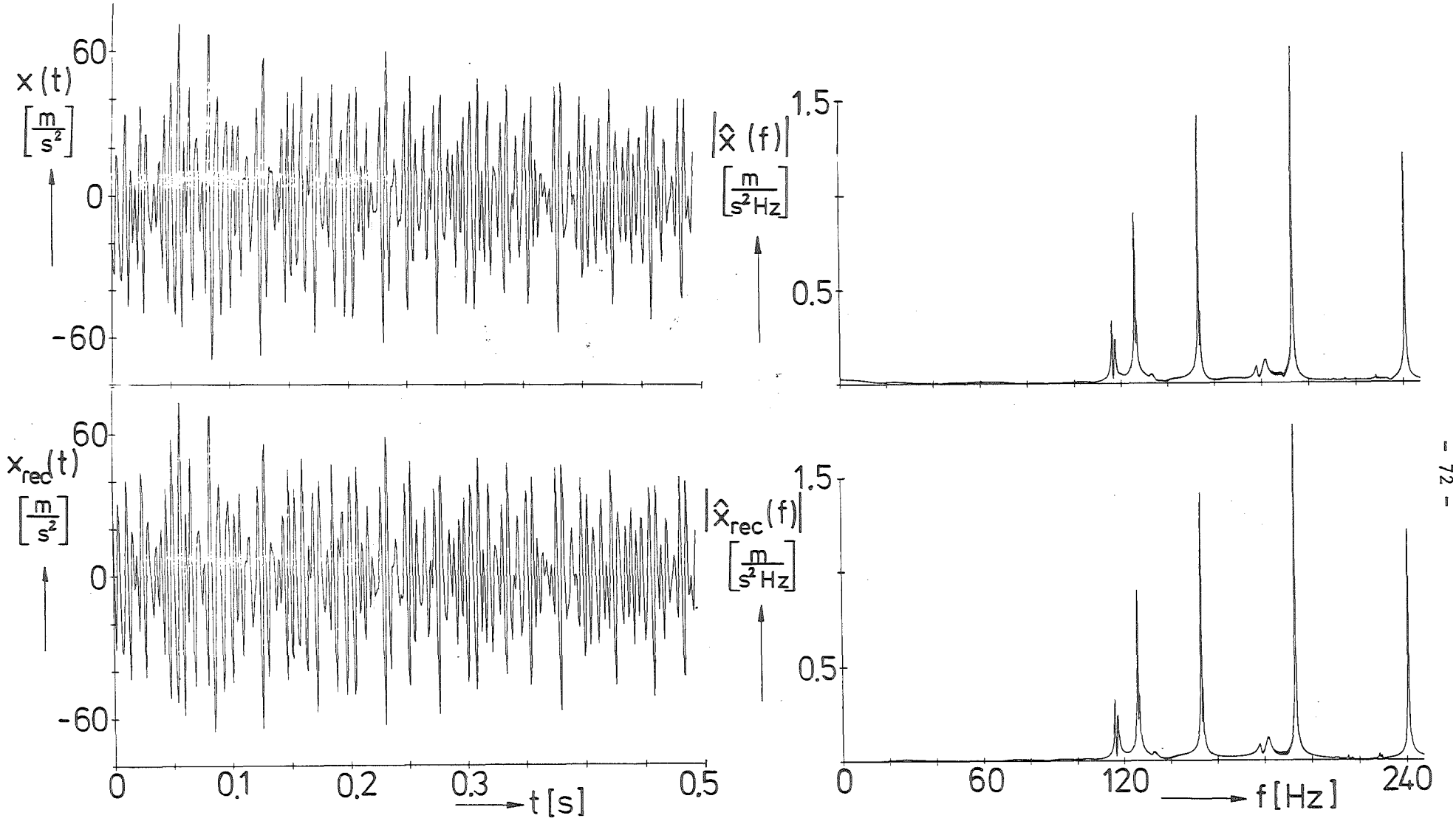

Fig.44: Comparison of the original input signal with the reconstructed input signal (test cylinder empty, excitation location $z_e = 800\,mm$, $\psi_e = 0°$; accelerometer position $z_a = 1000\,mm$, $\psi_a = 0°$)

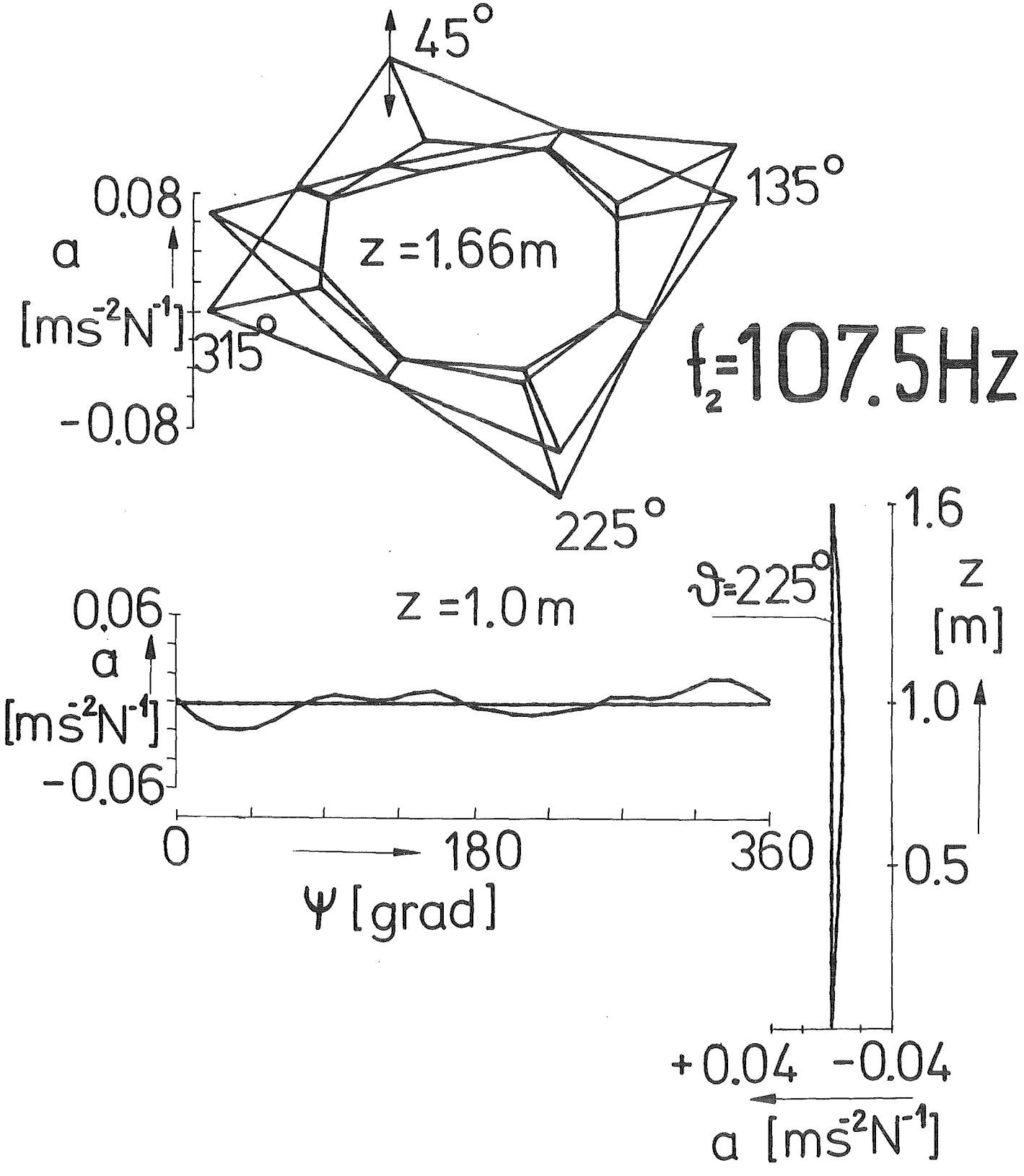

Fig.45 : Mode shape f_2 = 107.5 Hz

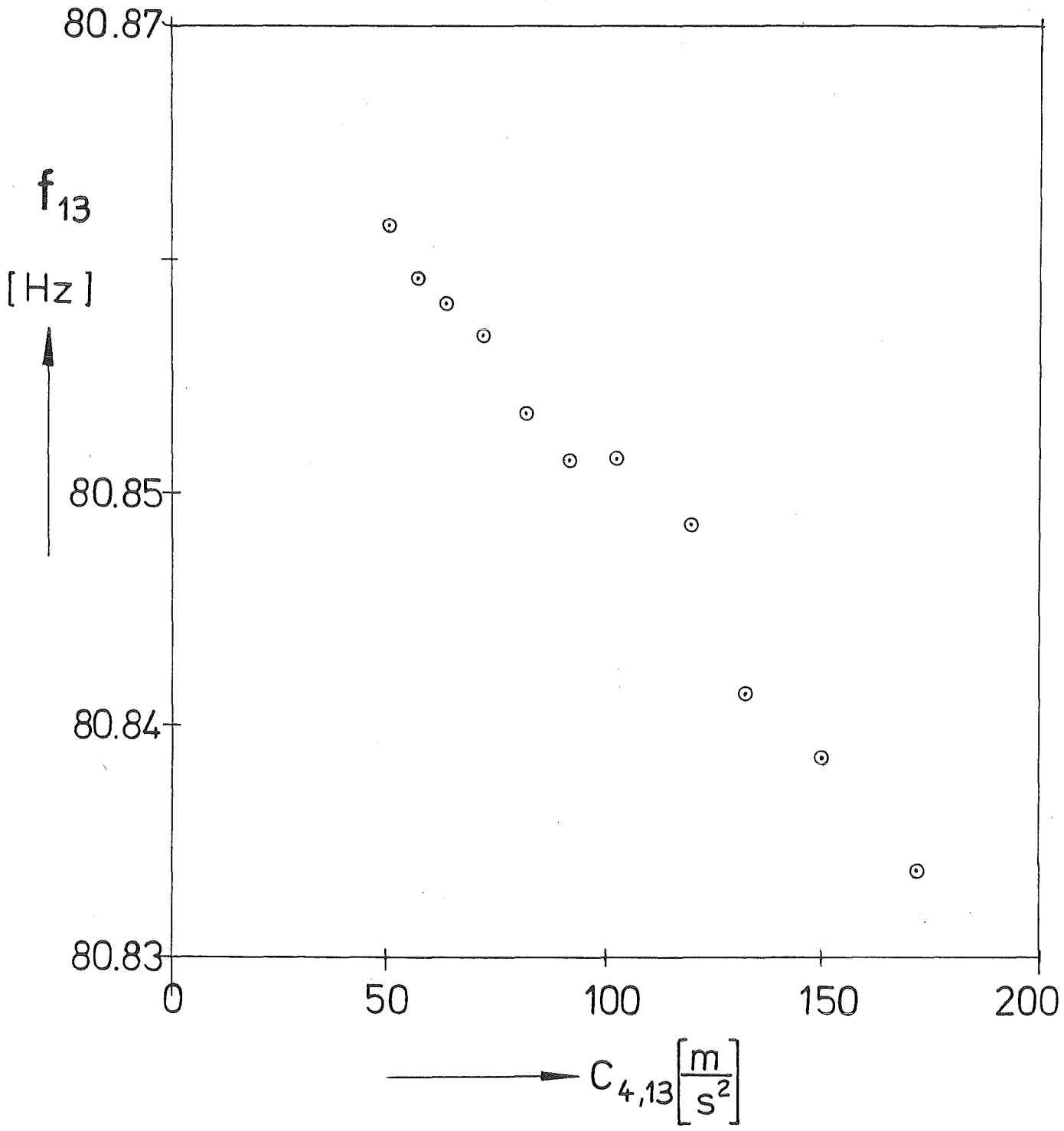

Fig. 46: Decrease of eigenfrequency f_{13} with increasing initial value of acceleration $C_{4,13}$

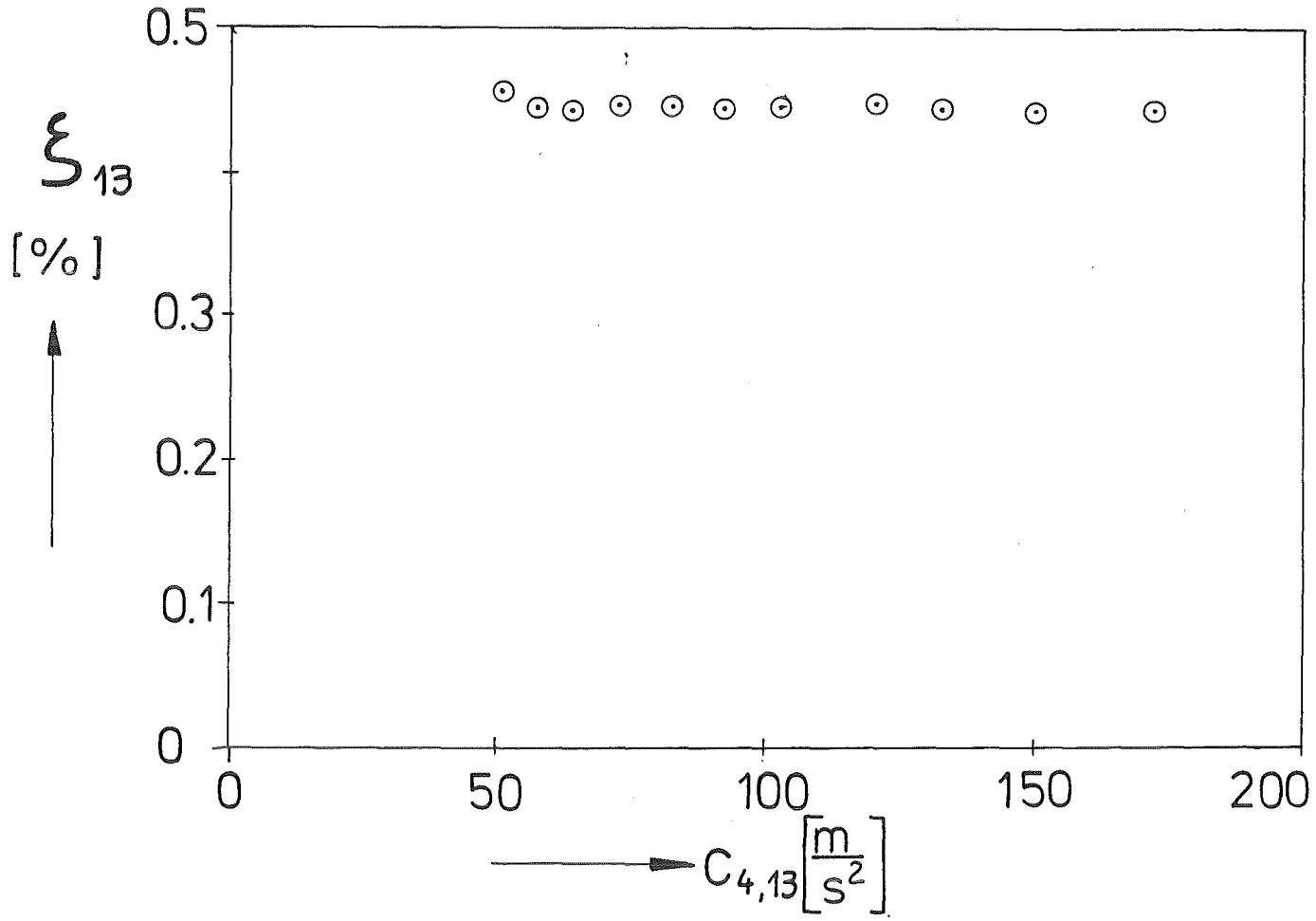

Fig. 47: Variation of critical damping ratio ξ_{13} with increasing initial value of acceleration $C_{4,13}$